

ผลของโครงสร้างของบิสไฟรีนิลยูเรียที่เชื่อมโดยสเปเซอร์พอลิเอทิลีนไกลคอลและเอไทม์ต่อ
ความสามารถในการจับแอนไอออน

นางสาวญาณิ์ ภารัตน์

วิทยานิพนธ์นี้เป็นส่วนหนึ่งของการศึกษาตามหลักสูตรปริญญาวิทยาศาสตรมหาบัณฑิต
สาขาวิชาเคมี ภาควิชาเคมี
คณะวิทยาศาสตร์ จุฬาลงกรณ์มหาวิทยาลัย
ปีการศึกษา 2554

ลิขสิทธิ์ของจุฬาลงกรณ์มหาวิทยาลัย
บทคัดย่อและแฟ้มข้อมูลฉบับเต็มของวิทยานิพนธ์ตั้งแต่ปีการศึกษา 2554 ที่ให้บริการในคลังปัญญาจุฬาฯ (CUIR)
เป็นแฟ้มข้อมูลของนิสิตเจ้าของวิทยานิพนธ์ที่ส่งผ่านทางบัณฑิตวิทยาลัย

The abstract and full text of theses from the academic year 2011 in Chulalongkorn University Intellectual Repository (CUIR)
are the thesis authors' files submitted through the Graduate School.

STRUCTURAL EFFECTS OF BISPYRENYL UREAS LINKED BY POLYETHYLENE
GLYCOL AND ETHYNE SPACERS TOWARD ANION BINDING ABILITIES

Miss Yanee Pharat

A Thesis Submitted in Partial Fulfillment of the Requirements
for the Degree of Master of Science Program in Chemistry

Department of Chemistry

Faculty of Science

Chulalongkorn University

Academic Year 2011

Copyright of Chulalongkorn University

ฎาณี ภารัตน์ : ผลของโครงสร้างของบิสไพร์นิลยูเรียที่เชื่อมโดยสเปเซอร์พอลิเอทิลีนไกลคอลและเอไทนต่อความสามารถในการจับแอนไอออน (STRUCTURAL EFFECTS OF BISPYRENYL UREAS LINKED BY POLYETHYLENE GLYCOL AND ETHYNE SPACERS TOWARD ANION BINDING ABILITIES) อ. ที่ปรึกษาวิทยานิพนธ์หลัก : ศ. ดร.ธวัชชัย ตันจุลานี, 113 หน้า.

ได้ออกแบบและสังเคราะห์อนุพันธ์ของบิสไพร์นิลที่สามารถจดจำแอนไอออนโมเลกุลเซ็นเซอร์ L1 ประกอบด้วยหมู่เอไมด์ที่มีความจำเพาะกับแอนไอออน มีวงเบนซิลเป็นสเปเซอร์โมเลกุลเซ็นเซอร์ L2 ประกอบด้วยหมู่ไทโอยูเรียเป็นหมู่จำเพาะกับแอนไอออน และมีสายพอลิเอทิลีนไกลคอลเชื่อมกับวงเบนซิลเป็นสเปเซอร์ และโมเลกุลเซ็นเซอร์ L3 ประกอบด้วยยูเรียเป็นหมู่จดจำแอนไอออน และ หมู่เอไทนเป็นสเปเซอร์ จากผลการสังเคราะห์ได้โมเลกุลเซ็นเซอร์ L1 และ L2 คิดเป็นร้อยละผลได้ของผลิตภัณฑ์เป็น 41 และ 51 ตามลำดับ ส่วนโมเลกุลเซ็นเซอร์ L3 ไม่สามารถสังเคราะห์ได้

ได้ศึกษาสมบัติการจดจำกับแอนไอออนของโมเลกุลเซ็นเซอร์ L1 และ L2 โดยใช้เทคนิคฟลูออเรสเซนซ์สเปกโตรโฟโตเมตรี ผลการศึกษาแสดงให้เห็นว่า L1 ไม่มีความจำเพาะกับแอนไอออนตัวใด เนื่องจากไม่มีการเปลี่ยนแปลงของสัญญาณฟลูออเรสเซนซ์ที่ชัดเจน ขณะที่ L2 มีการเปลี่ยนแปลงของสัญญาณฟลูออเรสเซนซ์แบบโมโนเมอร์เป็นแบบเอ็กไซเมอร์เมื่อมีการเติมแอนไอออน โดยสามารถเรียงอันดับการเปลี่ยนแปลงของอัตราส่วนความเข้มของสัญญาณเอ็กไซเมอร์ต่อโมโนเมอร์ดังนี้ $F^- > OH^- \gg AcO^- > BzO^- > H_2PO_4^- > Cl^- > Br^- \approx I^-$ เนื่องจากฟลูออไรด์มีขนาดเล็ก และมีความเป็นเบสสูง จึงสามารถเกิดพันธะไฮโดรเจนกับโปรตอนของไทโอยูเรียได้ดี นอกจากนี้ฟลูออไรด์และไฮดรอกไซด์ในปริมาณที่มากขึ้นจะเหนี่ยวนำให้เกิดการหลุดของโปรตอนที่ตำแหน่งไทโอยูเรีย ขณะที่อะซิเตตจะเกิดพันธะไฮโดรเจนเท่านั้น สารประกอบเชิงซ้อนระหว่าง L2 และ F^- เกิดจากการซ้อนทับกับของไพร์นต่างโมเลกุล ในขณะที่สารประกอบเชิงซ้อนระหว่าง L2 กับ AcO^- และ OH^- เกิดจากการซ้อนทับกันของไพร์นในโมเลกุลเดียวกัน

ภาควิชาเคมี..... ลายมือชื่อนิสิต

สาขาวิชาเคมี..... ลายมือชื่อ อ.ที่ปรึกษาวิทยานิพนธ์หลัก

ปีการศึกษา2554.....

5272288923 : MAJOR CHEMISTRY

KEYWORDS : PYRENE / EXCIMER / THIOUREA / INTER-INTRA
MOLECULAR EXCIMER

YANEE PHARAT : STRUCTURAL EFFECTS OF
BISPYRENYL UREAS LINKED BY POLYETHYLENE
GLYCOL AND ETHYNE SPACERS TOWARD ANION
BINDING ABILITIES. ADVISOR : PROF. THAWATCHAI
TUNTULANI, Ph.D., 113 pp.

Anion sensors possessing bispyrenyl derivatives have been designed and synthesized. Compound **L1** containing amide groups for binding anions and benzyl ring as spacer was synthesized in 41% yield. Compound **L2** containing thiourea groups as anion binding sites and polyethyleneglycol chains linked with benzyl ring as spacer was synthesized in 51% yield. Compound **L3** containing urea as anion binding sites and ethyne as spacer could not be synthesized.

Therefore, we have studied the anion abilities of **L1** and **L2** using fluorescence spectrophotometry. Compound **L1** did not interact with any anions as suggested by an insignificant change of the emission spectra. Emission spectra of compound **L2** changed from monomer band (410 nm) to excimer band (515 nm) upon addition of anions. The order of intensity ratio between excimer and monomer bands (I_E/I_M) in **L2** varied as $F^- > OH^- \gg AcO^- > BzO^- > H_2PO_4^- > Cl^- > Br^- \approx I^-$. Due to a smaller size and more basicity of F^- , it could form H-bonding interactions with protons of N-H thiourea of **L2**. A large amount of F^- and OH^- induced the deprotonation of N-H thiourea while AcO^- formed H-bonding interactions only. Complexation of **L2** and F^- occurred via intermolecular pyrene stacking while that of **L2** and AcO^- as well as OH^- occurred via intramolecular pyrene stacking.

Department : _____ Chemistry _____ Student's Signature _____
Field of Study : _____ Chemistry _____ Advisor's Signature _____
Academic Year : _____ 2011 _____

ACKNOWLEDGEMENTS

I wish to express appreciation to my thesis advisor, Professor Dr. Thawatchai Tuntulani, for the generous encouragement, help and provision to work and study in his laboratory. He gave guidance and spent time discussing my thesis. In addition, I would like to thank Assistant Professor Dr. Warinthorn Chavasiri, Assistant Professor Dr. Saowarux Fuangswasdi, and Dr. Gamolwan Tumcharern for their great suggestions and comments as thesis committee members.

I would like to thank the Human Resource Development in Science Project (Science Achievement Scholarship of Thailand, SAST) Scholarship. The Thailand Reserch Fund (RTA 5380003) is acknowledged for the research grant during my M.Sc. study. I thank to the Center of Excellence on Petrochemical and Materials Technology and Chulalongkorn University for research support.

I would like to express my highest gratitude to my family for their love, kindness, and financial support throughout my life. I would like to thank my mentor, Ms. Duangrat Thongkum, for her helps. Finally, my appreciation goes to all members in Supramolecular Chemistry Reserch Unit (SCRU).

CONTENTS

	Page
ABSTRACT IN THAI.....	iv
ABSTRACT IN ENGLISH.....	v
ACKNOWLEDGEMENTS.....	vi
CONTENTS.....	vii
LIST OF TABLES.....	x
LIST OF FIGURES.....	xi
LIST OF SCHEMES.....	xv
LIST OF ABBREVIATIONS.....	xvi
CHAPTER I INTRODUCTION.....	1
1.1 Concept of supramolecular chemistry.....	1
1.2 Molecular anion receptors.....	2
1.3 Molecular anion sensors.....	2
1.4 Optical anion sensors.....	3
1.4.1 Chromogenic sensors.....	3
1.4.2 Fluorogenic anion sensors.....	4
1.4.3 Excimer formation.....	6
CHAPTER II LITERATURE REVIEWS AND OBJECTIVE OF THIS RESEARCH.....	8
2.1 Literature reviews.....	8
2.1.1 Chromogenic fluoride sensors.....	8
2.1.2 Fluorogenic fluoride sensors.....	12
2.1.3 Excimer emission.....	16

	Page
2.2 Objective and scope of this research.....	26
2.2.1 Objective of this research.....	26
2.2.2 Scope of this research.....	26
CHAPTER III EXPERIMENTALS.....	27
3.1 General procedure.....	27
3.1.1 Analytical instruction.....	27
3.1.2 Materials.....	27
3.2 Synthesis.....	28
3.3 Complexation studies.....	38
3.3.1 Fluorescence studies.....	38
3.3.2 ¹ H NMR spectroscopy.....	50
3.4 Inter and Intramolecular pyrene stacking studies.....	54
3.5 Anion interference studies.....	54
CHAPTER IV RESULTS AND DISSCUSSION.....	55
4.1 Design and synthesize of anion receptors.....	55
4.2 Retrosynthesis of compounds L1-L3	56
4.2.1 Retrosynthesis of compound L1	56
4.2.2 Retrosynthesis of compound L2	56
4.2.3 Retrosynthesis pathway 1 of compound L3	58
4.2.4 Retrosynthesis pathway 2 of compound L3	59
4.3 Syntheses of compounds L1-L3	60
4.4 Characterization of L1 and L2	63
4.5 Anions binding studies.....	69
4.5.1 Anion binding studies using fluorescence spectrophotometry..	69
4.5.2 Anion binding studies using ¹ H NMR titrations.....	78
4.5.3 Determination of binding constants.....	82
4.6 Effects of concentrations on the emission spectra.....	85

	Page
CHAPTER V CONCLUSIONS.....	89
REFERENCES.....	91
APPENDIX.....	96
VITAE.....	113

LIST OF TABLES

Table	Page
1.1 Description of the photophysical species.....	7
3.1 The scale ratio between L1 with anions were used to fluorescence titration method.....	39
3.2 The scale ratio between L2 with fluoride ion were used to fluorescence titration method.....	41
3.3 The scale ratio between L2 with acetate ion were used to fluorescence titration method.....	44
3.4 The scale ratio between L2 with hydroxide ion were used to fluorescence titration method.....	46
3.5 Amount of L1 (2×10^{-6} M) and anion (2×10^{-6} M) that added in to a cuvette cell for Job's method.....	48
3.6 Amount of L2 (5×10^{-6} M) and anion (5×10^{-6} M) that added into a cuvette cell for Job's method.....	49
3.7 Amount of fluoride (0.04 M) was added into a cuvette cell of L2 (5×10^{-3} M) for Job's method ^1H NMR titration method.....	51
3.8 Amount of acetate (0.04 M) was added into a cuvette cell of L2 (5×10^{-3} M) for Job's method ^1H NMR titration method.....	52
3.9 Amount of hydroxide (0.04 M) was added into a cuvette cell of L2 (5×10^{-3} M) for Job's method ^1H NMR titration method.....	53
3.10 Amount of fluoride (0.24 M) was added into a cuvette cell of L2 (6×10^{-3} M) for Job's method ^1H NMR titration method.....	54
4.1 ^1H NMR data for L1 and L2 in d_6 -DMSO.....	64
4.2 ^{13}C NMR data for L1 and L2 in d_6 -DMSO.....	65
4.3 The emission parameters for compounds L1 and L2 in DMSO.....	68
4.4 Binding constant (M^{-1}) of receptor L2 and F^- , OH^- , and AcO^- in DMSO via SPECFIT 32 program.....	84

LIST OF FIGURES

Figure		Page
1.1	Scope of supramolecular chemistry.....	1
1.2	Principle of molecular sensors device (anion sensors).....	2
1.3	Compound 1 and the change in color of 1 in DMSO upon addition of various anions [10].....	3
1.4	The changes in color (Left) and the changes in the absorption spectra (Right) of 1 upon addition of fluoride in DMSO [9].....	4
1.5	Perrin-Jablonski diagram and illustration of the relative positions of absorption, fluorescence and phosphorescence spectra.....	5
1.6	Excimer formation, with the corresponding monomer (400 nm) and excimer (500 nm) bands.....	6
2.1	Structures of compounds 2 and 3	9
2.2	The proposed binding mode of compounds 4 and 5	10
2.3	Structure of compounds 6 (X=O) and 7 (X=S).....	11
2.4	Intermolecular proton transfer between 8 and the fluoride ion.....	11
2.5	Structure of compound 9	12
2.6	Structure of compound 10	13
2.7	Schematic representation of the different emission for 10 in the presence of fluoride ion [29].....	14
2.8	The proposed binding mechanisms of compound 11 with fluoride ion.....	14
2.9	Proposed interaction modes of compound 12 with fluoride ion.....	15

Figure	Page
2.10 The possible mechanism for the spectroscopic changes of 13 in the presence of fluoride ion.....	16
2.11 The Proposed binding mode of compound 14 and 15 upon addition fluoride ion.....	17
2.12 Structures of chemosensor 16-17 and it propose structures.....	18
2.13 The Proposed binding mode of compound 18 upon addition Cu(II) ion.....	19
2.14 Structures of compounds 19-22	20
2.15 Structure of compounds 23, 24, 25, and 26	21
2.16 Structure of compound 27 and its metal chelation.....	22
2.17 Structure of N-Pn-N or compound 28 and CB[8] [39].....	23
2.18 Cucurbit[8]uril-templated intramolecular photocycloaddition of N-Pn-N in aqueous solution [39].....	23
2.19 The concentration independent of I_e/I_m of CB[8] with various concentration of N-Pn-N (I_e : excimer intensity at 433 nm; I_m : monomer intensity at 373 nm) [39].....	24
2.20 The Proposed binding mode of compound 29	25
2.21 Structure of target molecules L1, L2, and L3	26
4.1 Structure of receptors L1, L2, and L3	55
4.2 The emission spectra of a) L1 and b) L2 in DMSO.....	66
4.3 Linear plot of anthracene standard in EtOH (Grad = 215818).....	67
4.4 Linear plot of L1 and L2 in DMSO (GradL1 = 196293, GradL2 = 216562).....	68

Figure		Page
4.5	Fluorescence emission of L1 (2×10^{-6} M) with 1000 equiv TBA anion salts in DMSO.....	69
4.6	Fluorescence emission of L1 (2×10^{-6} M) with 0-700 equiv of F^- salts in DMSO.....	70
4.7	Fluorescence emission of L1 (2×10^{-6} M) with a) 1.4 mL of DMSO b) 700 equiv of F^- salts in DMSO.....	70
4.8	Fluorescence emission of L2 (5×10^{-6} M) with 50 equiv. TBA anion salts in DMSO.....	72
4.9	Plot of the intensity ratio of excimer to monomer emission (I_E : 515 nm, I_M : 415 nm) of L2 (5×10^{-6} M) with 50 equiv TBA anion salts in DMSO.....	72
4.10	The color change observed for the receptor L2 (1×10^{-5} M) upon addition of 100 equiv. of anions (from left to right: L2 , L2 + F^- , L2 + Cl^- , L2 + Br^- , L2 + I^- , L2 + AcO^- , L2 + BzO^- , L2 + $H_2PO_4^-$, and L2 + OH^-) in DMSO.....	73
4.11	Fluorescence titration spectrum of L2 (1×10^{-5} M) with TBAF (0 - 1.4 equiv) in DMSO.....	75
4.12	Stepwise of fluorescence titration spectrum of L2 (1×10^{-5} M) with TBAF (0 - 231 equiv) in DMSO.....	75
4.13	Fluorescence titration spectrum of L2 (1×10^{-5} M) with TBAOH (0 – 7.2 equiv) in DMSO.....	76
4.14	Stepwise of fluorescence titration spectrum of L2 (1×10^{-5} M) with TBAOH (0 - 64 equiv) in DMSO.....	76
4.15	Fluorescence titration spectrum of L2 (1×10^{-5} M) with TBAOAc (0 - 2 equiv) in DMSO.....	77
4.16	Stepwise of fluorescence titration spectrum of L2 (1×10^{-5} M) with TBAOAc (0 – 10.8 equiv) in DMSO.....	77
4.17	1H NMR spectra of L2 in the presence of 0.5 equiv of TBAF, TBAOAc, and TBAOH in d_6 -DMSO at 400 MHz.....	78

Figure	Page
4.18 ^1H NMR titration spectra of L2 in the presence of 0-0.5 equiv. of TBAF, inset: partial ^1H NMR with 9 equivalents of TBAF in d_6 -DMSO at 400 MHz.....	80
4.19 ^1H NMR titration spectra of L2 in the presence of 0-0.8 equiv of tetra- <i>n</i> -butylammonium OH^- in d_6 -DMSO at 400 MHz.....	81
4.20 The fluorescence titration spectra of L2 (10^{-5} M) upon the gradual addition of a) F^- (0-1.8 equiv.), b) AcO^- (0-2 equiv), c) AcO^- (2-10.8 equiv), d) OH^- (0-7.2 equiv.), and e) OH^- (7.2-64 equiv.) in DMSO and the compared experiment data calculated data from fluorescence titration of L2 and f) F^- (0-1.4 equiv.), g) AcO^- (0-2 equiv), h) AcO^- (2-10.8 equiv), i) OH^- (0-7.2 equiv.), and j) OH^- (7.2-64 equiv.) for calculation of the binding constants (K_{ass}).....	82
4.21 Job's plot of L2 (5×10^{-6} M) with tetra- <i>n</i> -butylammonium fluoride in DMSO.....	85
4.22 Plot of I_E/I_M of various concentrations of L2 ($\times 10^{-8}$ M) with TBAF (2.5 equiv).....	86
4.23 The possible structure of L2 $\cdot\text{F}^-$ complex.....	86
4.24 Plot of I_E/I_M of various concentrations of L2 ($\times 10^{-7}$ M) with TBAOAc (1.0 equiv).....	87
4.25 Plot of I_E/I_M of various concentrations of L2 ($\times 10^{-7}$ M) with TBAOH (1.5 equiv).....	87
4.26 The possible structure of L2 $\cdot\text{OAc}^-$ and L2 $\cdot\text{OH}^-$ complex.....	88

LIST OF SCHEMES

Scheme		Page
3.1	Synthesis pathway of compound L3 in method 1.....	33
3.2	Synthesis pathway of compound L3 in method 2.....	36
4.1	Retrosynthesis of compound L1	56
4.2	Retrosynthesis of compound L2	57
4.3	Retrosynthesis pathway 1 of compound L3	58
4.4	Retrosynthesis pathway 2 of compound L2	59
4.5	Synthetic procedure of compound L1	60
4.6	Synthetic procedure of compound L2	61
4.7	Synthetic pathway 1 of compound L3	62
4.8	Synthetic pathway 2 of compound L3	63

LIST OF ABBREVIATIONS

AcO ⁻	Acetate ion
CH ₃ CN	Acetonitrile
K _{association} or K _{ass}	Binding Constant
BzO ⁻	Benzoate
Br ⁻	Bromide
¹³ C NMR	Carbon Nuclear Magnetic Resonance
δ	Chemical shift
CH ₃ OH	Chloroform
Cl ⁻	Chloride
<i>J</i>	Coupling constant
°C	Degree Celsius
CDCl ₃	Deuterated Chloroform
d ₆ -DMSO	Deuterated Dimethylsulfoxide
CH ₂ Cl ₂	Dichloromethane
DIEA	Diisopropylethylamine
H ₂ PO ₄ ⁻	Dihydrogenphosphate
DMAP	4-Dimethylaminopyridine
DMF	Dimethylformamide
Equiv.	Equivalent

EtOAc	Ethylacetate
Φ_F	Fluorescence quantum yields
F^-	Fluoride
g	Gram
Hz	Hertz
HCl	Hydrochloric acid
OH^-	Hydroxide
m/z	Mass per charge ratio
MeOH	Methanol
μL	Micro liter
mL	Milliliter
M	Molar
nm	Nanometer
ppm	Part per million
K_2CO_3	Potassium carbonate
$^1\text{H NMR}$	Proton Nuclear Magnetic Resonance
s, d, t, m	singlet, doublet, triplet, multiplet
Na_2SO_4	Sodium sulphate
TBA	Tetra- <i>n</i> -butylammonium
THF	Tetrahydrofuran
TLC	Thin layer chromatography
TsCl	Tosyl chloride

V

Volume

CHAPTER I

INTRODUCTION

1.1 Concept of supramolecular chemistry

Supramolecular chemistry is a branch of sciences which interest chemists, biochemists, physicists, engineers, and researchers in many fields. Supramolecular chemistry can be applied in many disciplines such as medicine, catalyst and chemical sensors. Basically, supramolecular chemistry studies mainly on non-covalent interactions such as hydrogen bonding, electrostatic, cation- π , π - π interactions, and van der Waals forces. Although these interactions are weak forces but they significantly effect complexation abilities of host and guest molecules. The concept of host-guest chemistry stems from the lock and key principle in which the host molecule can bind the guest molecule that fits it shape and size specifically (Figure 1.1) [1-3].

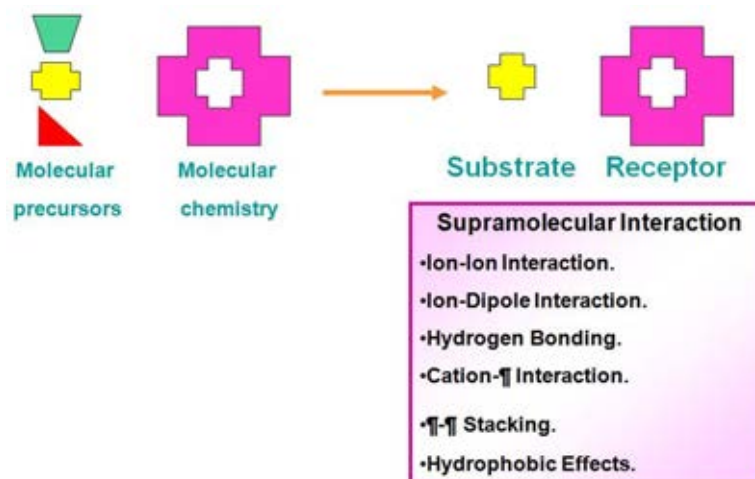


Figure 1.1 Scope of supramolecular chemistry [3].

1.2 Molecular anion receptors

To design host-guest molecule, not only non-covalent interactions between host and guest molecules but also steric and electronic effects can affect selectivity of the host-guest complex [4]. Therefore, concerning factors to display molecular recognition would be size and shape of the guest, cavity size of the host, solvation, preorganization and functional groups of the host molecule that involve in the interactions [1]. Designing of anion receptors was quite a challenge due to different shapes of anions: spherical, linear, V-shaped, trigonal planar and tetrahedral [5]. Nowadays, binding sites for anion receptors such as urea, thiourea, amide, phenol, or pyrrole subunits were widely used in the research. The interactions between host (anion receptors) and guest (anions) could be H-bonding interactions. Among them, thiourea was often used as anion binding sites in anion receptors because it is a superb H-bond donor group [6].

1.3 Molecular anion sensors

Molecular sensors are one of the applications of knowledge in supramolecular chemistry [7]. A molecule performing a sensing device contains binding sites, for ions or guest molecules, and sensing sites which are chemical transducers to convert the binding phenomena to a signal that can be detected by optical and electrochemical instruments (Figure 1.2).

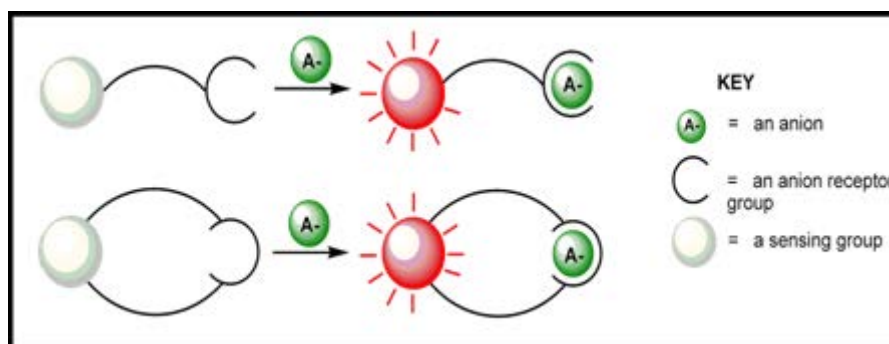


Figure 1.2 Principle of molecular sensors device (anion sensors).

1.4 Optical anion sensors

To develop the appropriate chemosensor, qualitative and quantitative determination of ion has been concerned. Aim to design the efficient chemosensor mainly focuses on maximizing the selectivity of the molecular recognition and the sensitivity of the physical signal. Both transformation of absorption and fluorescence signals have been utilized for 2 important classes of sensors: chromogenic and fluorogenic sensors. Beneficial of both spectrophotometry and fluorimetry are simple, rapid, nondestructive and suited to multicomponent analysis [8].

1.4.1 Chromogenic sensors

In 2005, Fabbrizzi, *et al.* synthesized compound **1** [9]. They found that the solution of **1** changed from green/yellow to purple in DMSO upon addition of various anions [10].



Figure 1.3 Compound **1** and the change in color of **1** in DMSO upon addition of various anions [10].

Later, the anion sensing properties of compound **1** were studied by UV-vis spectrophotometry. The color of a DMSO solution of **1** turned from yellow to red upon addition of F^- (Figure 1.4). Then, further addition of fluoride, up to ten equivalents, resulted in a blue color of the solution [9].



Figure 1.4 The changes in color (Left) and the changes in the absorption spectra (Right) of **1** upon addition of fluoride in DMSO [9].

1.4.2 Fluorogenic anion sensors

Transition processes between electronic state such as photon absorption, internal conversion, fluorescence, intersystem crossing, phosphorescence, delayed fluorescence and triplet-triplet transitions are presented in Figure 1.5. Singlet electronic state and triplet electronic state are represented in S and T symbols, respectively. The vibrational states are located between each electronic state [11].

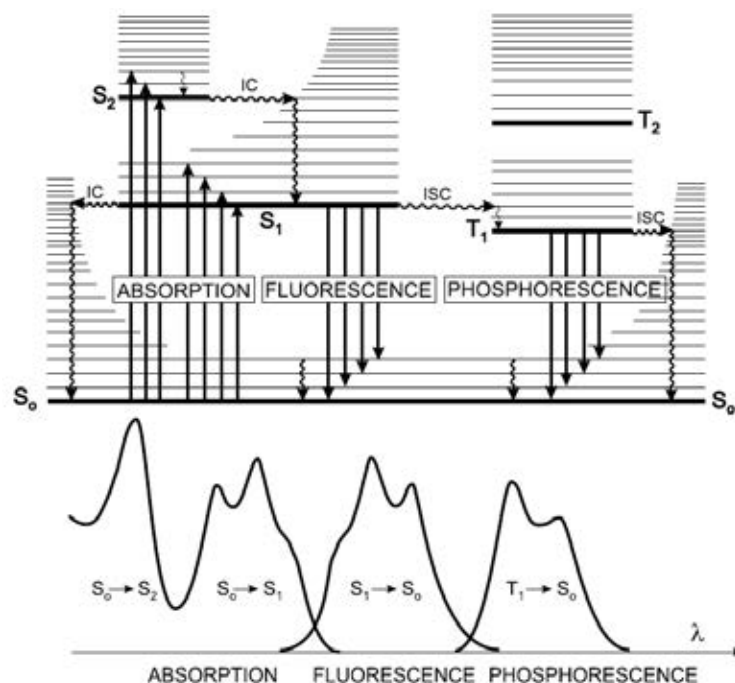


Figure 1.5 Perrin-Jablonski diagram and illustration of the relative positions of absorption, fluorescence and phosphorescence spectra.

Characteristic of fluorescence emission is started from transitions that involve the absorption of both $S_0 \rightarrow S_2$ and $S_0 \rightarrow S_1$ to pass internal conversion process and then, emission from $S_1 \rightarrow S_0$, so called fluorescence emission. However, the fluorescence spectrum is located at longer wavelengths (lower energy) than the absorption spectrum because of the energy loss in the excited state due to vibrational relaxation [11].

Moreover, fluorimetry is a higher sensitive technique up to 1000 times comparing to other spectrophotometry. Generally, fluorometric sensors for cations or anions contain two components: ionophore and fluorophore [12]. Ionophore is the selective binding site to substrate, while fluorophore gives signal when the ionophore binds the substrate. This may enhance or inhibit the fluorescence signal. The mechanism of the fluorophore that links with the substrate binding includes photoinduced electron transfer (PET), fluorescence resonance energy transfer (FRET), excimer/exciple formation or extinction, and photoinduced charge transfer (PCT) [13].

1.4.3 Excimer formation

Excimer is a complex between an excited fluorophore with another fluorophore in its ground state [11]. The first fluorophore is excited to the excited state. Therefore, the molecule becomes more polarization that affects interactions between aromatic rings involving a weak interaction as dipole- π and π - π interaction with another fluorophore in its ground state. As a result, the dimer form is more stable than the monomer form because the conjugation of the dimer form becomes more polarized than monomer form. This result suggests that the dimer form possesses a lower energy transition than that of the monomer form. Therefore, emission wavelength of the excimer is located at a longer wavelength than the monomer absorption, and it does not show vibronic bands as illustrated in Figure 1.6 [14-15]. The description of the photophysical species is collected in Table 1.1.

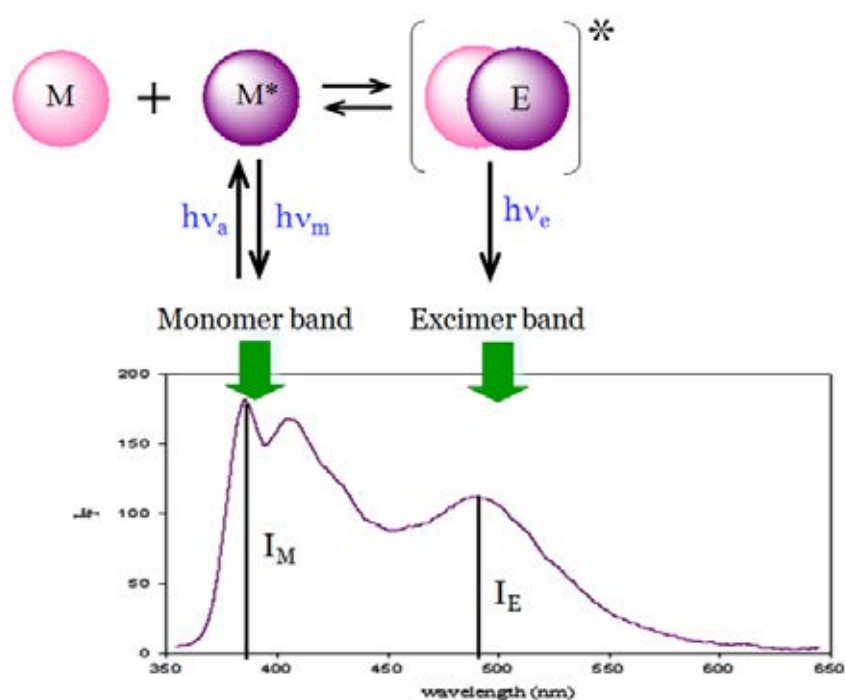


Figure 1.6 Excimer formation, with the corresponding monomer (400 nm) and excimer (500 nm) bands.

Table 1.1 Description of the photophysical species

Symbol	Description
M	Fluorophore in the ground state
M*	Monomer in the excited singlet state
E* or (MM)*	Excimer in the excited singlet state
$h\nu_a$	Photon energy absorption
$h\nu_m$	Photon energy of monomer emission
$h\nu_e$	Photon energy of excimer emission

CHAPTER II

LITERATURE REVIEWS AND OBJECTIVE OF THIS RESERCH

2.1 Literature reviews

2.1.1 Chromogenic fluoride sensors

Anions play an important role in chemical reactions, such as biological metabolisms or other processes [8]. Among anions, fluoride ion is of particular interest because of its role in dental caries and treatment of osteoporosis [16]. On the other hand, an overdose of fluoride anion can lead to fluorosis [17, 18], which is a type of fluoride toxicity to human health. Fluoride is found naturally at low concentration in drinking water and foods. Recently many sensors for detection of fluoride have been fabricated for using in environmental and biomedical research [19-22]. A chromogenic sensor is simple for users because changes in color can be detected by naked eyes.

In 2006, Ghosh *et al.* developed simple sensors **2** and **3** containing thiourea based coumarin for colorimetric and fluorescence sensing of benzoate and fluoride anions (Figure 2.1) [23]. Anion-binding properties of **2** and **3** were investigated by observing the changes in their fluorescence emission and absorption spectra in CH₃CN. Upon the addition of fluoride ion in solution of sensors **2**, the intensity of the absorption peak at 330 nm was remarkably reduced with a simultaneous growth of a new peak at 455 nm and the almost colorless solution turned yellow brown. In the case of benzoate, the absorption peak at 330 nm was shifted to 348 nm with a concomitant decrease in the intensity of the absorption and the solution turned light green. This reflected their binding constant values, which were measured by following the change in absorbance as a function of the concentration of the anions. It is clear that the association constants of both receptors for benzoate are greater than for fluoride ion. Fluoride ion, on the other hand, due to its small size and high charge density, initially forms a hydrogen bonded complex and then, in the presence of excess fluoride, causes deprotonation. Moreover, the selectivity of **2** with anions is

greater than **3**, due to the electron donating resonance effect of the phenyl group increases the charge density on the carboxylate group allowing it to form strong hydrogen bonds.

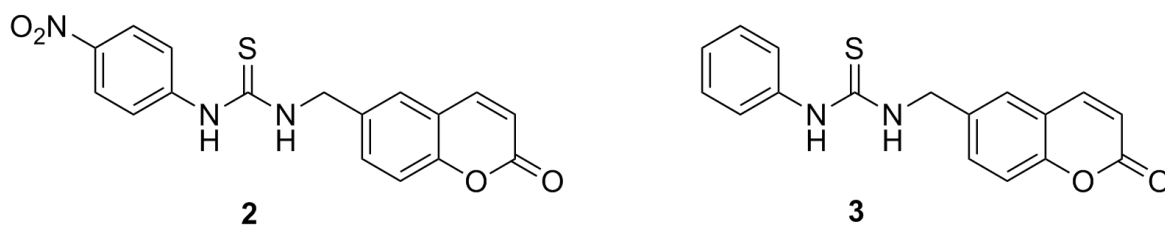
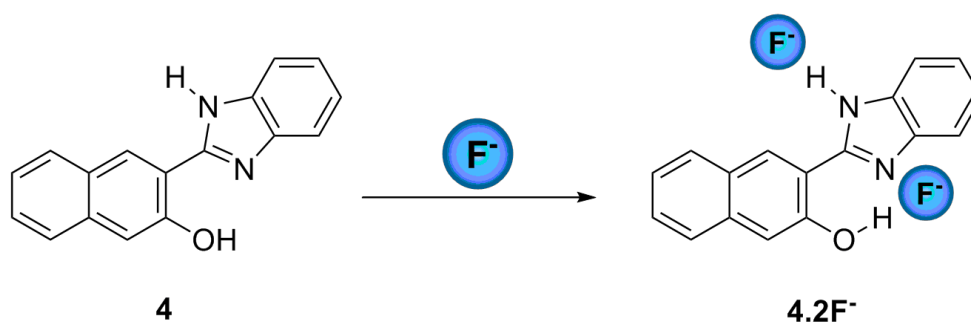


Figure 2.1 Structures of compounds **2** and **3**

In 2007, Kumar *et al.* reported compounds **4** and **5** containing naphthalene and binaphthalene for colorimetric and ratiometric fluorescence sensing of fluoride (Figure 2.2) [24]. Upon addition of fluoride, the appearance of a new absorption band between 400 and 440 nm in the case of **5** (but not in receptor **4**) resulted in a visible change in color from colorless to yellow. The spectral fitting of the absorbance data showed the formation of $L \cdot F_2$ in the case of **4**. With receptor **5**, a mixture of LF , LF_2 and LF_3 complexes was formed. The 1H NMR spectrum showed that for **4**, both the OH and NH protons formed H-bonding with fluoride simultaneously. However, in the case of **5**, at lower concentrations of fluoride ions the OH protons preferentially formed hydrogen bonding with fluoride and at higher concentrations of fluoride, stronger H-bonds between the benzimidazole NH and fluoride ions took place.



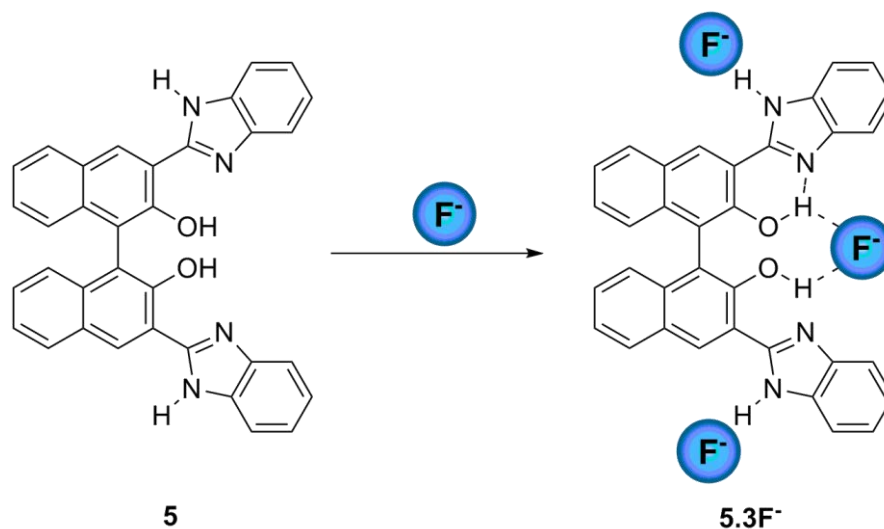


Figure 2.2 The proposed binding mode of compounds 4 and 5

In 2008, Chauhan *et al.* designed and synthesized new anion sensors **6** and **7** having urea/thiourea binding sites based on phenazine signaling unit (Figure 2.3) [25]. The receptors effectively and selectively recognized biologically important fluoride, acetate, and dihydrogenphosphate. However, fluoride interacted strongly with receptors **6** and **7** because of high electronegativity and small size compared to other halides. Moreover, colorimetric studies showed color changes of receptors **6** and **7** upon addition of fluoride which is due to hydrogen bonding interactions between fluoride ion and proton at N-H moieties of urea/thiourea. In addition, the color change of thiourea **7** was much more sensitive than that of the urea **6**. Upon addition of fluoride in DMSO, the characteristic absorption peaks of receptors **6** and **7** at 400 nm decreased gradually with a strong red shift and new peaks at 512 nm and 516 nm appeared in the spectrum. Association constants ($K_{\text{ass}}, \text{M}^{-1}$) of $\mathbf{6}\cdot\text{F}^-$ and $\mathbf{7}\cdot\text{F}^-$ were 5.6×10^4 and 9.1×10^5 , respectively. The result showed that fluoride bound more tightly with thiourea **7** than with urea **6**, indicating the formation of stronger hydrogen bonding interaction between the acidic N-H groups of thiourea **7** and fluoride.

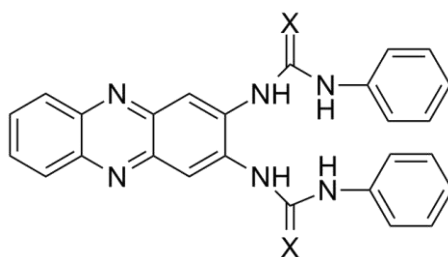


Figure 2.3 Structure of compounds **6** (X=O) and **7** (X=S)

In 2010, Tian *et al.* reported the colorimetric and a ratiometric red fluorescence for fluoride anion based on diketopyrrolopyrrole (DPP) compound **8** (Figure 2.4) [26]. When TBAF was added to the dichloromethane solution of **8**, an apparent color change from orange to purple in ambient light could be observed by the naked eye. On addition of fluoride, the absorption intensity at 497 nm was gradually decreased, and a large bathochromic shift (~ 80 nm) took place. The emission spectra also displayed a decrease of the emission at 563 nm and the emergence of a bathochromic emission band at 635 nm. From the result, a possible process for the ratiometric absorption changes is the intermolecular proton transfer (IPT) between the amide moiety and fluoride and its change from electronically neutral (Ar-DPP-NH-Ar) without a fluoride ion to negatively charged (Ar-DPP-N⁻-Ar) with a fluoride ion. In the presence of fluoride, the internal charge transfer (ICT) effect from the amide anion to the electron-withdrawing moiety was enhanced, which was facilitated by the deprotonation of the amide moiety. This enhancement in ICT effect also affords the reduced intensity and bathochromic shift of fluorescence as a function of fluoride concentration. ¹H NMR titrations confirmed the deprotonation of NH proton upon addition of fluoride.

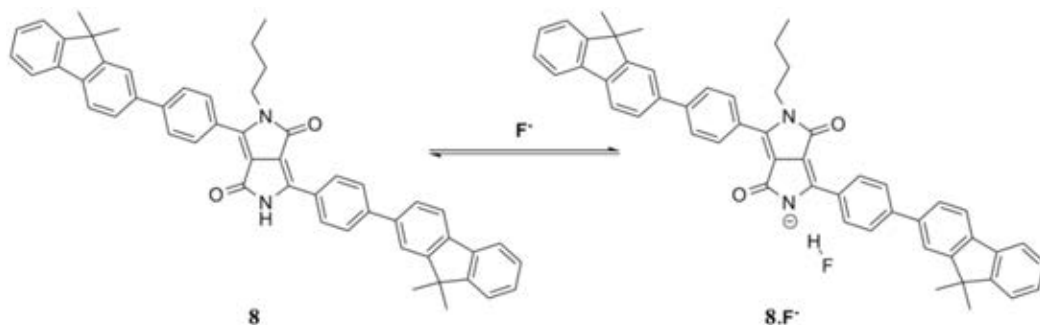


Figure 2.4 Intermolecular proton transfer between **8** and the fluoride ion

2.1.2 Fluorogenic fluoride sensors

Sensors based on anion-induced changes in fluorescence appear to be particularly attractive due to the simplicity and high detection limit of fluorescence. Particularly, fluoride is a biologically important anion because of its important role in dental care. In this regard, the fluorescent sensing of fluoride has attracted growing attention. In most cases, hydrogen bonding interactions between the N-H of urea, thiourea, amide, phenol, or pyrrole group and fluoride were used for recognition [27].

In 2004, Nam *et al.* synthesized chemosensor **9** based on a naphthalene urea derivative, which showed a unique fluorescence and absorption peak in the presence of fluoride (Figure 2.5) [28]. The absorption spectra of **9** displayed a red shift from 315 nm to 370 nm when addition of fluoride. The fluorescence study showed the same trend, that without the fluoride, the emission band appeared at 379 nm; while in the presence of 50 equiv of fluoride, the peak appeared at 448 nm. The interaction in **9**·F⁻ complex is the hydrogen bond interactions between fluoride and proton of the N-H moiety and the hydrogen at the aromatic ring. The ¹H NMR spectrum confirmed that in the presence of fluoride, two amide N-H signals disappeared rapidly and aromatic proton (H_a through H_f) signals shifted downfield or upfield due to the interactions between **9** and fluoride.

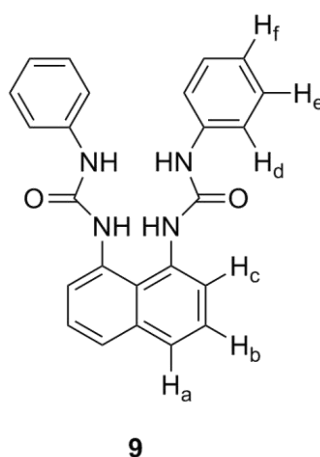


Figure 2.5 Structure of compound **9**

In 2006, Tian *et al.* designed and synthesized a novel fluoride ion-triggered dual fluorescence molecular switch based on naphthalimide (as energy donor: D) and

zinc-porphyrin (an energy acceptor: A) (**10**) in Figure 2.6 [29]. The fluorescence of the zinc porphyrin unit could be regulated “ON-OFF” on the excitation at 365 nm and “OFF-ON” on the excitation at 504 nm, respectively. When fluoride ion was added to the THF solution of **10**, a dramatic color change was observed from pale to dark orange. The Fluoride ion underwent hydrogen bonding interactions with NH proton at naphthalimide and deprotonation when more fluoride ions were added. The absorbance data showed absorption bands that were independent in the presence of fluoride. However, it depended on the extent intermolecular proton-transfer (IPT) in the amido nitrogen near the naphthalimide. Upon the addition of fluoride ion to **10**, the fluorescence intensity of the band at 608 nm was decreased at the excitation at 365 nm (“ON-Off”), while the excitation at 504 nm resulted in increasing intensity of the band at 608 nm (“Off-On”). There exist two competitive processes (PET and EET), but the changes in EET took responsibility for these dual changes in fluorescence spectra. When **10** was excited at 365 nm, EET gets weaker featured with the decreasing of absorption at 365 nm in the presence of F^- . Furthermore, with associated enhancement in the push-pull effect of the ICT transition, the photoinduced electron transfer from negatively charged naphthalimide ($[Naph]^-$) to the zinc porphyrin is also enhanced (“ON-Off”). In addition, EET turns over under the excitation at 504 nm (“Off-On”) (Figure 2.7).

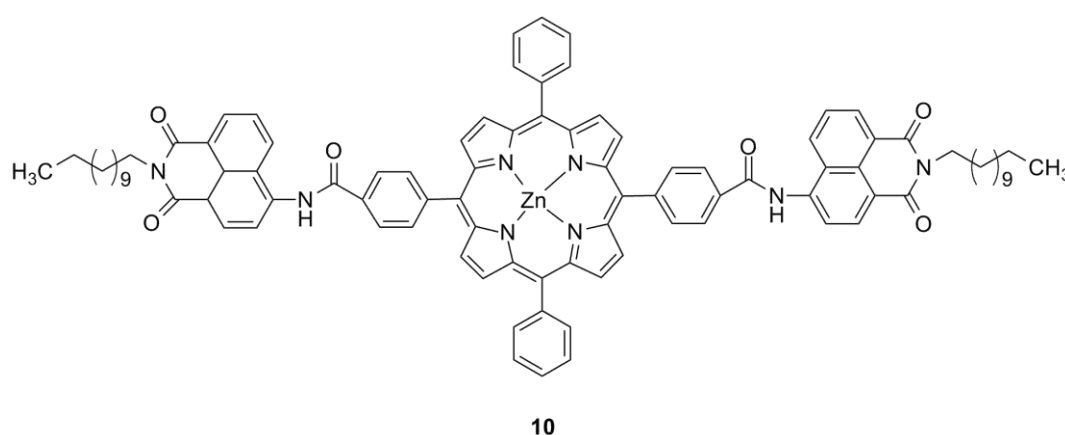


Figure 2.6 Structure of compound **10**

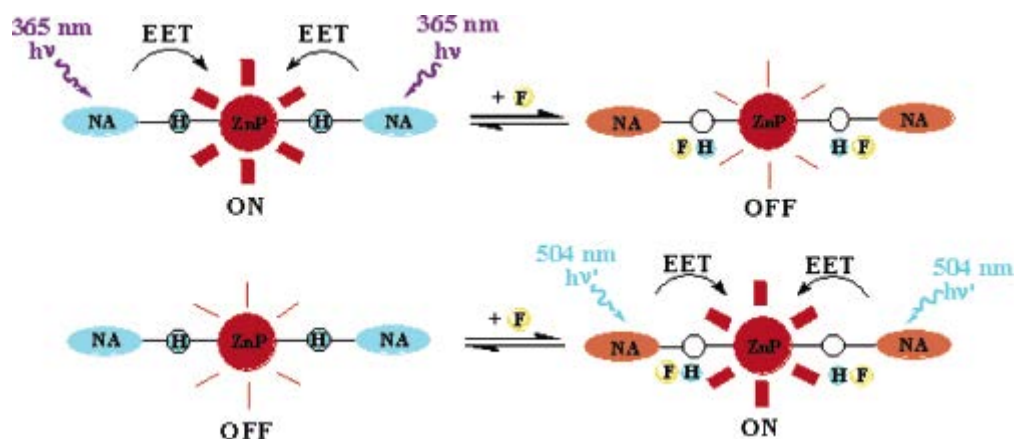


Figure 2.7 Schematic representation of the different emission for **10** in the presence of fluoride ion [29]

In 2006, Yoon *et al.* reported a new fluorescein derivative (**11**) containing a boronic acid group as a binding site (Figure 2.8) [27]. Since the fluorescein moiety was used as the fluorescent source, the emission changes can be monitored over 500 nm. Furthermore, off-on type fluorescence enhancement was observed by the blocking of the photoinduced electron transfer (PET) mechanism, which was induced by the interaction between fluoride and the boronic acid moiety. The fluorescence titration data displayed an intensity enhancement when the addition of fluoride ion was more than 3-folds. Upon the addition of fluoride, the fluoride ion interacted with the proton in the phenol moiety via hydrogen bonding. The phenolic hydrogen could make a strong hydrogen bond with fluoride as well as benzylic amine, which blocked the PET mechanism, resulting in fluorescence enhancement as proposed in Figure 2.8, which was confirmed by X-ray crystal structure.

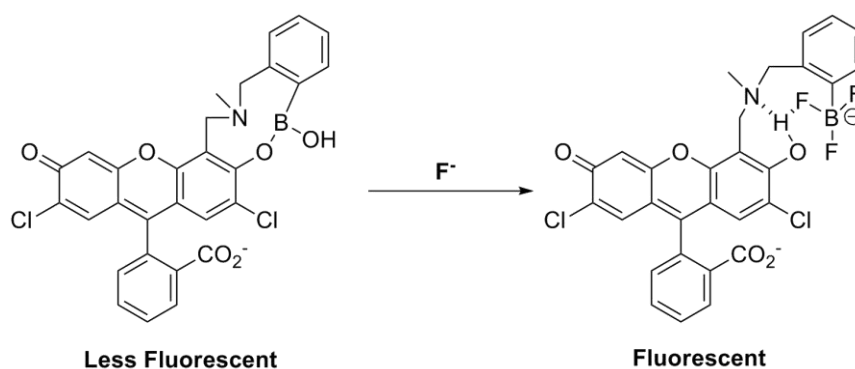


Figure 2.8 The proposed binding mechanism of compound **11** with fluoride

In 2007, Fang *et al.* synthesized compound **12**, containing the pyrrole recognition unit fused with the pyrene as fluorophore (Figure 2.9) [30]. Addition of fluoride to the solution of **12** caused a dramatic color change from greenish yellow to bright red, whereas other anions showed no apparent effect. The UV-vis absorption spectra displayed the vibronic peaks at 438 and 466 nm were significantly red-shifted upon fluoride titration, indicated that **12** underwent ground-state proton transfer in CH₃CN. The excitation at 440 nm led to the gradual growth of a new emission band maximized at 508 nm. Insufficient solubility of **12** in CD₃CN prohibited the ¹H NMR study. Thus, another compound that was soluble in CD₃CN and possessing functional similarity with **12** was synthesized. The deprotonation by fluoride in CH₃CN was confirmed by ¹H NMR studies.

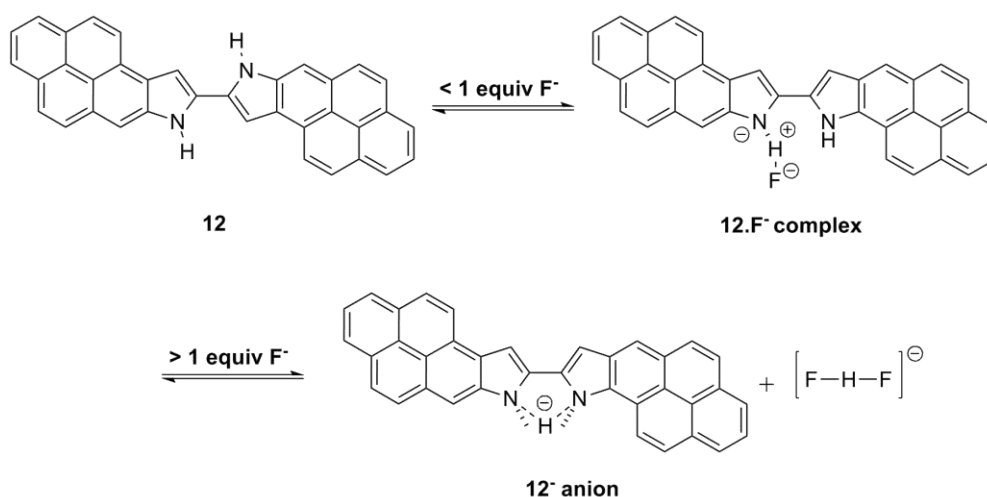


Figure 2.9 Proposed interaction modes of compound **12** with fluoride ion

In 2011, Kim *et al.* developed a novel colorimetric and ratiometric fluorescent sensor **13** for fluoride ion (Figure 2.10) [31]. When excess fluoride ion was added to **13** in MeCN, the colorless solution turned jade-green, these were clearly recognizable by the naked eyes. At a lower fluoride concentration (<40 μM) the absorption band at 365 nm decreased and a new band with a shoulder at 487 nm appeared. It corresponded to the ¹H NMR spectrum when 3 equiv of fluoride was added to **13**. The N-H signal at 7.46 ppm disappeared, whereas other protons toward upfield. As the fluoride concentration was further increased (> 50 μM), the shoulder at 487 nm decreased and the absorption band at 425 nm increased, indicating that the fluoride

promoted cleavage of the silyl ether. In the emission studies, when fluoride was added to **13**, the emission intensity at 449 nm decreased and at 508 nm increased. Hence, the initial decrease in the fluorescence intensity could be the deprotonation of N-H bond of **13**. When the fluoride concentration was further increased, the deprotection of the silyl ether moiety and the fluorescence intensity at 508 nm increased.

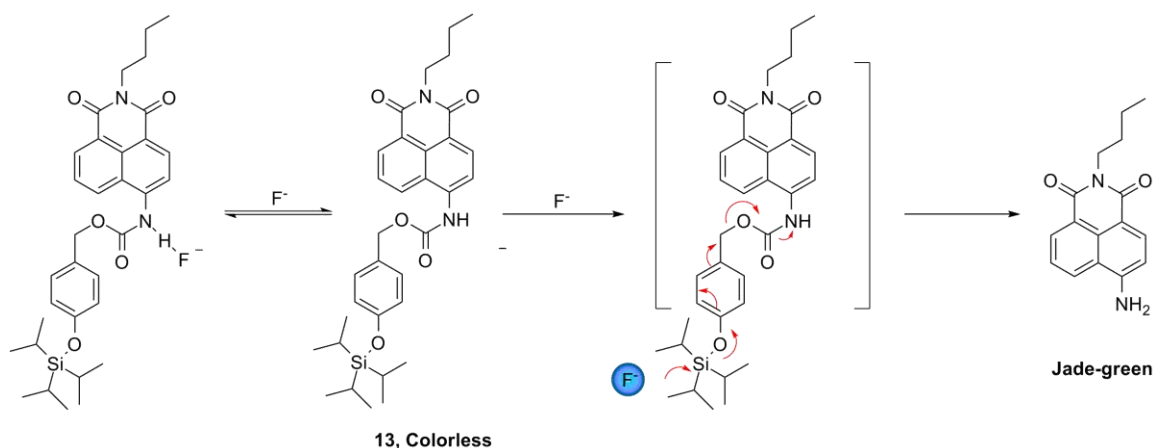


Figure 2.10 The possible mechanism for the spectroscopic changes of **13** in the presence of fluoride ion

2.1.3 Excimer emission

Pyrene is a popular fluorophore in fluorescence chemosensor. Furthermore, pyrene can induce excimer emission and more efficient fluorescence emission than other polyaromatic fluorophores. Two essential parameters are fluorescence intensity at monomer emission (I_M) and excimer emission (I_E). Relative intensity of I_E and I_M was used in case of pyrene linked with other systems as a sensing signal [32]

In 2006, Kim et al. developed anion sensing compounds **14** and **15** based on calix[4]arenes platform with 4-nitrophenylazo and pyrene moiety (Figure 2.11) [33]. In compound **14**, the -NH is directly connected to the pyrene moiety, while in compound **15**, there is an additional methylene spacer between -NH and pyrene. Upon addition of fluoride in the MeCN solution of compound **14**, the UV-vis spectra underwent a red shift by 54 nm, while in the case of compound **15** a bathochromically shifted band was observed at 614 nm. The red shift of **14**·F⁻ complexation could be explained by the photoinduced charge transfer (PCT). The PCT might have its origin

from the interaction between fluoride and the amide proton (-NH). However, the appearance of the peak at ~600 nm of compound **15** upon the fluoride complexation is related to the conversion of phenolic to phenolate forms. It should be noted that fluoride interacted with the amide protons of compound **14**, while it interacted with the phenolic protons of compound **15**. The addition of fluoride to the solution of compound **14** changed the characteristic excimer emission peak at 480 nm and formed a new emission peak at 460 nm, while compound **15** did not give such an excimer band. Notably, the main difference between compounds **14** and **15** was the elimination of methylene spacer between the pyrene moiety and amide group from **15** to form sensor **14**. Possibly, two pyrene moieties had an arrangement that were incapable of excimer formation in compound **15**. Theoretical calculations supported this regioselective binding of the fluoride, which was responsible for the different sensing characteristics displayed by **14** and **15**.

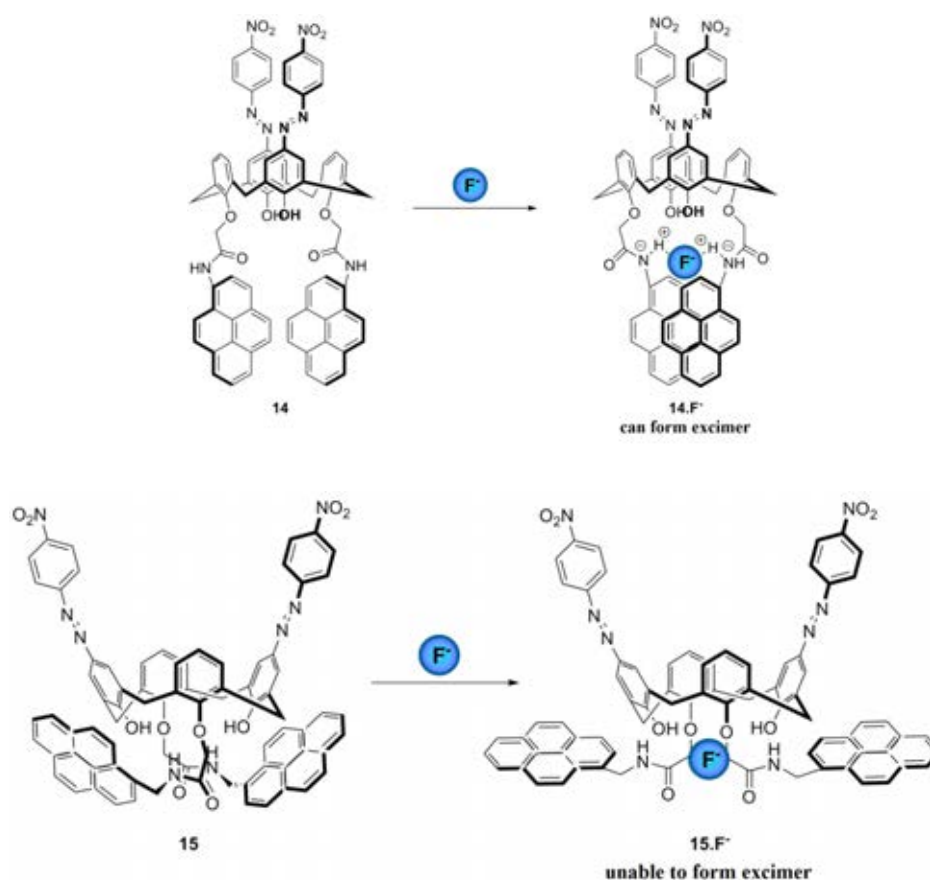


Figure 2.11 The proposed binding mode of compounds **14** and **15** upon addition of fluoride ion

In 2007, Gozin *et al.* synthesized chemosensor **16** and related macrocyclic chemosensor **17** (a model of the foled monomeric structure of **16**) (Figure 2.12) [34]. The molecular structure of chemosensor **16** formed a folded monomer (intramolecular excimer) and/or a dimer in the solution. Since the preferred configuration of the binding site of chemosensor **16** could not be easily determined by UV-vis or fluorescence spectroscopy measurements, anion-binding studies were used as a mapping tool to assess the preferred arrangement of the receptor of this chemosensor. There was a similar anion binding pattern for chemosensor **16** in both solvents, $\text{H}_2\text{PO}_4^- > \text{F}^- > \text{CH}_3\text{CO}_2^-$. This pattern could be explained by the size and shape of chemosensors and by the monoanions chemical structure and charge density. Specifically, the highest affinity of H_2PO_4^- toward chemosensor **16** was most probably due to the dihydrogenphosphate anion's geometry and its ability to form hydrogen bonds with more than one thiourea group. In contrast to chemosensor **16**, chemosensor **17** revealed different anion-binding patterns in chloroform and DMSO. The binding site of chemosensor **17** exhibited a preference toward smaller-size anions (F^- or CH_3CO_2^-), strongly suggested differences in the arrangement of the thiourea groups in the binding sites of these chemosensors. Thus, chemosensor **16** formed a dimer and not a folded excimer.

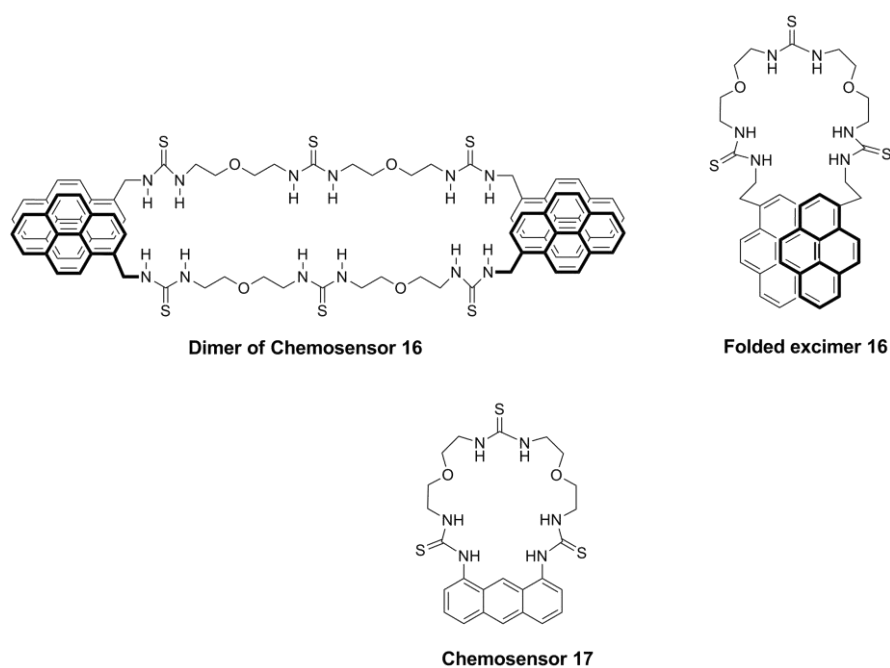


Figure 2.12 Structures of chemosensor **16-17** and their propose structures

In 2008, Kim *et al.* designed and synthesized compound **18** containing a pyrene unit linked with sulfonamide group as a sensor for copper ion (Figure 2.13) [35]. In the solution of **18** (CH₃CN/H₂O) displayed an absorption band at 342 nm, which was from the pyrene monomer. Addition of Cu(II) induced a band broadening and red-shift in the UV spectra, indicating the favored intermolecular π - π stacking dimerization of the two pyrene. Moreover, upon addition of Cu(II) ion, compound **18** gave a pyrene excimer emission at 455 nm and the pyrene monomer emission at 375 nm decreased concomitantly. The excimer emission, driven by formation of an intermolecular pyrene excimer upon copper ion binding to the sulfonamide group, was rationalized by experimental and theoretical DFT calculation results. These results showed the major binding mode in **18**·Cu²⁺ was the electrostatic interactions between Cu²⁺ and the electronegative nitrogen atoms in **18**, and the van der Waals interactions between the stacked pyrenes.

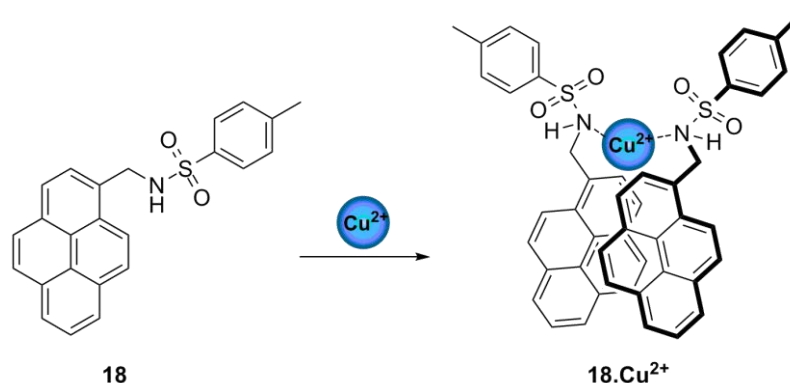


Figure 2.13 The proposed binding mode of compound **18** upon addition of Cu(II) ion

In 2009, Kim *et al.* reported the synthesis of new pyrene-derived Cu(II)-selective fluorescence sensor (Figure 2.14) [36]. Spacer lengths between the pyrene and quinolinylamide group of fluorogenic molecules **19-21** were varied ($n = 0, 1, 3$). Compound **22** were synthesized for comparing the binding mode of the 8-aminoquinoline nitrogen and carbonyl group to Cu(II) ion. Addition of Cu²⁺ to solution of **19** produced a new emission band at 460 nm with increasing intensity and provided a red shifted band in the UV-vis spectra. This attributed to the favorable intermolecular π - π stacking interactions of the two pyrenes in the ground state. The Job's plot showed the maximum point appears at the mole fraction of 0.65, close to

the typical ligand mole fraction (0.66) for a 2:1 ligand to metal complex. Upon addition of the Cu^{2+} ion, a solution of **22** gave negligible changes in the fluorescent spectra. From this result, it should be noted that both the quinoline host and pyrenylamide portions play an important role in selective binding to Cu(II) ion by a 2:1 complexation mode. The result from varying spacer length indicated that no methylene spacer between the pyrene and carbonyl unit of **19** optimized the intermolecular Py-Py* formation to show an intense static excimer band. The density functional theory calculations were executed for the energy minimized structures of **19-21** at the B3LYP/3-21G* level of theory. From calculations data indicated that, compound **19**, the H-bond is fairly weak due to the steric hindrance between the proximate pyrene groups. In the case of **20** and **21**, the stable hydrogen bonding between two amide groups was available to form stable dimers. Consequently, the binding energy for the dimer of **21** with two hydrogen bonds was highest. On the basis of this calculation, addition of the Cu^{2+} ion to the dimers of **20** and **21** disrupted the stable hydrogen bonding, which would perturb the stable electrostatic interactions between two monomer units which may be thermodynamically less favorable compared to the dimer of **19**.

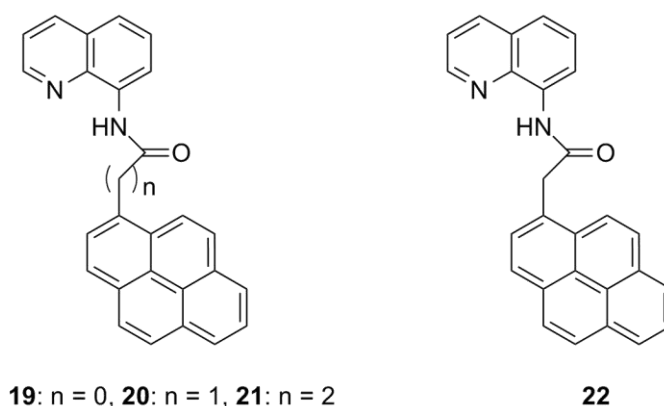


Figure 2.14 Structures of compounds **19-22**

In 2011, Tuntulani *et al.* synthesized new bispyrenyl thioureas linked by polyethylene glycol (PEG) chains, **23-25**, and methoxy benzene pyrene thiourea, **26** (Figure 2.15) [37]. The author have designed various chain lengths of polyethylene glycol (PEG), **23** > **24** > **25**, while **26** has not PEG chain. The emission intensity results showed a distinct pyrene excimer band of **23**, when fluoride was added in the

CHCl_3 solution of **23**, while **26** displayed the same intensity of both bands. The fluorescence titration spectra of **23** with fluoride ion displayed the fluorescence intensity enhancement of pyrene excimer band at 500 nm. These results suggested that the fluoride ion induced the formation of the π - π stacking interaction of pyrene resulting in the development of the excimer band. The Job's plot of **23** with fluoride displayed a maximum complexation at the mole fraction of 0.5 suggesting 1/1 or 2/2 complexation of **23** with fluoride. ^1H NMR spectrum supported that fluoride ion induced π - π stacking of the pyrene rings in the complex of $\mathbf{23}\cdot\text{F}^-$. Moreover, the relationship plot between the ratios of I_E/I_M of **23** in the presence of 100 equiv of fluoride ion with various concentrations of **23** were monitored. These results, showed that the fluorescence intensity ratios of excimer and monomer depended on the concentration of ligand, which gradually decreased in the concentration increased, suggested the pyrene stacking of $\mathbf{23}\cdot\text{F}^-$ complex proceeded via the intermolecular fashion. The binding constant from the titration study indicated that **23** possessing the longest podand chain showed the best binding ability and sensitivity toward fluoride ion while **26** showed the worst sensing and binding ability.

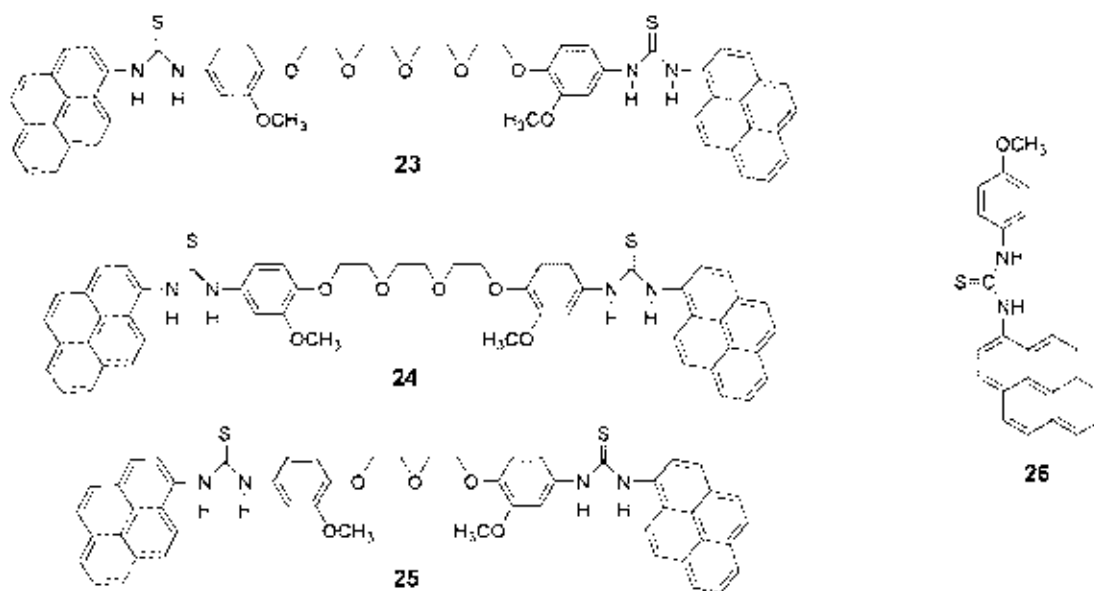


Figure 2.15 Structure of compounds **23**, **24**, **25**, and **26**

In 2006, Koshinen *et al.* introduced a molecular pincer based on a reversible metal chelation driven Salen-crown ether or compound **27** (Figure 2.16) [38]. The

pincer functionality and metal chelation ability of compound **27** was studied in MeOH/THF (1:1) solution by fluorescence spectroscopy. Without a chelated metal, compound **27** gave only weak fluorescence. However, when the solution was titrated with metal ions, an intense emission was observed at 475 nm. Upon addition of $\text{Zn}(\text{ClO}_4)_2$, the emission intensity increased until the concentration of ions reached 100 mol%. Moreover, the fluorescence intensity returned to the level of nonchelated **27** when 100 mol% of EDTA was added, which is known to trap transition metal ions. The ditopic chelation ability of **27** was studied by adding LiCl to the pincer- Zn^{2+} complex solution. The intensity dropped and then remained stable until 100 mol% because of Li^+ coordinating to the crown ether moiety, causing a disturbance in the pyrene excimer. Titration of **27** with LiCl indicated that the ditopic chelation is also possible with a single metal ion. Upon LiCl titration to **27**, the emission intensity increased linearly until 200 mol% of LiCl.

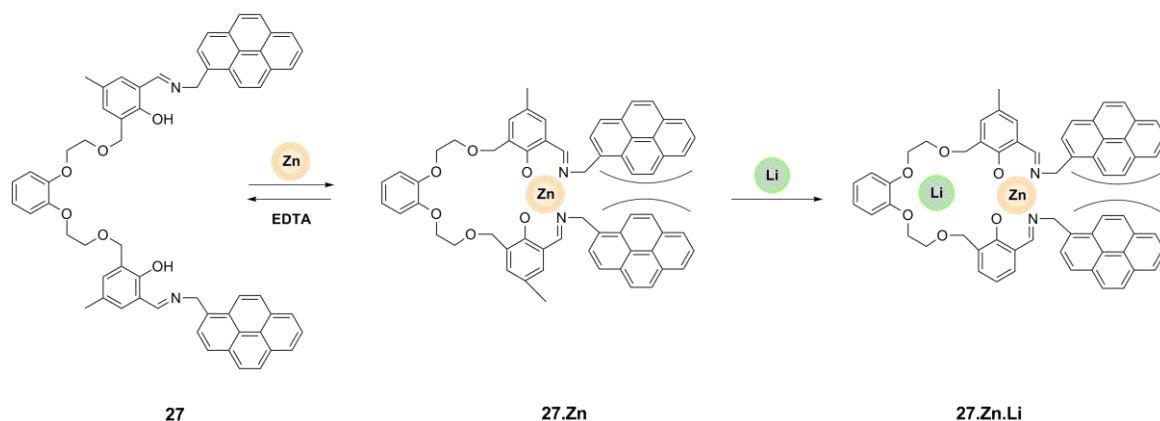


Figure 2.16 Structure of compound **27** and its metal chelation

In 2008, Wu *et al.* described the photodimerization of water-insoluble 2-naphthalene labeled poly (ethyl glycol) or **N-Pn-N** or compound **28** in cucurbit-[8]uril (**CB[8]**) aqueous solution (Figure 2.17) [39]. Cucurbit-[8]uril has a hydrophobic cavity and polar carbonyl groups surrounding the portals. Therefore, **CB[8]** can encapsulate hydrophobic or/and positively charged guest molecules in aqueous solution. **CB[8]** was able to accommodate two aromatic molecules such as naphthalene of **N-Pn-N** within the cavity forming a 1:1 complex, effected to intramolecular reaction of naphthalene of **N-Pn-N** (Figure 2.18). The interaction of **CB[8]** with **N-Pn-N** in aqueous solution was confirmed by UV-vis, fluorescence, and

^1H NMR spectroscopy. The fluorescence spectrum of **N-Pn-N** exhibited the monomer emission at 370 nm. The addition of **CB[8]** into **N-Pn-N** led to a growth of excimer emission at 430 nm. Furthermore, the ratio of fluorescence intensities of excimer to monomer was independent of the concentration used, suggesting that the excimer occurred intramolecularly (Figure 2.19).

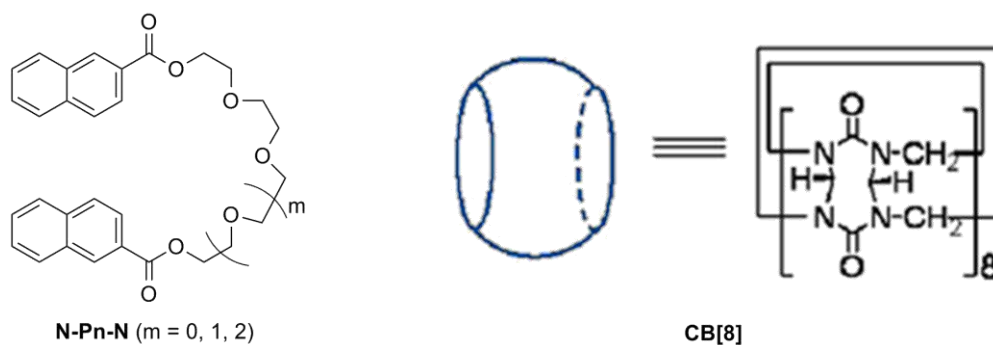


Figure 2.17 Structure of **N-Pn-N** or compound **28** and **CB[8]** [39]

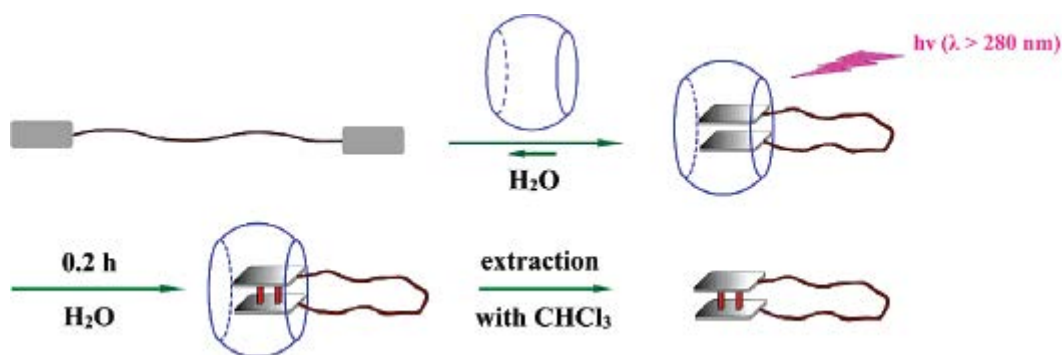


Figure 2.18 Cucurbit[8]uril-templated intramolecular photocycloaddition of **N-Pn-N** in aqueous solution [39]

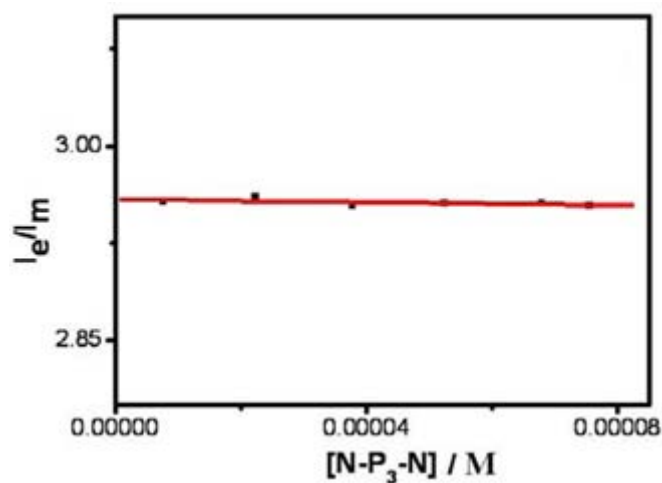


Figure 2.19 The concentration independent of I_e/I_m of **CB[8]** with various concentration of **N-Pn-N** (I_e : excimer intensity at 433 nm; I_m : monomer intensity at 373 nm) [39]

In 2010, Yao *et al.* synthesized a new pyrene-based derivative bearing an azadiene group as a ratiometric chemosensor for Hg^{2+} (**29**) (Figure 2.20) [40]. The absorption spectrum of **29** showed typical pyrene absorption bands at 238, 283, and 326 nm, along with a slightly low-energy band centered at 395 nm attributed to the imino bridge. Upon addition of Hg^{2+} ions, most significant changes were broadening of the absorption bands around 350-520 nm, and a new red-shifted band was formed at 442 nm. The formation of the new low-energy band may attribute to the interaction of Hg^{2+} ions with the imino nitrogens leading to the intramolecular charge transfer from the pyrene moieties to the imino groups. The fluorescence titration spectra of solution of **29** in $\text{CH}_3\text{CN}/\text{HEPES}$ upon addition of 10 equiv of Hg^{2+} showed the enhancement of fluorescence and a continuous red shift of the emission peak from 406 to 462 nm. ^1H NMR spectroscopy results suggest that Hg^{2+} coordinated to the imino unit of the Schiff base formed Hg-N bonding and that O atoms of ethermethylene forms Hg-O bonding, which forced the two pyrene moieties to fold. The conformational changes resulted in a switch from the weak pyrene monomer emission to the strong pyrene excimer emission.

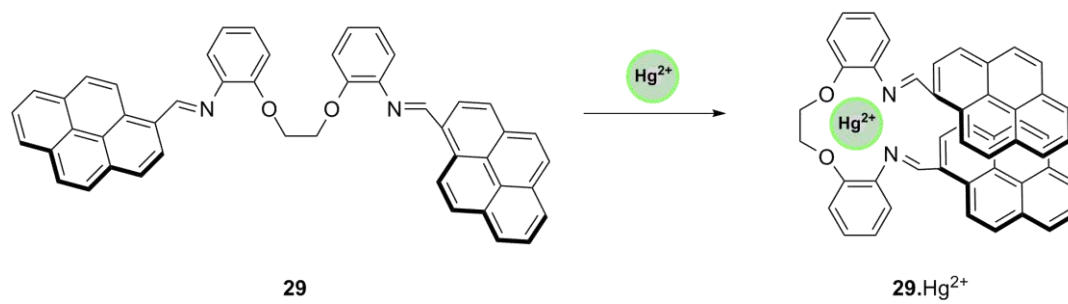


Figure 2.20 The Proposed binding mode of compound 29

2.2 Objective and scope of this research

2.2.1 Objective of this research

1. Synthesis of bispyrenyl urea linked with polyethylene glycol chains and ethyne for anion recognition.
2. Study the complexation between sensor molecules and anions by fluorescence spectrophotometry and ^1H NMR spectroscopy.

2.2.2 Scope of this research

Synthesis the target molecules, **L1**, **L2**, and **L3** (Figure 2.21) was carried out. **L1** contained benzyl amide like to pyrene unit. **L2** possessed ethylene glycol chains as spacers connecting two methoxy benzene and pyrene thiourea unit as sensing of an anion. While, **L3** is containing ethyne as spacer, that link with two pyrene urea groups. From different types of spacers in molecular structures of **L1**, **L2**, and **L3** that effect the rigidity of each molecule, it is interesting to study the abilities of these compounds towards anions.

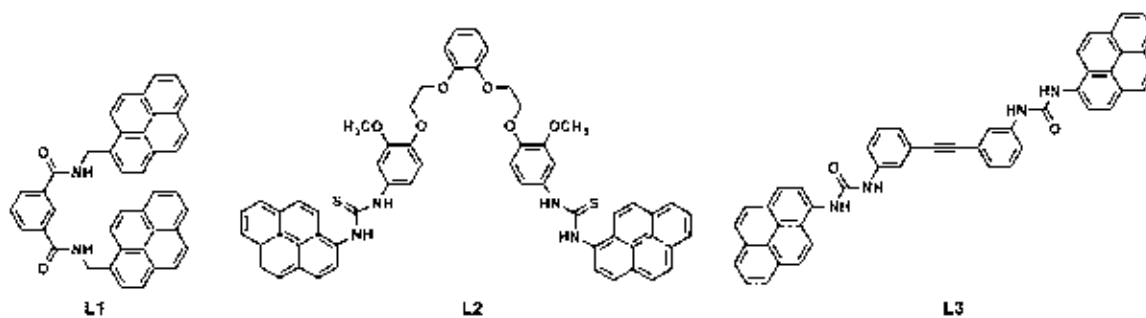


Figure 2.21 Structure of target molecules **L1**, **L2**, and **L3**

CHAPTER III

EXPERIMENTALS

3.1 General procedure

3.1.1 Analytical instruction

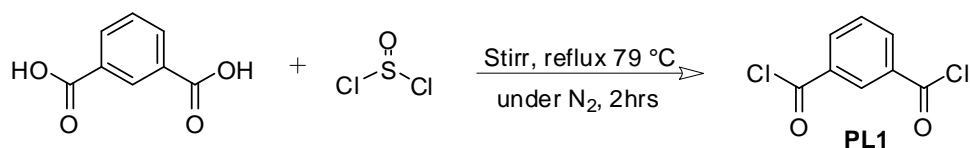
^1H NMR and ^{13}C NMR spectra were recorded by a Varian Mercury Plus 400 NMR spectrometry and Bruker UltrashieldTM Plus 400 NMR spectrometry. Fluorescence spectra were recorded using a Varian Cary Eclipse fluorescence spectrophotometer. UV-Vis spectra were recorded by a Varian Cary 50 UV-Vis spectrometer. d_6 -DMSO and CDCl_3 were used as solvent in ^1H NMR and ^{13}C NMR spectroscopy. All anion were used in the form of tetrabutylammonium salts. Binding constants between ligand and anions were obtained from SPECFIT 32 program.

3.1.2 Materials

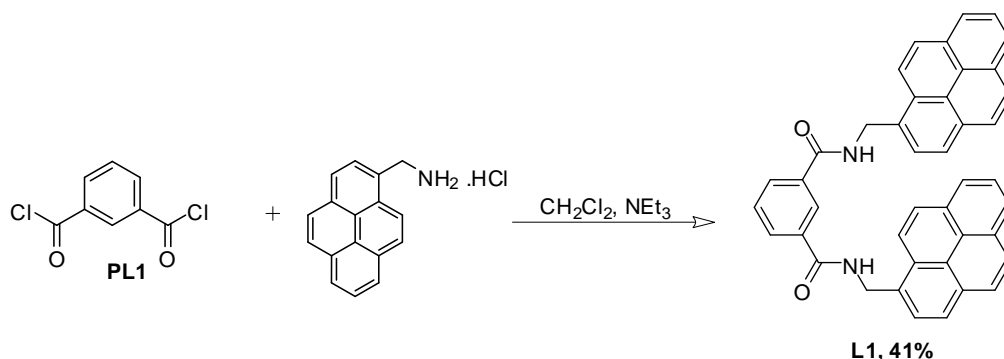
Compound **L1**, 1-pyrenemethylamine hydrochloride was obtained from Aldrich. Compound **L2**, 1-isothiocyanatopyrene was synthesized from the procedure reported previously [41]. All materials and reagents were standard analytical grade, and used without further purification. Commercial grade solvents, methanol, dichloromethane, ethyl acetate, were distilled before use. Column chromatography was carried out on silica gel (Kieselgel 60, 0.063-0.200 mm, Merck).

3.2 Synthesis

Compound L1



Isophthalic acid (0.10 g, 6.02×10^{-4} mol) was mixed with thionyl chloride (5 mL), stirred and refluxed at 79 °C under nitrogen atmosphere for 2 hours. The reaction was colorless solution. The solvent was then removed by a rotary evaporator. The product (compound **PL1**) was used in the next step without further purification.



The compound **PL1** was dissolved in CH_2Cl_2 (5 mL) and added dropwise to the mixture of 1-pyrenemethylamine hydrochloride (0.13 g, 4.83×10^{-4} mol) in CH_2Cl_2 (5 mL) and triethylamine (0.5 mL, 3.61×10^{-3} mol). The reaction was colorless. The solvent was subsequently removed by a rotary evaporator. The product was washed by H_2O and MeOH to give compound **L1** as white solid (0.0947 g, 41%).

Characterization data for compound L1.

^1H NMR spectrum (400 MHz, d_6 -DMSO): δ 9.37 (s, 2H), 8.51 (s, 1H), 8.48 (d, $J = 6$ Hz, 2H), 8.31-8.06 (m, 18H) 7.58 (t, $J = 8$ Hz, 1H), 5.23 (d, $J = 5.6$ Hz, 4H).

^{13}C NMR spectrum (100 MHz, d_6 -DMSO): δ 165.83, 134.55, 132.78, 130.76, 130.27, 130.07, 129.99, 128.45, 128.08, 127.55, 127.35, 127.00, 126.70, 126.54, 126.21, 125.22, 125.13, 124.67, 124.01, 123.91, 123.21, 41.09 ppm.

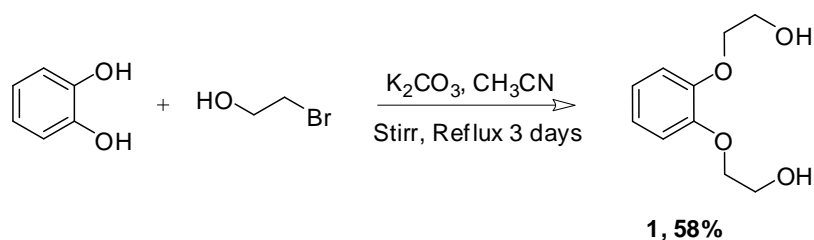
Elemental analysis:

Anal. Calcd for C₄₂H₂₈N₂O₂ C, 85.11; H, 4.76; N 4.73

Found C, 85.20; H, 5.11; N 4.71

ESI-MS (m/z): calcd 594.23, found 593.22.

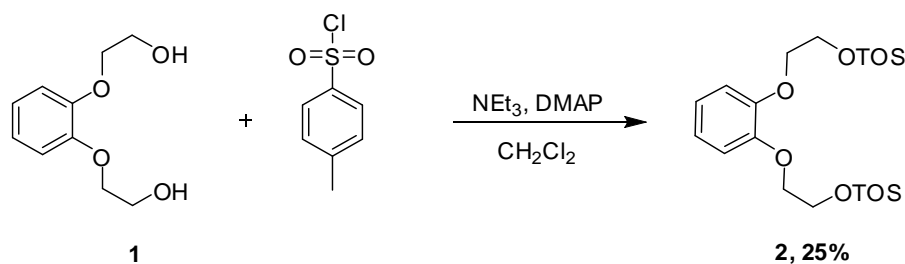
IR (KBr): 1634 (ν_{sym.} CO) cm⁻¹.

Compound L2

Compound 1. The mixture of pyrocatechol (1.0 g, 9.08 mmol), bromoethanol (4.0 mL, 5.67x10⁻² mol), K₂CO₃ (12.55 g, 9.10x10⁻² mol), and CH₃CN (100 mL) was stirred and refluxed at 79 °C under nitrogen atmosphere for 3 days, the reaction was brown solution. After that, the solvent was removed by a rotary evaporator and the pH was adjusted to 1 by 3M HCl. The residue was extracted with CH₂Cl₂ and H₂O. The organic phase was isolated and dried over anhydrous Na₂SO₄. The solvent was removed to give compound **1** as brown oil (1.050 g, 58%).

Characterization data for compound 1.

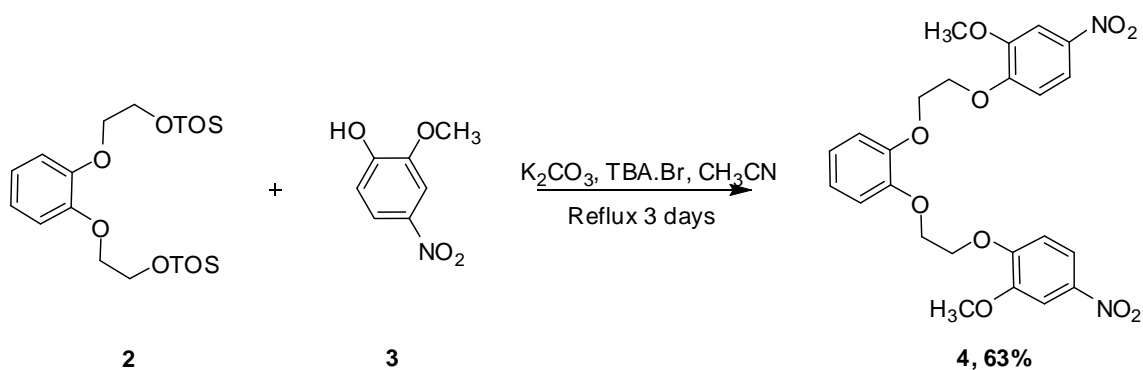
¹H NMR spectrum (400 MHz, CDCl₃): δ 6.98-6.79 (m, 4H), 4.11 (q, *J* = 4.4 Hz, 4H), 3.96 (td, *J* = 4.4 Hz, 4H), 2.58 (s, 2H).



Compound **2**. Compound **1** (0.153 g, 7.72×10^{-4} mol), triethylamine (1.08 mL, 7.75×10^{-3} mol), DMAP (1/3 spoon) were dissolved in CH_2Cl_2 (20 mL). The mixture was stirred at room temperature under nitrogen. The reaction was stirred at 0°C under N_2 for 15 minutes. Then, TsCl (0.221 g, 1.16×10^{-3} mol) in CH_2Cl_2 (10 mL) was added dropwise to the reaction at 0°C and keep stirring at room temperature for 3 days. Then, the pH was adjusted to pH 1 by adding 3M HCl and the mixture was extracted with CH_2Cl_2 and H_2O . The organic phase was isolated and dried over anhydrous Na_2SO_4 . The solvent was removed. The crude was purified by column chromatography with CH_2Cl_2 : EtOAc (9:1) as eluent to give the product as colorless oil (0.096 g, 25 %)

Characterization data for compound **2**.

^1H NMR spectrum (400 MHz, CDCl_3): δ 7.79 (d, $J = 8.4$ Hz, 4H), 7.33 (d, $J = 8$ Hz, 4H), 6.90 (q, 2H), 6.80 (q, 2H), 4.32 (t, $J = 4.8$ Hz, 4H), 4.15 (t, $J = 4.8$ Hz, 4H), 2.434 (s, 6H).

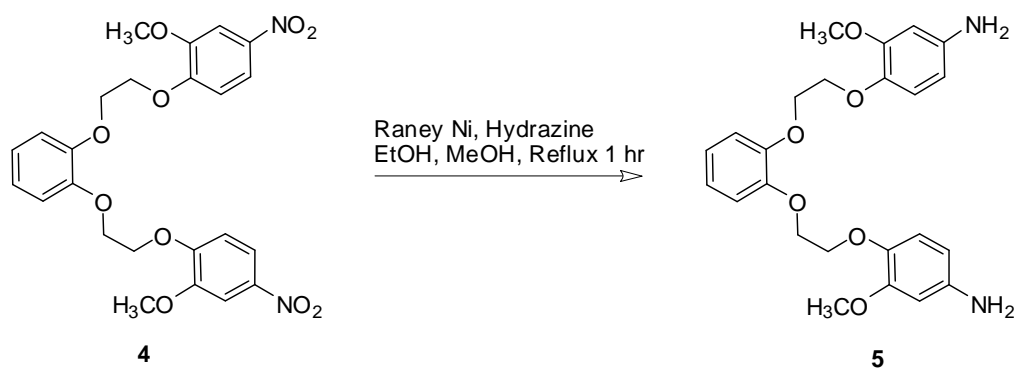


Compound **4**. The mixture of compound **2** (0.075 g, 1.48×10^{-4} mol), compound **3** [37] (0.05 g, 2.96×10^{-4} mol), K_2CO_3 (0.205 g, 1.48×10^{-3} mol), tetrabutylammonium bromide (1/3 spoon), and CH_3CN (50 mL) was stirred and refluxed for 3 days. Then, the solvent was removed by a rotary evaporator and the pH was adjusted to 1 by 3M HCl. The residue was extracted with CH_2Cl_2 and H_2O . The organic phase was isolated and dried over anhydrous Na_2SO_4 . The solvent was removed, and MeOH and CH_2Cl_2 was added to precipitate compound **4** (0.041 g, 63 %).

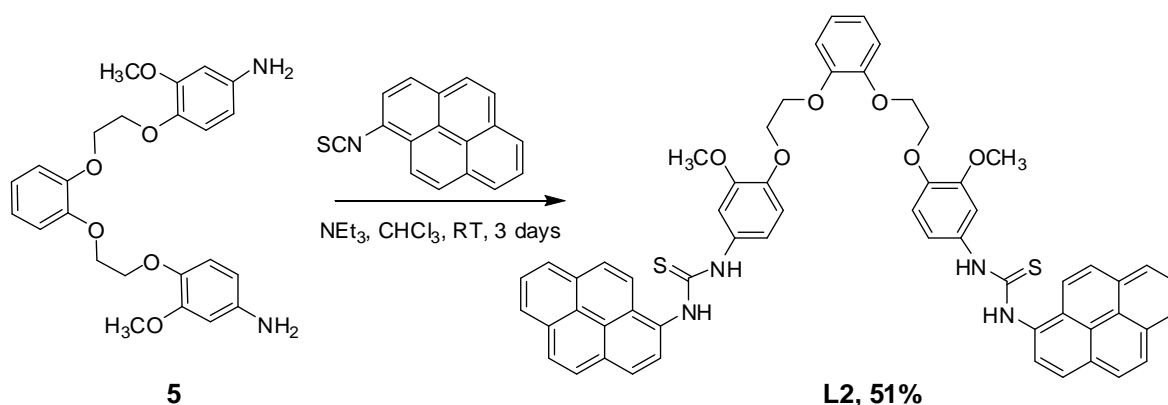
Characterization data for compound **4**.

1H NMR spectrum (400 MHz, $CDCl_3$): δ 7.85 (d, $J = 8.8$ Hz, 2H), 7.72 (s, 2H), 7.01 (m, 6H), 4.44 (d, $J = 7.2$ Hz, 8H), 3.91 (s, 6H).

^{13}C NMR spectrum (100 MHz, $CDCl_3$): δ 149.25, 148.774, 141.811, 122.38, 117.57, 115.60, 111.83, 106.87, 68.17, 67.98, 56.26, 29.71 ppm



Compound **5** [37]. The mixture of compound **4** (0.025 g, 5.68×10^{-5} mol) in CH_3OH (1.25 mL) and EtOAc (5 mL) was stirred under nitrogen. Then, Raney Ni (1/4 spoon) and hydrazine (0.5 mL) were added and reflux for 1 hour. Raney Ni was removed by filtration and the solvent was removed by a rotary evaporator. The crude was extracted with CH_2Cl_2 and H_2O . The organic phase was isolated and dried over anhydrous Na_2SO_4 . The solvent was removed, and the product was used in the next step without further purification.



Compound **L2**. The mixture of compound **5** (5.68×10^{-5} mol) in CHCl_3 (10 mL) and triethylamine (0.06 mL, 4.33×10^{-4} mol) was stirred under nitrogen at room temperature for 30 min. Then, 1-isothiocyanatopyrene (0.037 g, 1.43×10^{-4} mol) in CHCl_3 (10 mL) was added dropwise and the reaction was stirred under nitrogen at room temperature for 3 days. The reaction was extracted with CH_2Cl_2 and H_2O . The organic phase was isolated and dried over anhydrous Na_2SO_4 . The solvent was removed and CH_2Cl_2 and CH_3OH was added to precipitate compound **L2** as yellow solid (0.028, 51%).

Characterization data for compound **L2**.

^1H NMR spectrum (400 MHz, d_6 -DMSO): δ 10.05 (s, 2H), 9.72 (s, 2H), 8.29-8.02 (m, 18H), 7.17 (s, 2H), 7.05 (d, $J = 3.8$ Hz, 2H), 7.04-6.95 (m, 4H), 6.92 (t, $J = 3$ Hz, 2H), 4.29 (dd, $J_1 = 16$ Hz, $J_2 = 4$ Hz, 4H), 4.25 (dd, $J_1 = 16$ Hz, $J_2 = 4$ Hz, 4H), 3.70 (s, 6H).

^{13}C NMR spectrum (100 MHz, d_6 -DMSO): δ 181.23, 148.58, 148.20, 145.22, 133.11, 132.81, 130.55, 130.37, 129.16, 127.26, 127.08, 126.92, 126.62, 126.37, 126.27, 125.24, 125.02, 124.77, 124.37, 123.74, 122.64, 121.40, 116.75, 114.67, 113.36, 109.79, 67.50, 67.46, 55.46 ppm.

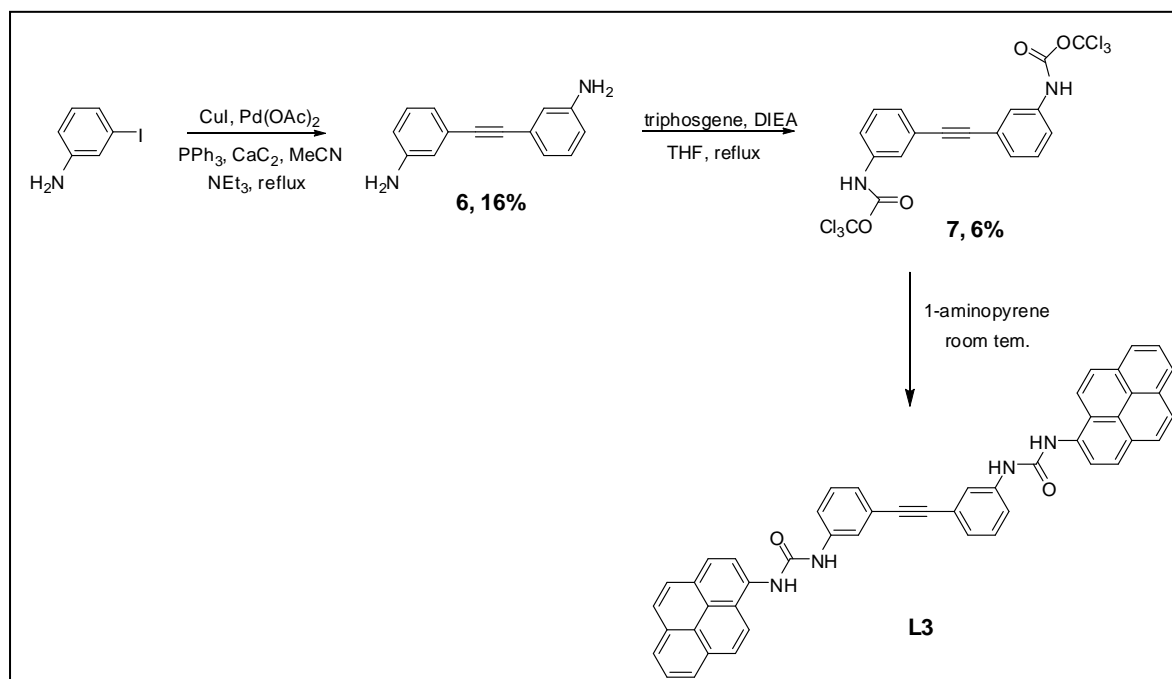
Elemental analysis:

Anal. Calcd for $C_{58}H_{46}N_4O_6S_2$ C, 72.63; H, 4.83; N 5.84

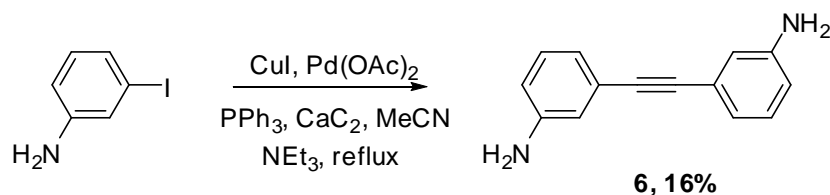
Found C, 72.70; H, 5.06; N 5.79

ESI-MS (m/z): calcd 959.14, found 959.28.

IR (KBr): 3221.74 ($\nu_{\text{sym.}}\text{-NH}$) cm^{-1} , 3056.31, 2923.50, 2846.60 ($\nu_{\text{sym.}}\text{-C=C-H}$), 2156.52 ($\nu_{\text{sym.}}\text{-C=C}$), 1500 ($\nu_{\text{sym.}}\text{-C=S}$).

Compound L3**Method 1**

Scheme 3.1 Synthesis pathway of compound **L3** in method 1



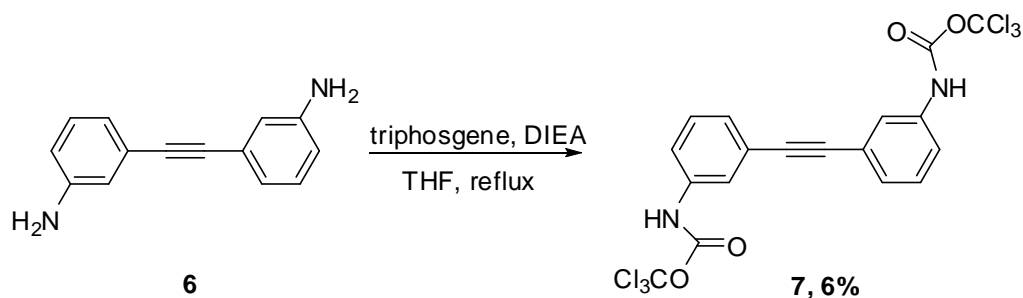
Compound **6** was synthesized using the published method [42]. The mixture of copper iodide (0.017 g, 1.142×10^{-4} mol), palladium (II) acetate (0.010 g, 4.567×10^{-5} mol), and triphenyl phosphine (0.024 g, 9.135×10^{-5} mol) in CH_3CN was stirred and refluxed for 15 mins. Then, triethylamine (0.379 mL, 2.740×10^{-3} mol), 3-iodoaniline (0.2 g, 9.135×10^{-4} mol), and calcium carbide (0.176 g, 2.740×10^{-3} mol) were added and refluxed for 1 day. The reaction was filtered and the solvent was removed by a rotary evaporator. The orange oil was purified by 2% EtOAc in CH_2Cl_2 to give compound **6** as yellow oil (0.03 g, 16%).

Characterization data for compound **6**.

^1H NMR spectrum (400 MHz, $\text{d}_6\text{-DMSO}$): δ 7.12 (t, $J = 8$ Hz, 2H), 6.92 (dd, $J_1 = 0.8$ Hz, $J_2 = 0.8$ Hz, 2H), 6.84 (s, 2H), 6.66 (t, $J = 1$ Hz, 1H), 6.64 (t, $J = 1$ Hz, 1H), 3.61 (s, 4H).

^{13}C NMR spectrum (100 MHz, $\text{d}_6\text{-DMSO}$): δ 146.30, 129.28, 124.05, 122.10, 117.86, 115.57, 115.31, 89.06, 29.71 ppm.

MALDI-TOF (m/z): calcd 208.10, found 208.20.

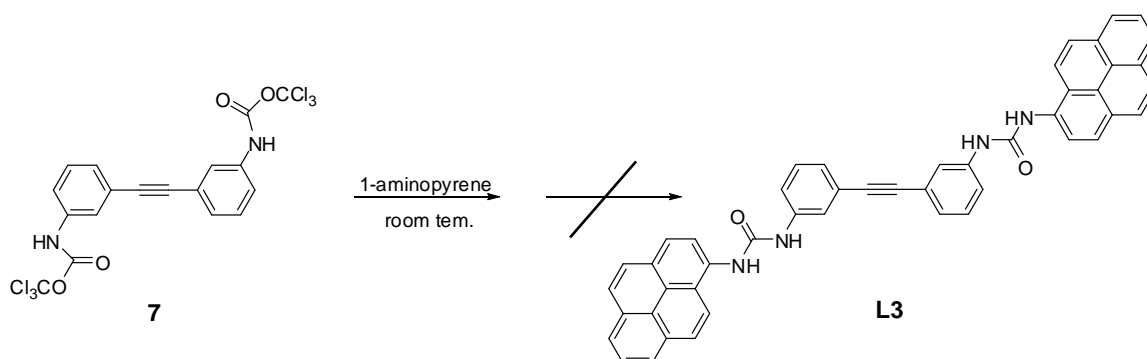


Compound **7** was synthesized using the published method [43]. In a solution of compound **6** (0.724 g, 3.48×10^{-3} mol) and diisopropylethylamine, DIEA, (3.031 mL, 0.017 mol) in THF, triphosgene (4.132 g, 0.014 mol) in THF was dropwised at 0 °C under nitrogen. The mixture was stirred at room temperature overnight. The reaction was filtered and the solvent was removed by a rotary evaporator. The residue was chromatographed on a silica gel column (dichloromethane or chloroform as an eluent) to give compound **7** (0.110 g, 6%).

Characterization data for compound **7**.

^1H NMR spectrum (400 MHz, d_6 -DMSO): δ 9.808 (s, 2H), 7.651 (s, 2H), 7.482 (d, $J = 8$ Hz, 2H), 7.330 (t, $J = 8$ Hz, 2H), 7.174 (d, $J = 7.6$ Hz, 2H).

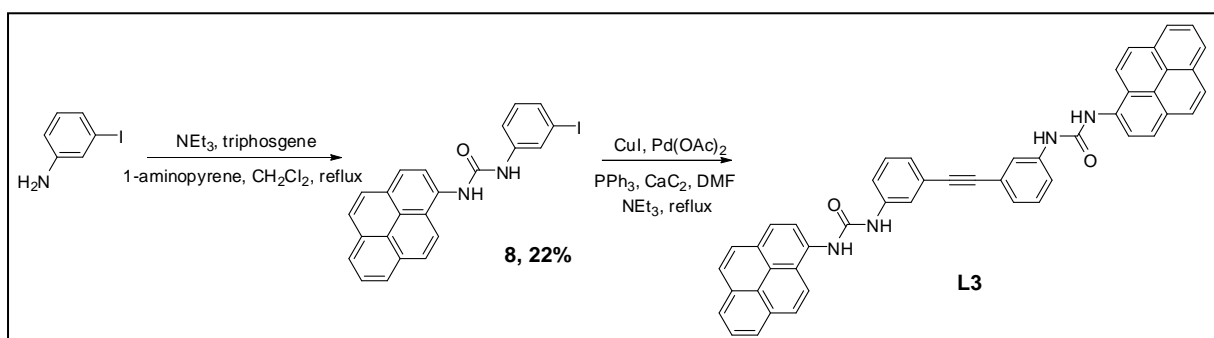
^{13}C NMR spectrum (100 MHz, d_6 -DMSO): δ 153.94, 153.49, 140.00, 139.48, 129.28, 125.33, 122.44, 120.52, 118.65, 89.13, 88.95 ppm.



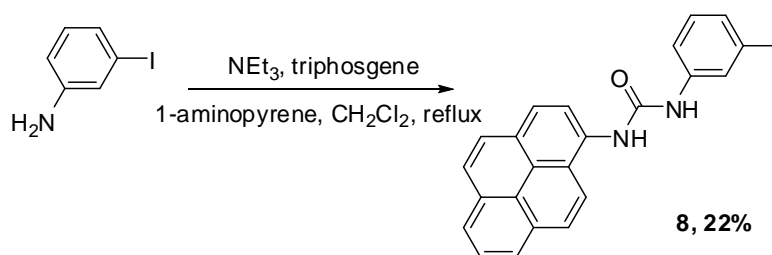
Compound **L3** [43]. A mixture of compound **7** (0.108 g, 2.034×10^{-4} mol) and 1-aminopyrene (0.132 g, 6.101×10^{-4} mol) in THF was stirred at room temperature overnight. The solvent was removed by a rotary evaporator. The residue was

chromatographed on silica gel (in CH_2Cl_2 as an eluent) to give a yellow solid (0.104 g). The characterization results suggested a yellow solid was 1-aminopyrene (the starting material)

Method 2



Scheme 3.2 Synthesis pathway of compound **L3** in method 2



Compound **8**. The mixture of 3-iodoaniline (0.1 g, 4.567×10^{-4} mol) and triethylamine (0.18 mL, 1.370×10^{-3} mol) in CH_2Cl_2 was stirred and refluxed under nitrogen for 30 mins. Then, triphosgene (0.27 g, 9.135×10^{-4} mol) was added. The reaction was stirred and refluxed for 3 hours. Then, the mixture of 1-aminopyrene (0.198 g, 9.135×10^{-4} mol) and triethylamine (0.379 mL, 2.740×10^{-3} mol) was added. The reaction was stirred and refluxed for 2 days. The reaction was filtered and MeOH was added to precipitate a green solid of compound **8** (0.05g, 22%).

3.3 Complexation studies

Compounds **L1** and **L2** containing pyrene as fluorophore, therefore function of spectrofluorometry were excited at 340 nm and the emission spectra were recorded at 360-700 nm.

3.3.1 Fluorescence studies

3.3.1.1 Anion binding study.

Anion binding abilities of two ligands were studied by using tetrabutylammonium (TBA) salts of anions in DMSO solution. The TBA salts of anions F^- , Cl^- , Br^- , I^- , OAc^- , BzO^- , $H_2PO_4^-$, and OH^- were used as anions. Concentration of **L1** was prepared at 2×10^{-6} M and concentration of anions were prepared at 10^{-2} M. In the case of **L2**, was prepared at 5×10^{-6} M and concentration of anions were prepared at 8×10^{-3} M. In an anion binding study, adding 1000 equiv. of anions into a solution of ligand **L1** and 50 equiv. of anions into a solution of ligand **L2** were using in spectrofluorometry.

3.3.1.2 Complexation studies of compounds **L1** and **L2** with anions.

Solution of compound **L1** (2×10^{-6} M) and **L2** (1×10^{-5} M) were prepared 10 mL in volumetric flask and 2 mL of each was added to a 1 cm path length quartz cuvette. The solution of anions, 2×10^{-3} M and 8×10^{-3} M, for compounds **L1** and **L2**, respectively, were prepared in 10 mL volumetric flask and added into 2 mL of ligand using microburette and microsyringe. Addition of anions to compound **L1** was carried out according to Table 3.1. In the case of **L2**, volumetric scale of each anion (fluoride, acetate, and hydroxide) was prepared according to Tables 3.2, 3.3, and 3.4, respectively. Emission spectra of each addition were measured after the mixture was stirred for 3 min.

A binding constant (K_{ass} , M^{-1}) was calculated from fluorescence titration data using SPECFIT 32 program.

Table 3.1 The scale ratio between **L1** (2×10^{-6} M) with anions (2×10^{-3} M) were used to fluorescence titration method

Point	V of anions (μL)	V total of anions (μL)	V total (mL)	anions / L1
1	0	0	2.000	0
2	10	10	2.010	5
3	10	20	2.020	10
4	10	30	2.030	15
5	10	40	2.040	20
6	10	50	2.050	25
7	10	60	2.060	30
8	10	70	2.070	35
9	10	80	2.080	40
10	10	90	2.090	45
11	10	100	2.100	50
12	40	140	2.140	70
13	40	180	2.180	90
14	40	220	2.220	110

Table 3.1 The scale ratio between **L1** (2×10^{-6} M) with anions (2×10^{-3} M) were used to fluorescence titration method (continued)

Point	V of anions (μL)	V total of anions (μL)	V total (mL)	anions / L1
15	40	260	2.260	130
16	40	300	2.300	150
17	80	380	2.380	190
18	80	460	2.460	230
19	80	540	2.540	270
20	80	620	2.620	310
21	80	700	2.700	350
22	100	800	2.800	400
23	100	900	2.900	450
24	100	1000	3.000	500
25	100	1100	3.100	550
26	100	1200	3.200	600
27	100	1300	3.300	650
28	100	1400	3.400	700

Table 3.2 The scale ratio between **L2** (1×10^{-5} M) with fluoride ion were used to fluorescence titration method

Point	V of F^- (μ L)	V total of F^- (μ L)	V total (mL)	$F^-/L2$
1	0.0	0.0	2.0000	0.0
2	0.5	0.5	2.0005	0.2
3	0.5	1.0	2.0010	0.4
4	0.5	1.5	2.0015	0.6
5	0.5	2.0	2.0020	0.8
6	0.5	2.5	2.0025	1.0
7	0.5	3.0	2.0030	1.2
8	0.5	3.5	2.0035	1.4
9	0.5	4.0	2.0040	1.6
10	0.5	4.5	2.0045	1.8
11	0.5	5.0	2.0050	2.0
12	0.5	5.5	2.0055	2.2
13	0.5	6.0	2.0060	2.4
14	0.5	6.5	2.0065	2.6
15	0.5	7.0	2.0070	2.8
16	0.5	7.5	2.0075	3.0
17	5.0	12.5	2.0125	5.0
18	5.0	17.5	2.0175	7.0

Table 3.2 The scale ratio between **L2** (1×10^{-5} M) with fluoride ion were used to fluorescence titration method (continued)

Point	V of F^- (μ L)	V total of F^- (μ L)	V total (mL)	$F^-/L2$
19	5.0	22.5	2.0225	9.0
20	5.0	27.5	2.0275	11
21	5.0	32.5	2.0325	13
22	5.0	37.5	2.0375	15
23	5.0	42.5	2.0425	17
24	5.0	47.5	2.0475	19
25	10.0	57.5	2.0575	23
26	10.0	67.5	2.0675	27
27	10.0	77.5	2.0775	31
28	10.0	87.5	2.0875	35
29	10.0	97.5	2.0975	39
30	10.0	107.5	2.1075	47
31	20.0	127.5	2.1275	55
32	20.0	147.5	2.1475	63
33	20.0	167.5	2.1675	71
34	50.0	217.5	2.2175	91
35	50.0	267.5	2.2675	111
36	50.0	317.5	2.3175	131
37	50.0	367.5	2.3675	151

Table 3.2 The scale ratio between **L2** (1×10^{-5} M) with fluoride ion were used to fluorescence titration method (continued)

Point	V of F^- (μ L)	V total of F^- (μ L)	V total (mL)	$F^-/L2$
38	50.0	417.5	2.4175	171
39	50.0	467.5	2.4675	191
40	50.0	517.5	2.5175	211
41	50.0	567.5	2.5675	231
42	50.0	617.5	2.6175	251

Table 3.3 The scale ratio between **L2** (1×10^{-5} M) with acetate ion were used to fluorescence titration method

Point	V of AcO^- (μL)	V total of AcO^- (μL)	V total (mL)	$\text{AcO}^-/\mathbf{L2}$
1	0.0	0.0	2.0000	0.0
2	0.5	0.5	2.0005	0.2
3	0.5	1.0	2.0010	0.4
4	0.5	1.5	2.0015	0.6
5	0.5	2.0	2.0020	0.8
6	1.0	3.0	2.0030	1.2
7	1.0	4.0	2.0040	1.6
8	1.0	5.0	2.0050	2.0
9	1.0	6.0	2.0060	2.4
10	1.0	7.0	2.0070	2.8
11	1.0	8.0	2.0080	3.2
12	1.0	9.0	2.0090	3.6
13	1.0	10.0	2.0100	4.0
14	1.0	11.0	2.0110	4.4
15	2.0	13.0	2.0130	5.2
16	2.0	15.0	2.0150	6.0
17	2.0	17.0	2.0170	6.8
18	2.0	19.0	2.0190	7.6
19	2.0	21.0	2.0210	8.4

Table 3.3 The scale ratio between **L2** (1×10^{-5} M) with acetate ion were used to fluorescence titration method (continued)

Point	V of AcO ⁻ (μL)	V total of AcO ⁻ (μL)	V total (mL)	AcO ⁻ /L 2
20	2.0	23.0	2.0230	9.2
21	2.0	25.0	2.0250	10.0
22	2.0	27.0	2.0270	10.8

Table 3.4 The scale ratio between **L2** (1×10^{-5} M) with hydroxide ion were used to fluorescence titration method

Point	V of OH ⁻ (μL)	V total of OH ⁻ (μL)	V total (mL)	OH ⁻ /L2
1	0	0	2.000	0.0
2	2	2	2.002	0.8
3	2	4	2.004	1.6
4	2	6	2.006	2.4
5	2	8	2.008	3.2
6	2	10	2.010	4.0
7	2	12	2.012	4.8
8	2	14	2.014	5.6
9	2	16	2.016	6.4
10	2	18	2.018	7.2
11	2	20	2.020	8.0
12	2	22	2.022	8.8
13	2	24	2.024	9.6
14	2	26	2.026	10.4
15	2	28	2.028	11.2
16	2	30	2.030	12.0
17	5	35	2.035	14.0
18	5	40	2.040	16.0
19	5	45	2.045	18.0

Table 3.4 The scale ratio between **L2** (1×10^{-5} M) with hydroxide ion were used to fluorescence titration method (continued)

Point	V of OH ⁻ (μL)	V total of OH ⁻ (μL)	V total (mL)	OH ⁻ /L2
20	5	50	2.050	20.0
21	5	55	2.055	22.0
22	5	60	2.060	24.0
23	5	65	2.065	26.0
24	5	70	2.070	28.0
25	5	75	2.075	30.0
26	5	80	2.080	32.0
27	5	85	2.085	34.0
28	5	90	2.090	36.0
29	5	95	2.095	38.0
30	5	100	2.100	40.0
31	5	105	2.105	42.0
32	5	110	2.110	44.0
33	5	115	2.115	46.0
34	5	120	2.120	48.0
35	5	125	2.125	50.0
36	5	130	2.130	52.0
37	5	135	2.135	54.0
38	5	140	2.140	56.0

3.3.1.3 Determination of the stoichiometry of the L1 and L2 with anion complexes by Job's method

Solution of **L1** and anions in DMSO (2×10^{-6} M) were prepared in a 20 mL of a volumetric flask. Solution of **L1** and an anion was added to a 1 cm path length quartz cuvette to provide the total volume of 2 mL according to Table 3.5.

Solution of **L2** and anion (F^- or AcO^- or OH^-) in DMSO (5×10^{-6} M) were prepared in a 30 mL of a volumetric flask. Solution of **L2** and an anion was added to a 1 cm path length quartz cuvette to provide the total volume of 3 mL according to Table 3.6.

Emission spectra of each addition were measured after the mixture was stirred for 2 min.

Table 3.5 Amount of **L1** (2×10^{-6} M) and anion (2×10^{-6} M) that added in to a cuvette cell for Job's method

Point	Volume of anion (mL)	Volume of L1 (mL)
1	0	2.00
2	0.20	1.80
3	0.40	1.60
4	0.60	1.40
5	0.80	1.20
6	1.00	1.00
7	1.20	0.80
8	1.40	0.60
9	1.60	0.40
10	1.80	0.20
11	2.00	0

Table 3.6 Amount of **L2** (5×10^{-6} M) and anion (5×10^{-6} M) that added into a cuvette cell for Job's method

Point	Volume of anion (mL)	Volume of L2 (mL)
1	0	3.00
2	0.50	2.50
3	0.80	2.00
4	1.10	1.80
5	1.00	1.50
6	1.20	1.40
7	1.30	1.30
8	1.40	1.20
9	1.50	1.00
10	1.80	1.10
11	2.00	0.80
12	2.50	0.50
13	3.00	0

3.3.1.4 Quantum yield

The fluorescence quantum yields, Φ_F , were estimated using the integrate emission intensity of anthracene as standard in ethanol via equation (1).

$$\Phi_F = \Phi'_{ST}(\text{Grad}_F/\text{Grad}_{ST})(\eta^2_F/\eta^2_{ST})\dots\dots\dots(1)$$

1) Determination of L2 quantum yield value

Solution of **L2** was prepared for analysis using UV-visible concomitant with fluorescence spectrophotometry. In the case of absorbance peak, each point of signal should be lower than 0.1 Abs. In experimental, the first step was analyzed the most concentrate of **L2** then, the solution was diluted to continue analysis. One set of study took around 8-10 points. All absorption and emission intensity data were calculated following equation (1).

2) Determination of L2·F⁻ quantum yield value

Determination steps of **L2·F⁻** were performed in the same manner as step of **L2** quantum yield. However, the preparation of the solution was different. Solution of **L2** was prepared certainly concentration with added of fluoride at 2.5 equiv of **L2** mole that was stock solution. And the **L2·F⁻** solution underwent to determination of quantum yield value step following in determination of **L2** quantum yield value steps.

3.3.2 ¹H NMR spectroscopy

3.3.2.1 Excess anion study

Solution of compound **L1** (5×10^{-3} M) and compound **L2** (5×10^{-3} M) were prepared in 0.4 mL of d₆-DMSO in a NMR tube. The solution of anions (0.5 M for **L1** and 0.04 M for **L2**) were prepared in 1 mL and added into 0.4 mL of ligand by a microsyringe. ¹H NMR spectra were recorded by a Varian Mercury Plus 400 NMR spectrometer.

3.3.2.2 Complexation study of L2 with anions (F^- , OH^- , and AcO^-) using 1H NMR titration method

Solution of compound **L2** (5×10^{-3} M) was prepared in 0.4 mL of d_6 -DMSO in a NMR tube. The solution of anions (0.04 M) were prepared in 1 mL and added into 0.4 mL of ligand by a microsyringe, according to Tables 3.7, 3.8, and 3.9 for fluoride, acetate, and hydroxide, respectively.

Table 3.7 Amount of fluoride (0.04 M) was added into a cuvette cell of **L2** (5×10^{-3} M) for Job's method 1H NMR titration method

Point	V of F^- (μ L)	V total of F^- (μ L)	$F^-/L2$
1	2.50	2.50	0.05
2	2.50	5.00	0.10
3	2.50	7.50	0.15
4	5.00	10.0	0.20
5	5.00	15.0	0.30
6	5.00	20.0	0.40
7	5.00	25.0	0.50

Table 3.8 Amount of acetate (0.04 M) was added into a cuvette cell of **L2** (5×10^{-3} M) for Job's method ^1H NMR titration method

Point	V of AcO^- (μL)	V total of AcO^- (μL)	$\text{AcO}^-/\text{L2}$
1	2.50	2.50	0.05
2	2.50	5.00	0.10
3	2.50	7.50	0.15
4	5.00	10.0	0.20
5	5.00	15.0	0.30
6	5.00	20.0	0.40
7	5.00	25.0	0.50

Table 3.9 Amount of hydroxide (0.04 M) was added into a cuvette cell of **L2** (5×10^{-3} M) for Job's method ^1H NMR titration method

Point	V of OH^- (μL)	V total of OH^- (μL)	$\text{OH}^-/\text{L2}$
1	2.50	2.50	0.05
2	2.50	5.00	0.10
3	2.50	7.50	0.15
4	5.00	10.0	0.20
5	5.00	15.0	0.30
6	5.00	20.0	0.40
7	5.00	25.0	0.50
8	5.00	30.0	0.60
9	5.00	35.0	0.70
10	5.00	40.0	0.80

In case of fluoride ion, changing of ^1H NMR signal when fluoride ion was added into **L2** was studied specifically. The solution of **L2** (6×10^{-3} M) and fluoride ion (0.24 M) were prepared, the quantity of fluoride was added into **L2** according to Table 3.10, and data were recorded 0-18 ppm.

Table 3.10 Amount of fluoride (0.24 M) was added into a cuvette cell of **L2** (6×10^{-3} M) for Job's method ^1H NMR titration method

Point	V of F^- (μL)	V total of F^- (μL)	$\text{F}^-/\text{L2}$
1	3.00	3.00	3
2	3.00	6.00	6
3	3.00	9.00	9
4	3.00	12.00	12
5	3.00	15.00	15
6	5.00	20.00	20
7	5.00	30.00	30

3.4 Inter and Intramolecular pyrene stacking studies

Solutions of anions (8×10^{-3} M) were prepared as stock solutions. The stock solution of anion was added to various concentrations of **L2** (5×10^{-6} M, ..., 10^{-7} M) by fixing relative concentration of anions to **L2** at 2.5, 1.5 and 1.0 equiv for F^- , OH^- and AcO^- , respectively. Emission spectra of each experiment were measured after the mixture was stirred for 2 min.

3.5 Anion interference studies

Solution of compound **L2** (5×10^{-6} M) were prepared in volumetric flask (20 mL) and 2 mL of each was added to a 1 cm path length quartz cuvette. The solutions of anions (8×10^{-3} M) were prepared in volumetric flask (5 mL). Solution of compound **L2** (5×10^{-6} M, 2 mL) with fluoride (8×10^{-3} M, 2.5 eq) was prepared as a reference. Subsequently, other anions (8×10^{-3} M, 100 eq) were added into the mixture of compound **L2** and fluoride.

CHAPTER IV

RESULTS AND DISCUSSION

4.1 Design and synthesis of anion receptors

Receptors **L1**, **L2** and **L3** were designed and synthesized as anion receptors. The structures of **L1**, **L2** and **L3** are different in term of anion binding sites and types of spacers. Receptor **L1** containing benzyl group as spacer linked to two amides as anion binding site. Receptor **L2** including polyethylene glycol chains with benzyl ring as spacer linked to two thioureas as anion binding site. Receptor **L3** combining an ethyne as spacer linked to two ureas as anion binding site. All receptors have the same signaling unit, pyrene. Therefore, the effects of structures of the receptors toward anion binding abilities were studied and compared.

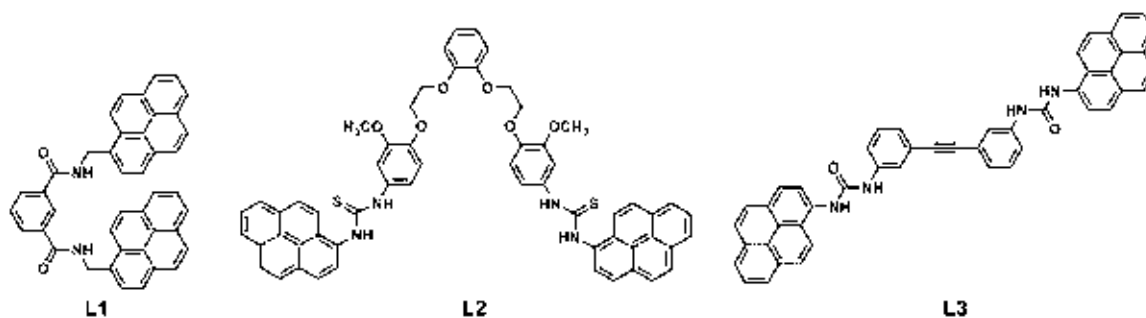
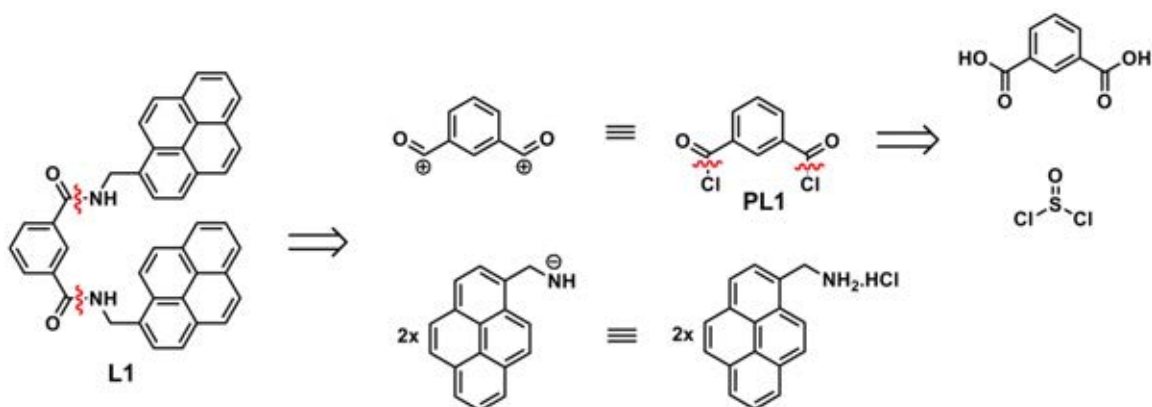


Figure 4.1 Structures of receptors **L1**, **L2**, and **L3**

4.2 Retrosynthesis of compounds L1-L3

4.2.1 Retrosynthesis of compound L1

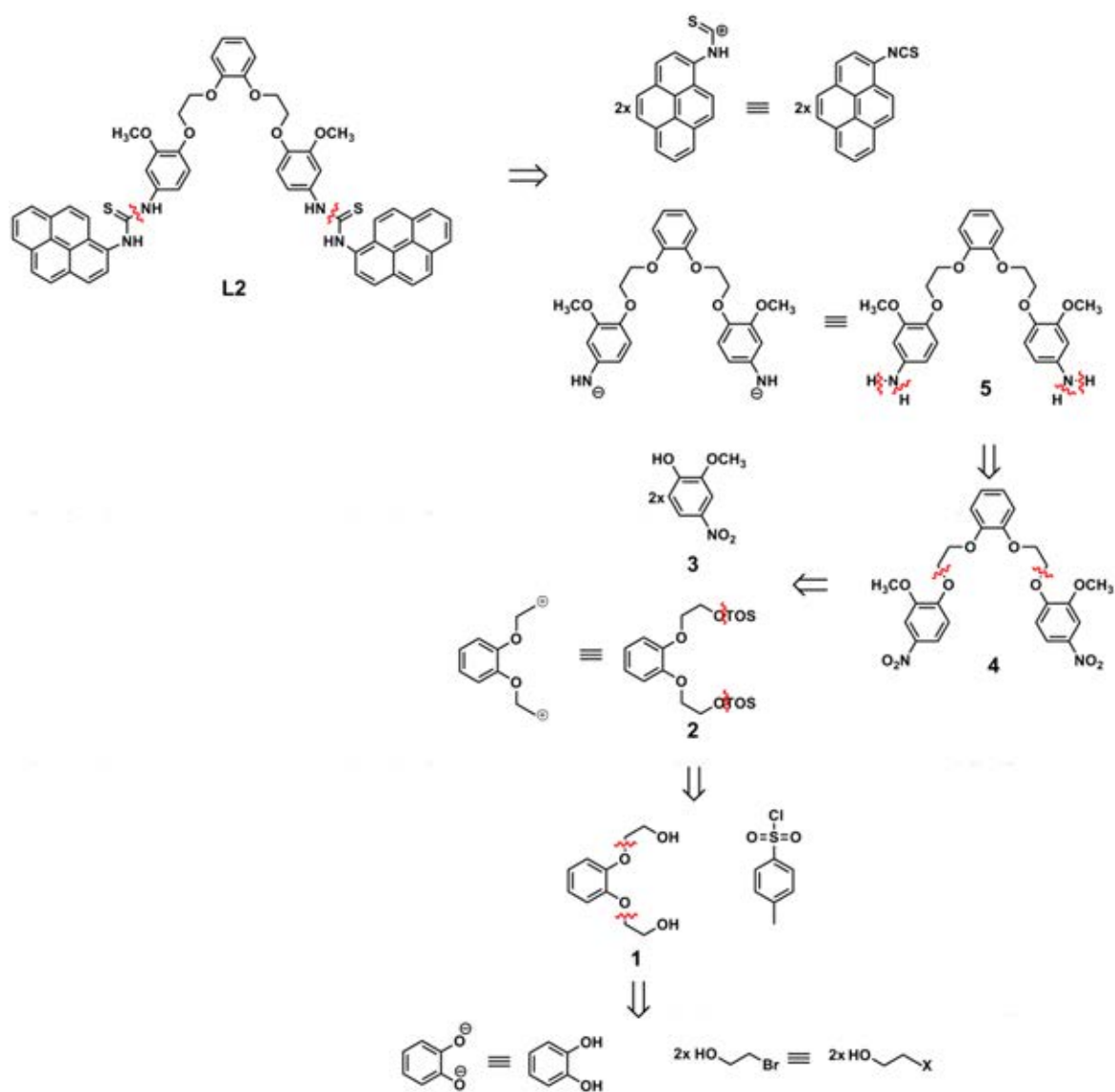


Scheme 4.1 Retrosynthesis of compound L1

Compound **L1** can be separated by disconnection at the amide bond to give two synthons: 1-pyrenemethylamine hydrochloride and isophthalamide (**PL1**). Isophthalamide (**PL1**) can be divided into two synthons, isophthalic acid and thionyl chloride, as shown in Scheme 4.1.

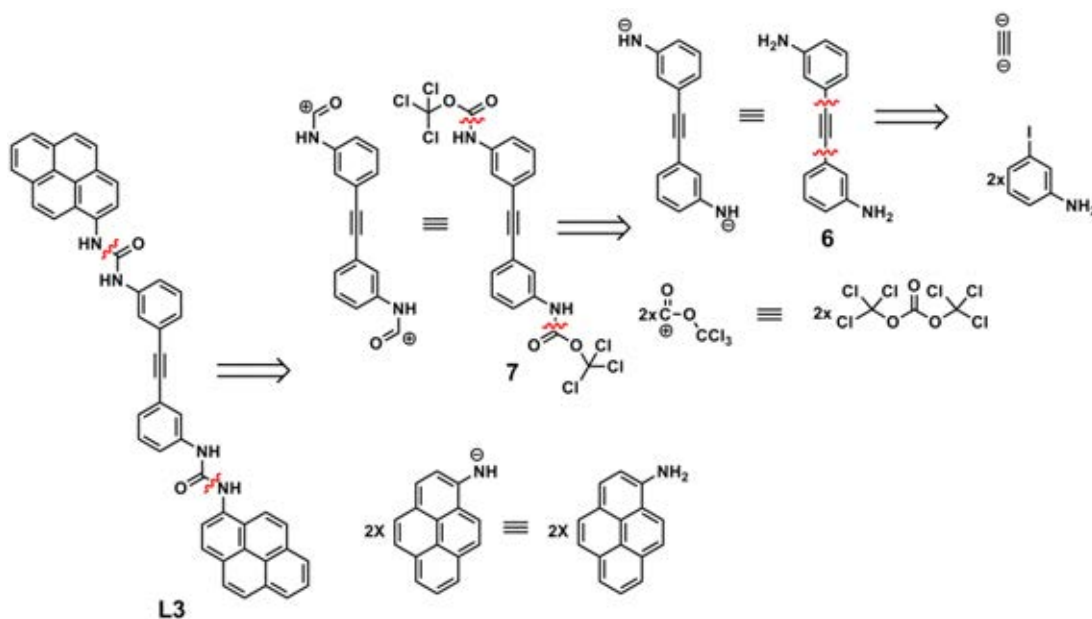
4.2.2 Retrosynthesis of compound L2

Compound **L2** (Scheme 4.2) can be separated disconnected at the thiourea bond to give thiocyanatopyrene and compound **5**. Disconnecting of compound **5** at the N-H bond gives compound **4** containing nitro groups. Then, disconnecting at the bonds of ethylene glycol chains gives two synthons: compound **3** and compound **2**. Disconnection of compound **2** gives compound **1** and tosyl chloride. Consequently, disconnection of compound **1** gives two synthons: pyrocatechol and bromoethanol.



Scheme 4.2 Retrosynthesis of compound L2

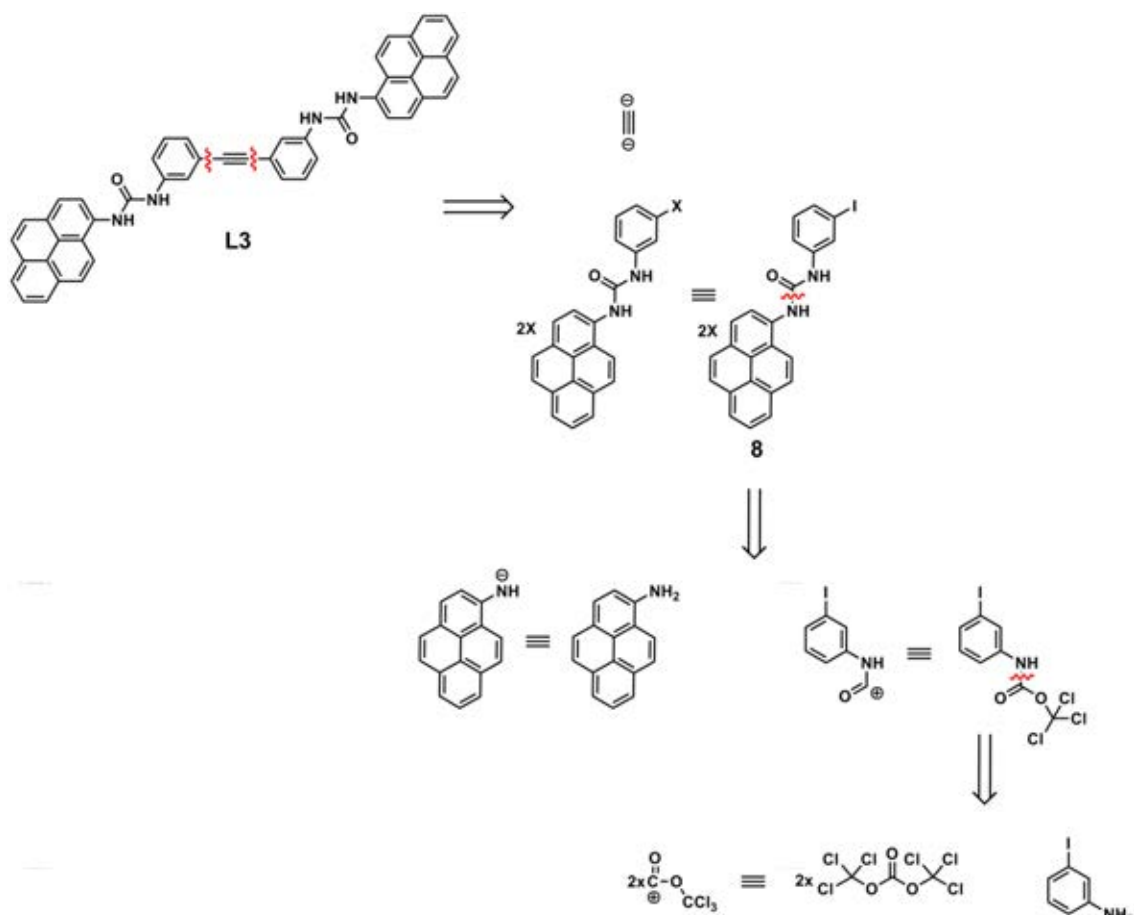
4.2.3 Retrosynthesis pathway 1 of compound L3



Scheme 4.3 Retrosynthesis pathway 1 of compound L3

The disconnection of compound L3 in pathway 1 gives two synthons as 1-aminopyrene and compound 7. Subsequently, compound 7 can be disconnected at the amide bond to give two synthons: triphosgene and compound 6. Then, the disconnection of compound 6 gives ethyne and 3-iodoaniline as shown in Scheme 4.3.

4.2.4 Retrosynthesis pathway 2 of compound L3

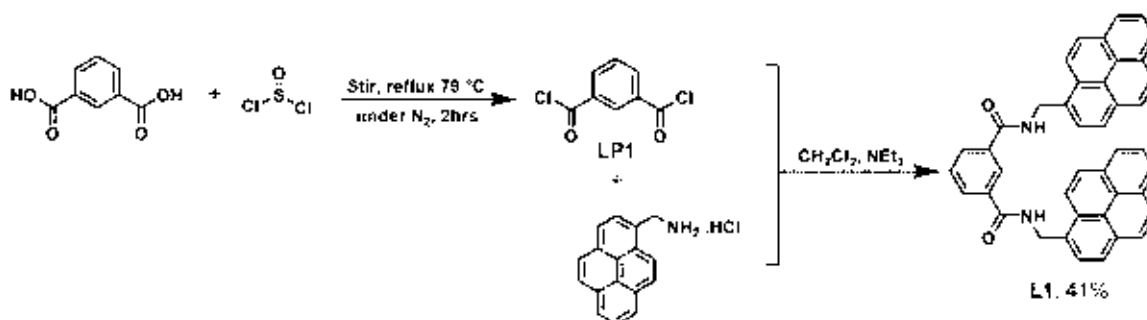


Scheme 4.4 Retrosynthesis pathway 2 of compound **L2**

Disconnection of the C-C bond that linked between benzene and the ethyne group of **L3** gives ethyne and compound **8**. Subsequently, compound **8** can be disconnected to give 1-aminopyrene and 3-iodoaniline linked with triphosgene as shown in Scheme 4.4.

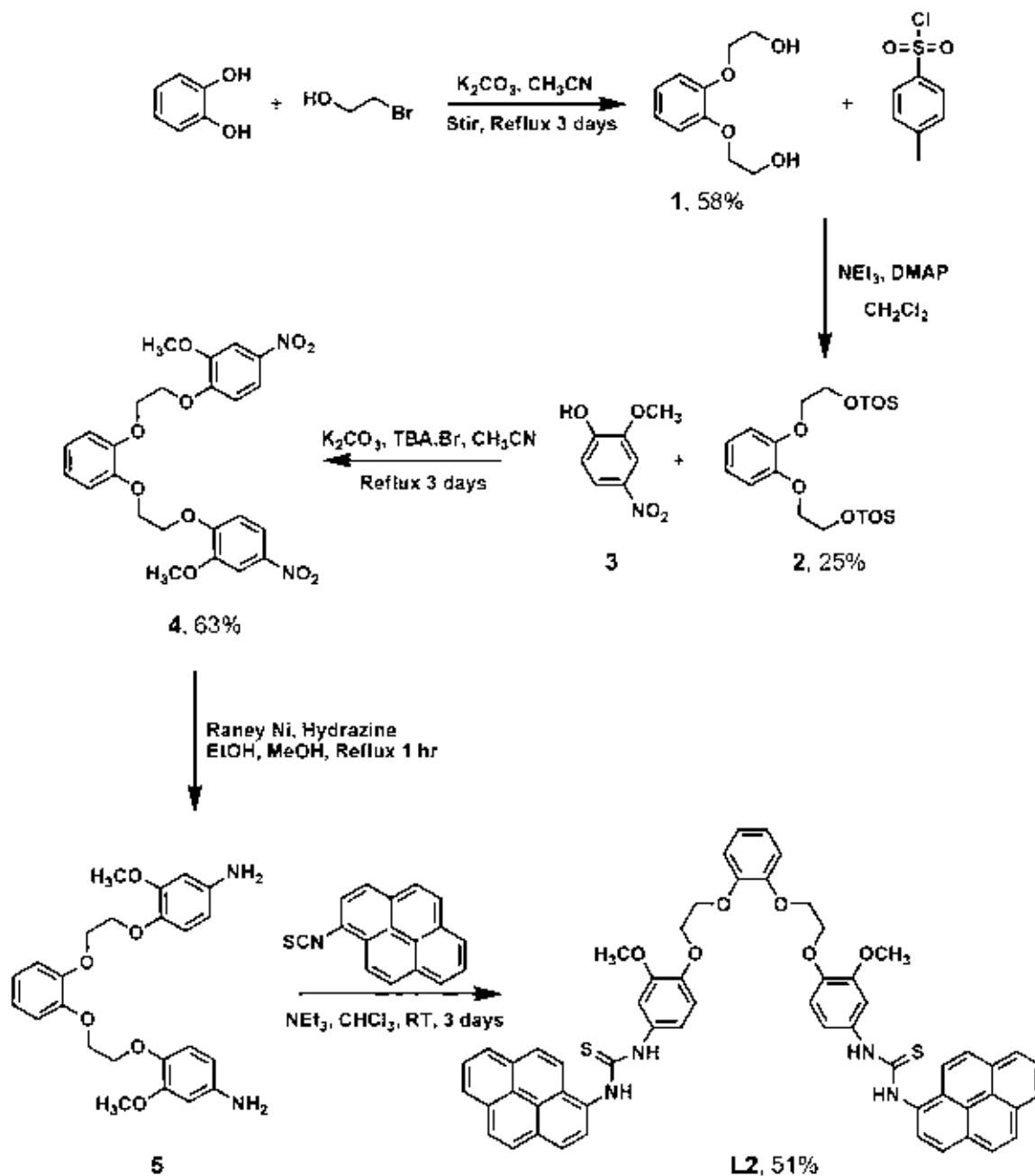
4.3 Syntheses of compounds L1-L3

Compound **L1** containing two pyrene moieties linked to isophthalamide as anion receptor was synthesized by the procedure shown in Scheme 4.5. Isophthalic acid and thionyl chloride underwent a substitution reaction to yield isophthalamide. Further reaction with 1-pyrenemethylamine hydrochloride in CH_2Cl_2 gave compound **L1** in 42% yield. Compound **L1** dissolves in DMSO only. ^1H NMR and ^{13}C NMR spectroscopy, mass spectrometry, elemental analysis, infrared spectroscopy were used to substantiate the structure of compound **L1**.



Scheme 4.5 Synthetic procedure of compound **L1**

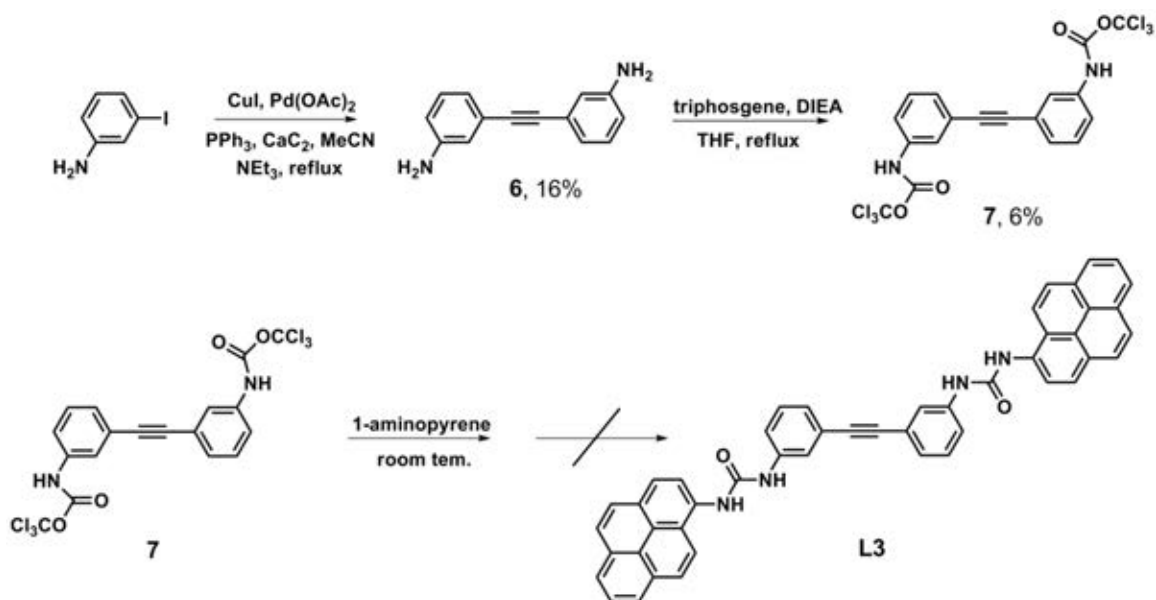
Compound **L2** possessing a longer polyethylene glycol chain linked to two pyrene moieties as fluorophore and thiourea sites as anion receptor was synthesized using the procedure shown in Scheme 4.6. Pyrocatechol reacted with bromoethanol by a substitution reaction in CH_3CN to give compound **1** in 58% yield. Substitution reaction of compound **1** with TsCl using triethylamine as base and DMAP as catalyst in CH_2Cl_2 gave compound **2** in 25% yield. Compound **2** reacted with compound **3** by a substitution reaction using K_2CO_3 as base and tetrabutylammonium bromide as phase transfer catalyst in CH_3CN to give compound **4** in 63% yield. Reduction of compound **4** with Raney Ni and hydrazine gave compound **5** in a quantitative yield. Coupling reaction between compound **5** and 1-isothiocyanatopyrene in CHCl_3 at room temperature gave compound **L2** in 51% yield. Compound **L2** dissolves in DMSO only. ^1H NMR and ^{13}C NMR spectroscopy, elemental analysis, mass spectrometry and infrared spectroscopy were used to confirm structures of **L2**.



Scheme 4.6 Synthetic procedure of compound **L2**

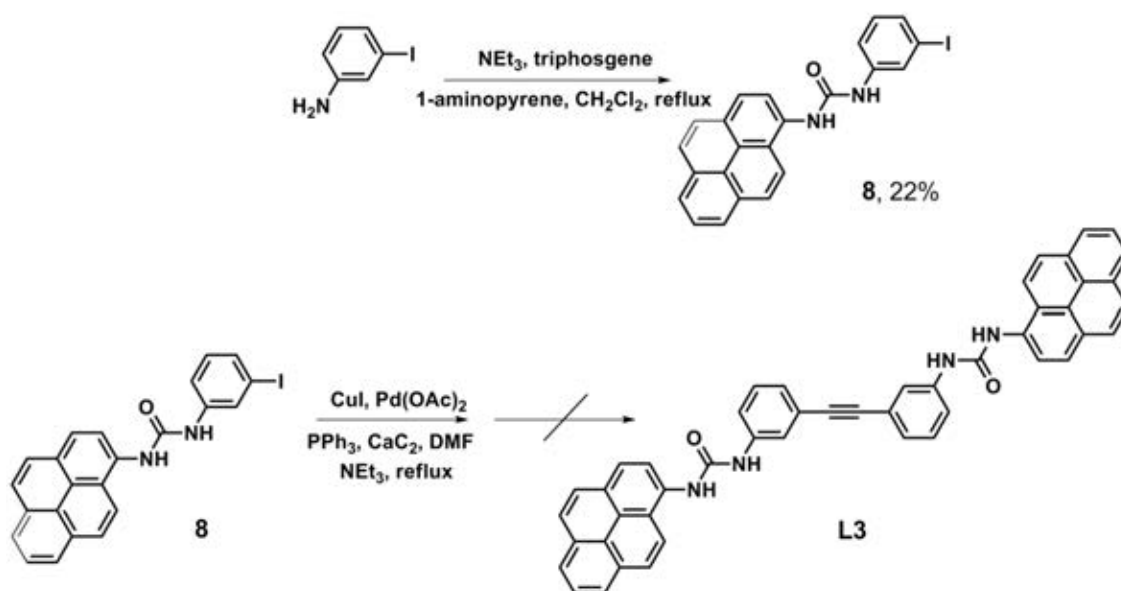
Compound **L3** was attempted to synthesize according to pathways 1 and 2 shown in Scheme 4.7 and 4.8, respectively. From experimental results, Sonogashira coupling of 3-iodoaniline and CaC_2 gave compound **6** in 16% yield whereas compound **6** reacted with triphosgene to give compound **7** in 6% yield. ^1H and ^{13}C

NMR spectroscopy confirm the structure of compounds **6** and **7** as shown in Figure A13, Figure A14, Figure A16, and Figure A17. However, the final product (**L3**) cannot be synthesized.



Scheme 4.7 Synthetic pathway 1 of compound **L3**

In pathway 2, Compound **8** was synthesized in 22% yield from the reaction of 3-iodoaniline and triphosgene. The structure of **8** was confirmed by ^1H NMR, ^{13}C NMR and mass spectroscopy as shown in Figures A18-A20. Compound **8** underwent Sonogashira coupling with CaC_2 , but the desired compound **L3** could not be obtained.



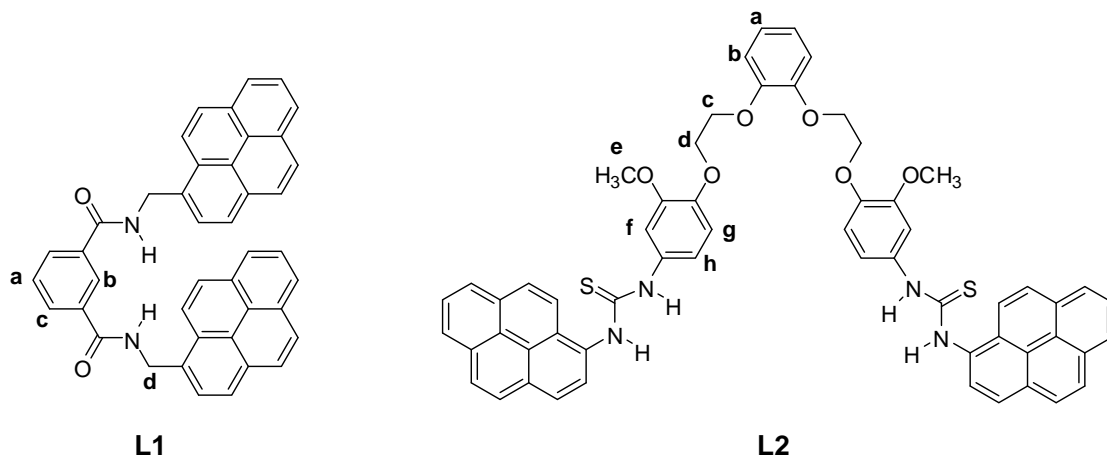
Scheme 4.8 Synthetic pathway 2 of compound L3

4.4 Characterization of L1 and L2

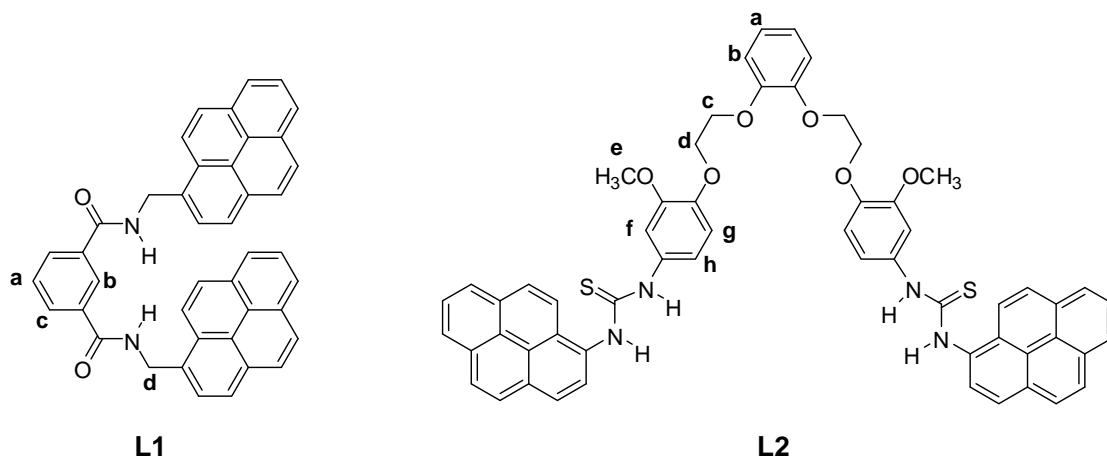
NMR spectroscopy was used to determine structures of L1 and L2. ¹H NMR and ¹³C NMR spectra were recorded in d₆-DMSO. The ¹H NMR data of L1 and L2 were shown in Table 4.1. The proton at NH of amide showed a singlet peak at 9.37 ppm and benzene protons, H_a, H_b and H_c, showed the resonance signal around 7.58-8.51 ppm. The H_d proton showed a doublet signal at 5.23 ppm. Moreover, the spectra of aromatic ring of pyrene showed a multiplet peak in the range of 8.31-8.06 ppm. Due to the effect of amide electron withdrawing group to benzene protons, H_b and H_c appeared more downfield than the proton of pyrene. For L2, the benzene protons, H_a showed a triplet peak at 6.92 ppm. H_b showed a doublet peak at 7.05 ppm. H_g and H_h, showed the resonance multiplet peak around 7.04-6.95 ppm and the benzene proton of H_f displayed a singlet peak at 7.17 ppm. The polyethylene glycol protons, H_c and H_d, showed a doublet of doublet peak at 4.25 and 4.29 ppm, respectively. H_d displayed a higher chemical shift than H_c due to effect of the benzene ring anisotropy. The methoxy protons of H_e displayed a singlet peak at 3.70 ppm. Signals of the aromatic ring protons of pyrene showed a multiplet signal in the range of 8.29-8.02 (m). The protons of thiourea moieties showed two singlet signals at 10.05 and 9.72 ppm. The

^{13}C NMR data of **L1** and **L2** were collected in Table 4.2. ESI-mass spectrum confirmed the structure of **L2** (Figure A11).

Table 4.1 ^1H NMR data for **L1** and **L2** in d_6 -DMSO



H-Position	L1(ppm)	L2(ppm)
a	7.58 (t)	6.92 (t)
b	8.51 (s)	7.05 (d)
c	8.48 (d)	4.25 (dd)
d	5.23 (d)	4.29 (dd)
e	-	3.70 (s)
f	-	7.17 (s)
g	-	7.04-6.95 (m)
h	-	7.04-6.95 (m)
pyrene	8.31-8.06 (m)	8.29-8.02 (m)
NH	9.37 (s)	10.05 (s), 9.72 (s)

Table 4.2 ^{13}C NMR data for **L1** and **L2** in d_6 -DMSO

C-Position	L1(ppm)	L2(ppm)
a	130.7	121.4
b	130.2	122.6
c	132.7	67.5
d	41.0	67.4
e		55.4
f	-	116.7
g	-	113.3
h	-	109.7
$\underline{\text{C}}_{\text{Ar}}\text{-C=O}$	134.5	-
C=O	165.8	-
pyrene	130.0-123.2	130.5-123.7
$\underline{\text{C}}_{\text{Ar}}\text{-OCH}_3$	-	145.2
$\underline{\text{C}}_{\text{Ar}}\text{-OCH}_2$	-	148.2
$\underline{\text{C}}_{\text{Ar}}\text{-N}$	-	132.8
$\underline{\text{C}}_{\text{pyr}}\text{-N}$	-	133.1
C=S	-	181.2

The fluorescence emission spectra of **L1** and **L2** were studied in DMSO and were excited at 340 nm. Since the concentration at 2×10^{-6} M displayed the intensity of the monomer band (375-400 nm) around 700 a.u. which can be observed the changing obviously when adding anions (Figure 4.2a), the fluorescence emission of **L1** were measured in 2×10^{-6} M concentration. In the case of **L2**, the emission study of **L2** was performed at the concentration of 5×10^{-6} M and 1×10^{-5} M. Monomer bands of **L2** appeared in the region between 380-415 nm as shown in Figure 4.2b. The concentration of **L2** at 5×10^{-6} M was carried out for the complexation study, Job's plot, inter- and intramolecular interactions, and anion interference. Since the concentration at 5×10^{-6} M was appropriate for monitoring changing of both monomer and excimer emission. However, the concentration at 1×10^{-5} M was carried out to repeat titration experiments and Job's plot of concentration at 5×10^{-6} M because the concentration at 1×10^{-5} M gave distinctive changes. The data obtained were then analyzed by SPECFIT 32 program.

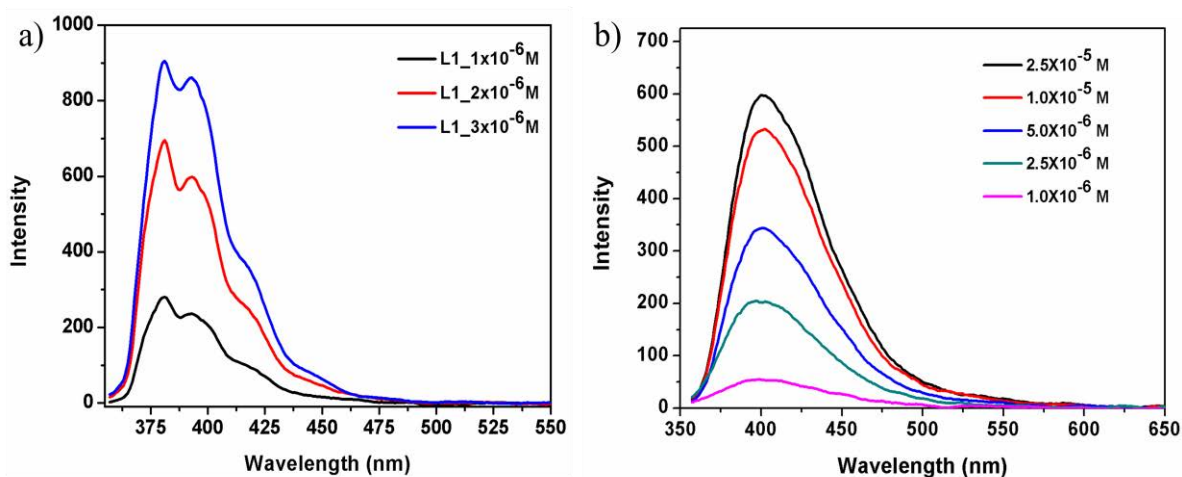


Figure 4.2 The emission spectra of a) **L1** and b) **L2** in DMSO

The fluorescence quantum yields, Φ_F , were estimated using the integrate emission intensity of anthracene as standard in ethanol via equation (1). The anthracene standard had been selected because its solution and all synthesized ligand solutions have identical absorbance at the same excitation wavelength (340 nm) to ensure their absorption of the same number of photons.

$$\Phi_F = \Phi'_{ST}(\text{Grad}_F/\text{Grad}_{ST})(\eta^2_F/\eta^2_{ST})\dots\dots\dots(1)$$

The subscripts:

ST: data of standard

F: data of test

Φ_F : Fluorescence quantum yield

Grad: The gradient from the plot of integrated fluorescence intensity versus absorbance

η : The refractive index of solvent ($\eta_{\text{EtOH}} = 1.3614$ and $\eta_{\text{DMSO}} = 1.4785$)

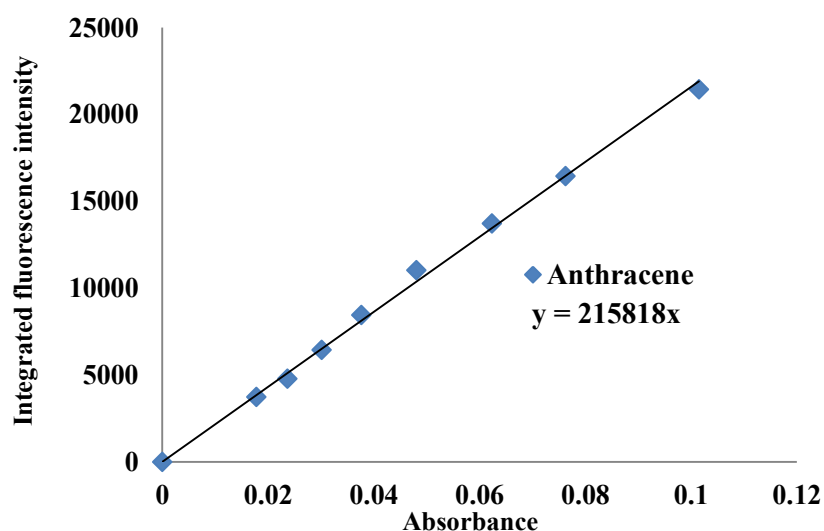


Figure 4.3 Linear plot of anthracene standard in EtOH (Grad = 215818)

Absorbance data of **L1** and **L2** were collected at 346 and 350 nm, respectively. The relative of absorbance data versus the integrated fluorescence intensity gave linear plots of **L1** and **L2** (Figure 4.4). The linear plot was used to calculate Grad of **L1** and **L2** to be 196293 and 216562, respectively. All parameter value was calculated following equation (1) to find the fluorescence quantum yields (Φ_F) of **L1** and **L2** given the values 0.29 and 0.32, respectively (Table 4.3). From the data obtained, **L2** possesses higher fluorescence quantum yields than the shorter chain length, **L1**.

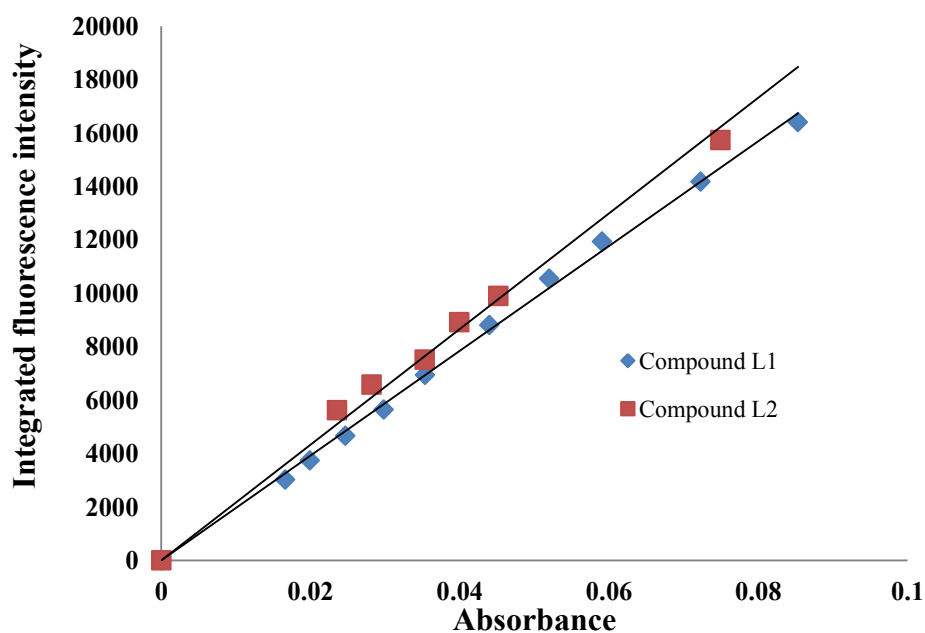


Figure 4.4 Linear plot of **L1** and **L2** in DMSO ($\text{Grad}_{L1} = 196293$, $\text{Grad}_{L2} = 216562$)

Table 4.3 The emission parameters for compounds **L1** and **L2** in DMSO

Compound	Absorbance	Emission	
	λ_{abs} (nm)	λ_{em} (nm)	Φ_F
L1	346	381	0.29
L2	350	410	0.32

4.5 Anions binding studies

4.5.1 Anion binding studies using fluorescence spectrophotometry

4.5.1.1 Anion binding ability of L1

Anions binding abilities of **L1** were studied in DMSO solution using fluorescence spectrophotometry. Tetrabutylammonium salts of F^- , Cl^- , Br^- , I^- , AcO^- , BzO^- , $H_2PO_4^-$, and OH^- were added to the solution of **L1** (2×10^{-6} M). Changing of ligand **L1** excimer emission intensity around 500 nm was not observed when these anions were added (Figure 4.5). A slightly change of **L1** monomer emission (at 375-400) was observed depending on anions. Therefore, anion titration at 0 to 700 equiv. was then performed to verify the effect of anion on **L1** monomer emission intensity in DMSO. The titration results showed slightly decreasing of **L1** monomer emission intensity when the volume of anion in DMSO increase as presented in Figure 4.6 and Figures A21-A27.

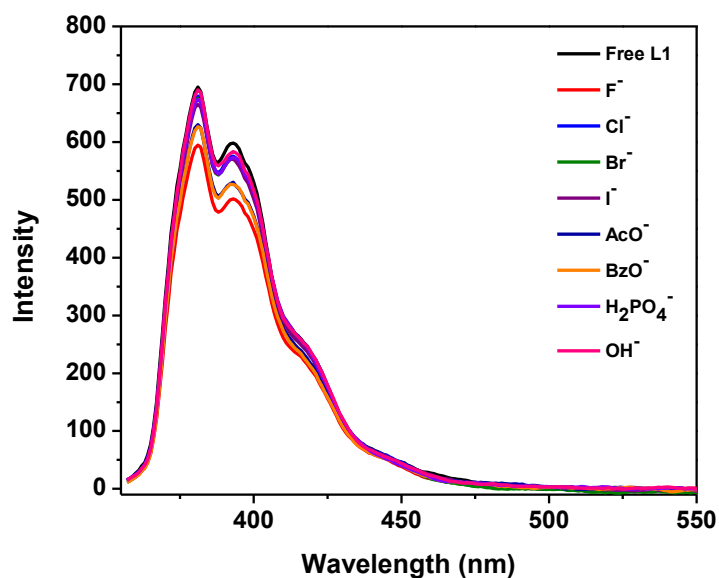


Figure 4.5 Fluorescence emission of **L1** (2×10^{-6} M) with 1000 equiv TBA anion salts in DMSO

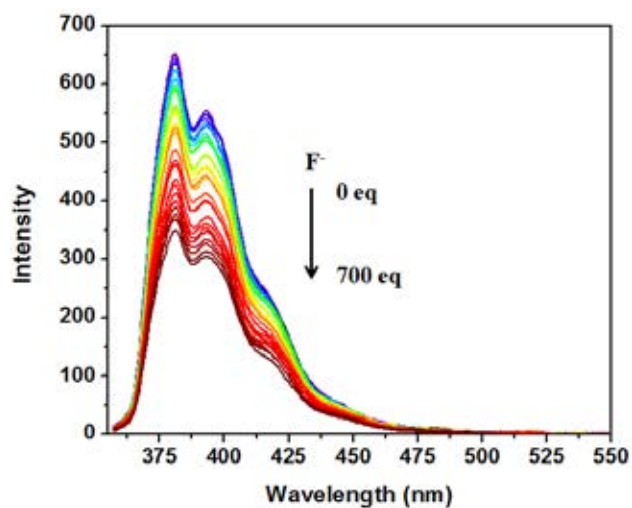


Figure 4.6 Fluorescence emission of **L1** (2×10^{-6} M) with 0-700 equiv of F^- salts in DMSO

The blank test has been carried out to confirm anions titration result by added DMSO in **L1** solution. Fluorescence spectra result of blank test and F^- titration has been compared as presented in Figure 4.7. This result indicated that decreasing of **L1** monomer emission intensity occurred from the dilution effect of added DMSO solution.

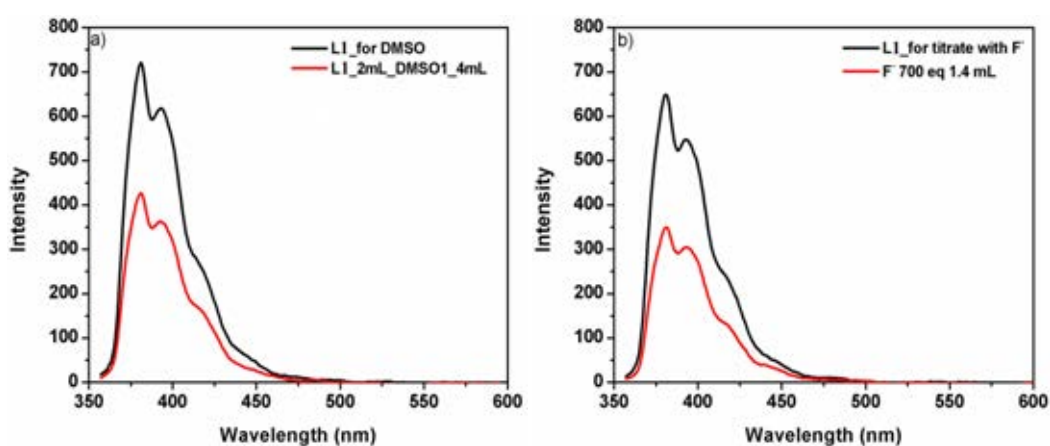


Figure 4.7 Fluorescence emission of **L1** (2×10^{-6} M) with a) 1.4 mL of DMSO b) 700 equiv of F^- salts in DMSO

From this result, anions induced slightly changes in the monomer band and no changes in the excimer band. The result may stem from the less acidic NH protons of **L1** and resulted in the less binding ability.

4.5.1.2 Anion binding ability of **L2**

Anions binding abilities of **L2** were studied in DMSO solution using fluorescence spectrophotometry. Tetrabutylammonium salts of various anions were added to the solution of **L2** (5×10^{-6} M). Only fluorescence spectra of **L2**·F⁻, **L2**·OH⁻, and **L2**·OAc⁻ displayed pyrene excimer band at 515 nm (Figure 4.8). Excimer emission intensity of **L2** may stem from the negative charge brought by the anion-stabilized excited state of the first pyrene molecule. The first pyrene molecule was excited and polarized to interact with another pyrene molecule in its ground state. Decreasing of **L2** monomer emission intensity was detected whereas the excimer emission intensity increasing upon adding anions. The order of intensity ratio between excimer and monomer bands (I_E/I_M) in **L2** varied as F⁻ > OH⁻ >> AcO⁻ > BzO⁻ > H₂PO₄⁻ > Cl⁻ > Br⁻ ≈ I⁻ as shown in Figure 4.9. Anions of F⁻, OH⁻, and AcO⁻ bound to the N-H thiourea of **L2** via hydrogen bonding interactions. F⁻ gave a distinct excimer band when interacted with **L2**. Furthermore, two F⁻ acted as a very strong base [44] and provided a large affinity toward H⁺. Moreover, the smallest atomic size of fluoride was suitable to encapsulate in the receptor while OH⁻ was bigger and became less favorable. In the case of oxoanion, AcO⁻ > BzO⁻ > H₂PO₄⁻, two consecutive oxygen atoms can form N-H···O with thiourea. The interaction was crucially electrostatic and was related to the intrinsic basicity of the anion [45].

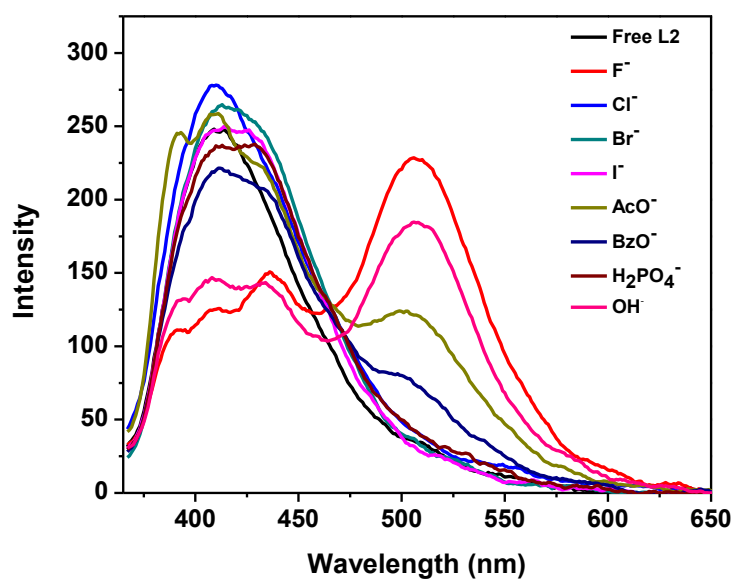


Figure 4.8 Fluorescence emission of **L2** (5×10^{-6} M) with 50 equiv. TBA anion salts in DMSO

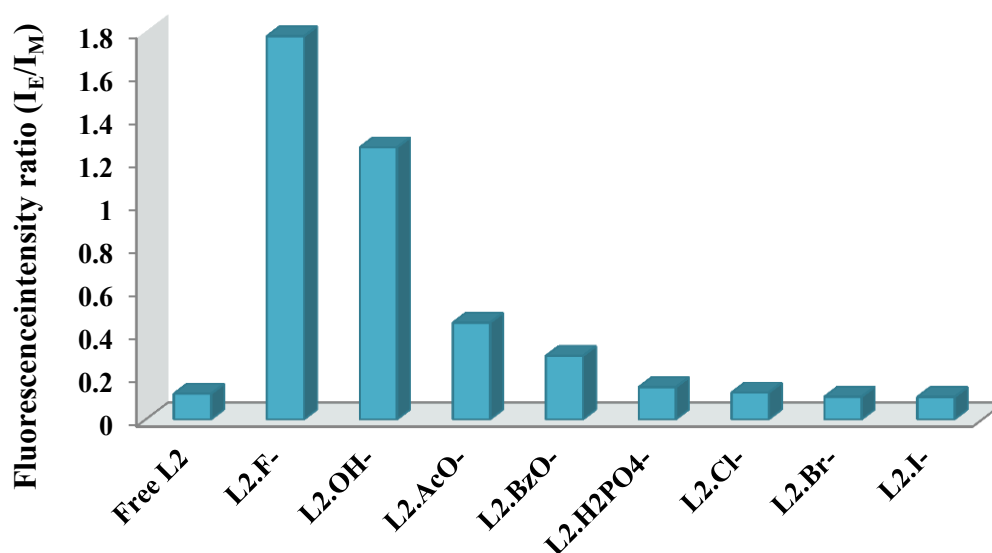


Figure 4.9 Plot of the intensity ratio of excimer to monomer emission (I_E : 515 nm, I_M : 415 nm) of **L2** (5×10^{-6} M) with 50 equiv TBA anion salts in DMSO.

The color changes were observed after the addition of various anions to **L2** solution as shown in Figure 4.10. Moreover, addition of F^- , OH^- , and AcO^- induced

the color changes of **L2** solution from colorless to yellow. Changing of color stem from the negative charge of anions affected the charge-transfer transition and stabilized the excited state of the chromophore [9].

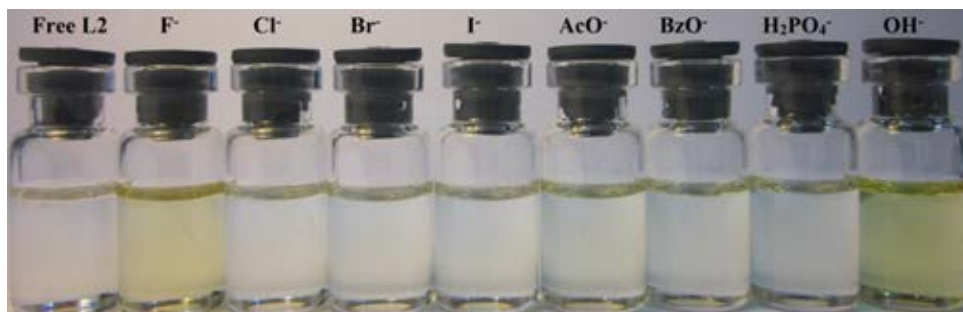
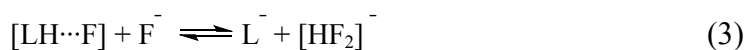
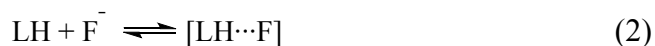
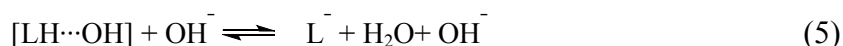


Figure 4.10 The color change observed for the receptor **L2** ($1 \times 10^{-5} \text{M}$) upon addition of 100 equiv. of anions (from left to right: **L2**, **L2**+ F^- , **L2**+ Cl^- , **L2**+ Br^- , **L2**+ I^- , **L2**+ AcO^- , **L2**+ BzO^- , **L2**+ H_2PO_4^- , and **L2**+ OH^-) in DMSO.

According to the results from fluorescence titrations, monomer emission intensity of the free ligand **L2** (10^{-5}M) has been monitored at 415 nm. Upon addition of anions (F^- , OH^- , and AcO^-), the monomer emission intensity decreased while the excimer emission intensity at 515 nm increased (Figures 4.11, 4.13, and 4.15 for F^- , OH^- , and AcO^- , respectively). Upon addition of F^- , OH^- , and AcO^- , the emission intensity were found to give 3 different bands. The monomer emission intensity at 415 nm decreased, while the excimer emission intensity at 515 nm increased. We assumed that **L2** formed H-bonding interactions with F^- , OH^- and AcO^- which presupposed by equilibrium in equation 2 [45]. A small change of the excimer emission intensity was found and a large change of the emission intensity by an appearance of a new peak when adding excess F^- and OH^- was observed. From this result, it could be assumed that F^- induced N-H deprotonation as illustrated in equation 3 [45].



In the case of OH^- , 0-7.2 equiv of OH^- induced a decreasing monomer at 415 nm and increasing excimer at 515 nm (Figure 4.14). When more equivalents of OH^- (7.2-64 equiv.) were added to **L2** solution, a new peak at 436 nm was developed. The deprotonation process was assumed in a similar fashion to F^- . Thus, the following equilibria (4) and (5) were proposed.



Addition of 0-2 equiv. of AcO^- induced a decreasing in monomer emission intensity at 415 nm and a increasing of excimer emission intensity at 515 nm (Figure 4.15). We assumed that AcO^- formed H-bonding interactions with **L2**. Then, the emission at 515 nm turn to monomer at higher AcO^- concentration (2-10.8 equiv) (Figure 4.16). It was assumed that **L2** formed two N-H \cdots O bonds with two consecutive oxygen atoms of the AcO^- . The molecular structure of **L2** \cdot 2 OAc^- probably prevented it to give the excimer emission.

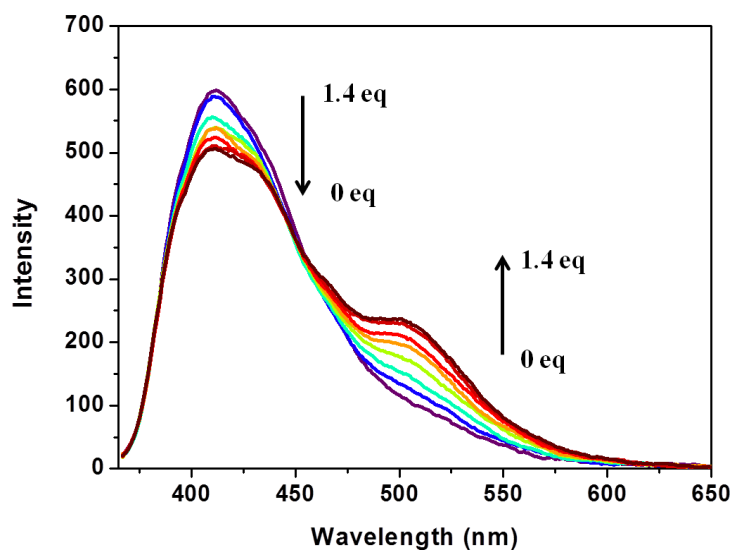


Figure 4.11 Fluorescence titration spectrum of **L2** (1×10^{-5} M) with TBAF (0 - 1.4 equiv) in DMSO.

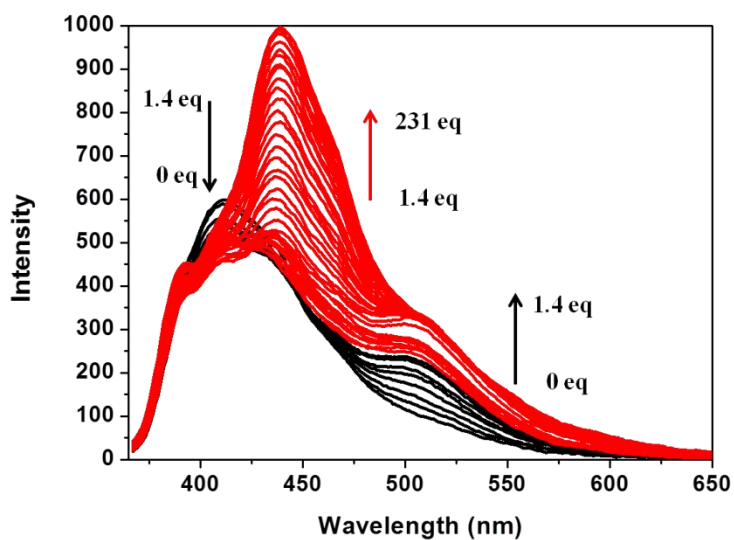


Figure 4.12 Overall fluorescence titration spectrum of **L2** (1×10^{-5} M) with TBAF (0 - 231 equiv) in DMSO.

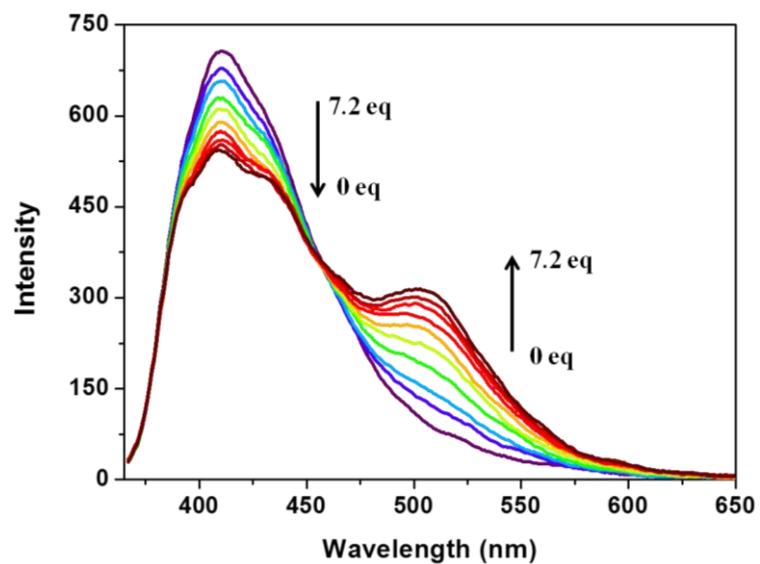


Figure 4.13 Fluorescence titration spectrum of **L2** (1×10^{-5} M) with TBAOH (0 – 7.2 equiv) in DMSO.

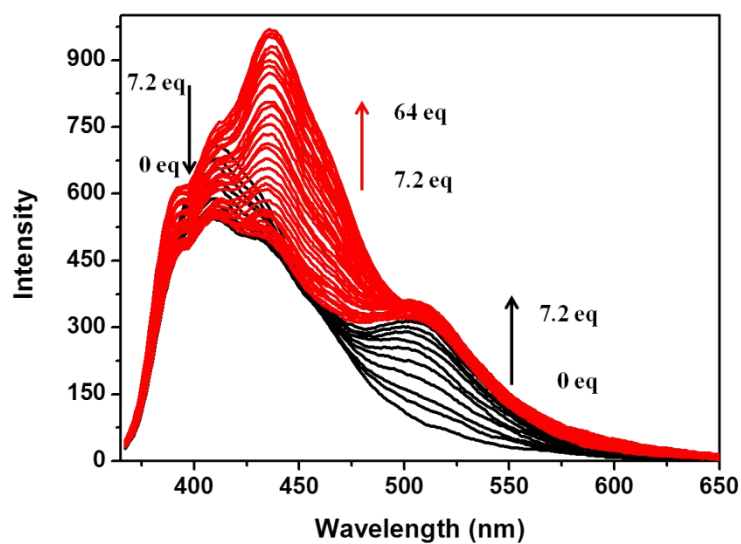


Figure 4.14 Overall fluorescence titration spectrum of **L2** (1×10^{-5} M) with TBAOH (0 - 64 equiv) in DMSO.

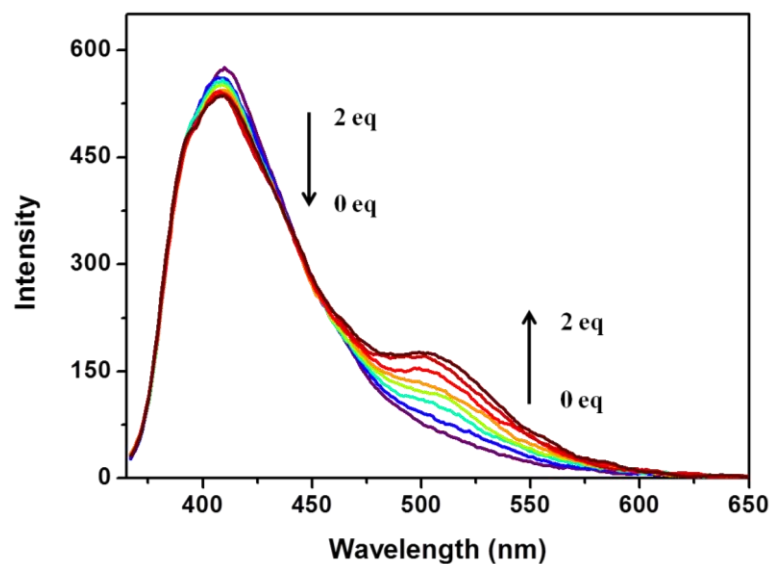


Figure 4.15 Fluorescence titration spectrum of **L2** (1×10^{-5} M) with TBAOAc (0 - 2 equiv) in DMSO.

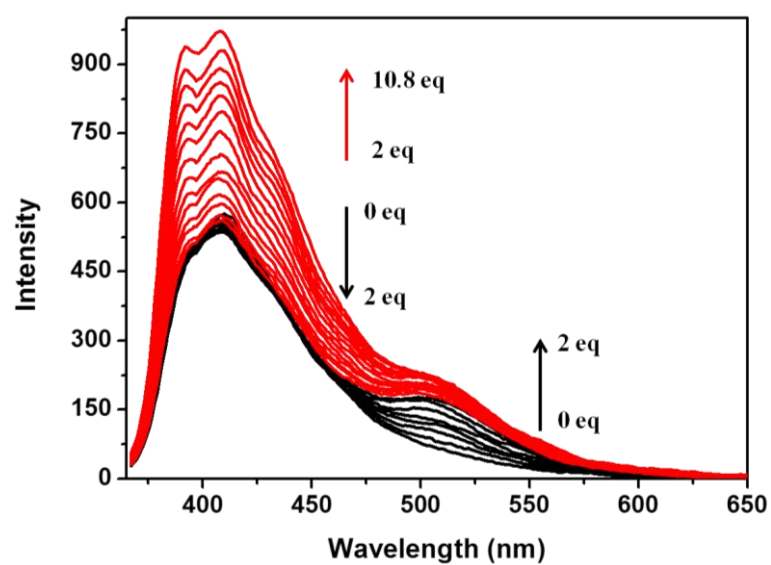


Figure 4.16 Overall fluorescence titration spectrum of **L2** (1×10^{-5} M) with TBAOAc (0 - 10.8 equiv) in DMSO.

4.5.2 Anion binding studies using ^1H NMR titrations

^1H NMR spectroscopy supported the structure of **L2** and structure of **L2** complexing with anions (F^- , AcO^- , and OH^-). In figure 4.17, 0.5 equiv. of anions could form hydrogen bonding with N-H protons of **L2**. The N-H protons broadened and shifted downfield due to the effect of electronegativity of anions that induced electron deshielding of proton at thiourea and H_f proton. Moreover, the singlet H_f proton also broadened and shifted downfield.

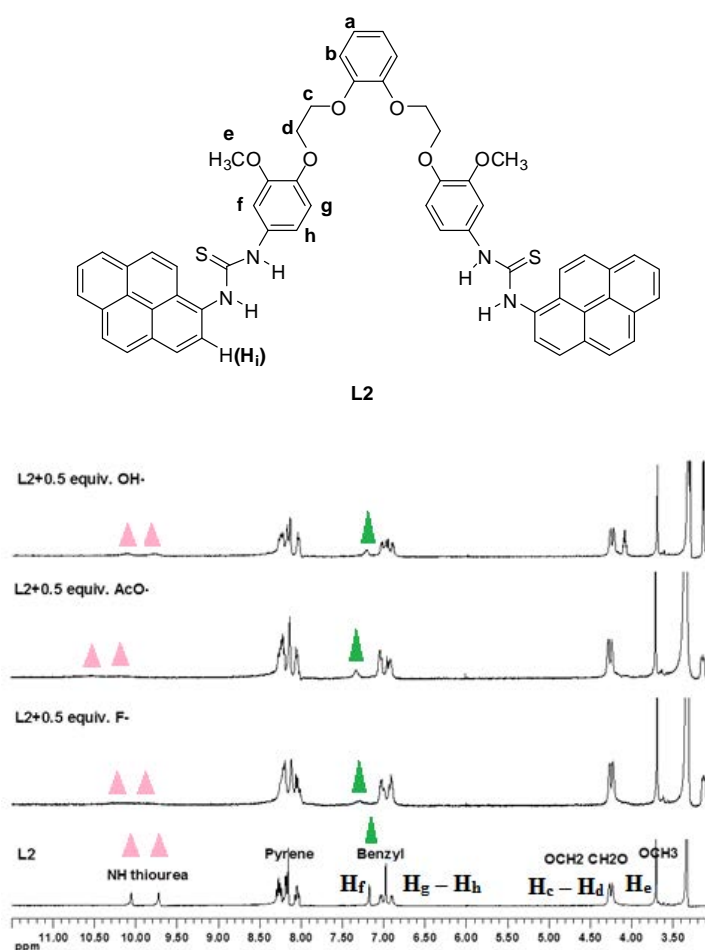


Figure 4.17 ^1H NMR spectra of **L2** in the presence of 0.5 equiv of TBAF, TBAOAc, and TBAOH in d_6 -DMSO at 400 MHz

^1H NMR spectra suggested that interactions of **L2** with F^- , AcO^- and OH^- formed H-bonding interactions, as indicated in the downfield shift of N-H protons and a singlet H_f proton in Figure 4.17. Moreover, the N-H proton at thiourea site disappeared upon

adding 0.5 equiv. of TBAF (Figure 4.18) and TBAOAc (Figure A28), while, TBAOH used 0.8 equiv for N-H proton disappear (Figure 4.19).

In Figure 4.18, 0-0.5 equiv. of F^- induced the N-H protons of thiourea and a singlet proton at benzene ring (H_f) to broaden and shift to downfield region. Both singlet protons at benzene ring and N-H protons of thiourea disappeared when F^- concentration was higher than 0.5 equivalents. At 0.15 equivalents of F^- , a $NH\cdots F^-$ hydrogen bond was formed. This hydrogen bond was indicated by the emerging of broadness and downfield shift of N-H proton of thiourea. The downfield shift of H_f was formed, due to the through space effect of the hydrogen bond (polarization of the C-H bond) [46]. Moreover, addition of 0.5 equivalents of F^- , N-H protons of thiourea and $-CH-$ at a singlet proton of benzene ring (H_f) disappeared. The N-H protons were deprotonated. With excess F^- (9 equiv.), the proton peak of $[FHF]^-$ was observed at $\delta=16.10$ ppm as shown in Figure 4.18 (inset), supporting the deprotonation mechanism. Interestingly, Figure 4.18 (inset) showed the upfield shift of pyrene signal from 8.29-8.02 ppm to around 7.77-8.12 ppm, and the singlet signal at 8.43 ppm was assumed to be the signal of H_i proton of pyrene. Figure 4.18 (inset) indicated that F^- induced the deprotonation of the N-H proton. From 1H NMR titration spectra confirmed that at low concentration of F^- H-bonding interaction occurred, while at high concentration of F^- could induce deprotonation of the NH thiourea.

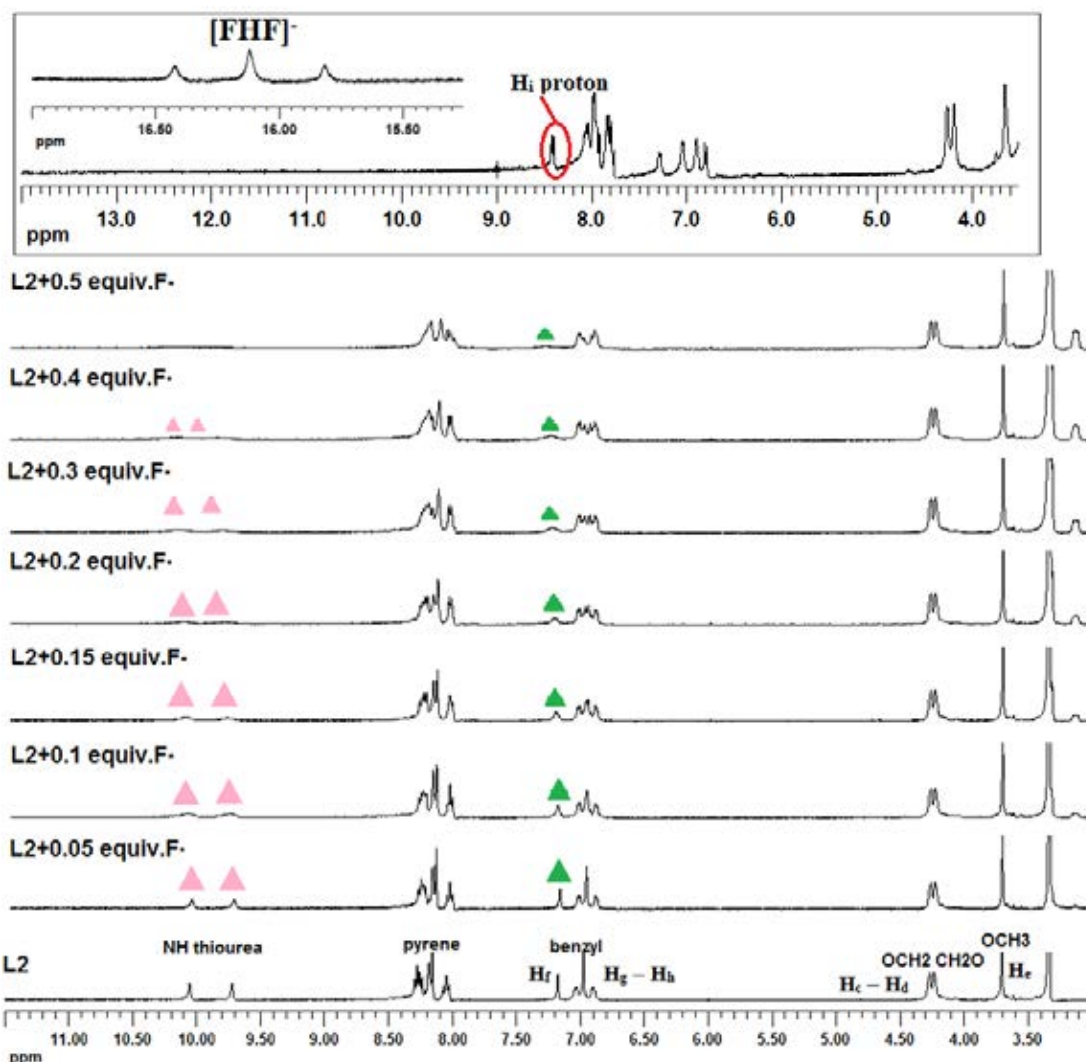


Figure 4.18 ^1H NMR titration spectra of **L2** in the presence of 0-0.5 equiv. of TBAF, inset : partial ^1H NMR with 9 equivalents of TBAF in d_6 -DMSO at 400 MHz.

^1H NMR titration spectra (Figure 4.19) suggested the H-bonding interactions and N-H deprotonation when adding 0-0.8 equiv of OH^- to **L2** solution. Downfield shifts and broadens of N-H proton and H_f proton suggested that OH^- formed H-bonding interactions with the N-H proton. Due to high electronegativity of oxygen in OH^- the N-H proton and H_f proton of **L2** shifted downfield. Interestingly, the spectrum at $\delta \approx 4.13$ and 3.33 ppm due to hydroxide and water formed from the deprotonation of N-H proton by OH^- . Figure 4.19 (inset), upfield shift of the pyrene proton (7.88-8.07 ppm) and H_i pyrene proton (8.42 ppm) was observed. This result suggested that OH^- induced deprotonation at NH thiourea in a similar manner to F^- .

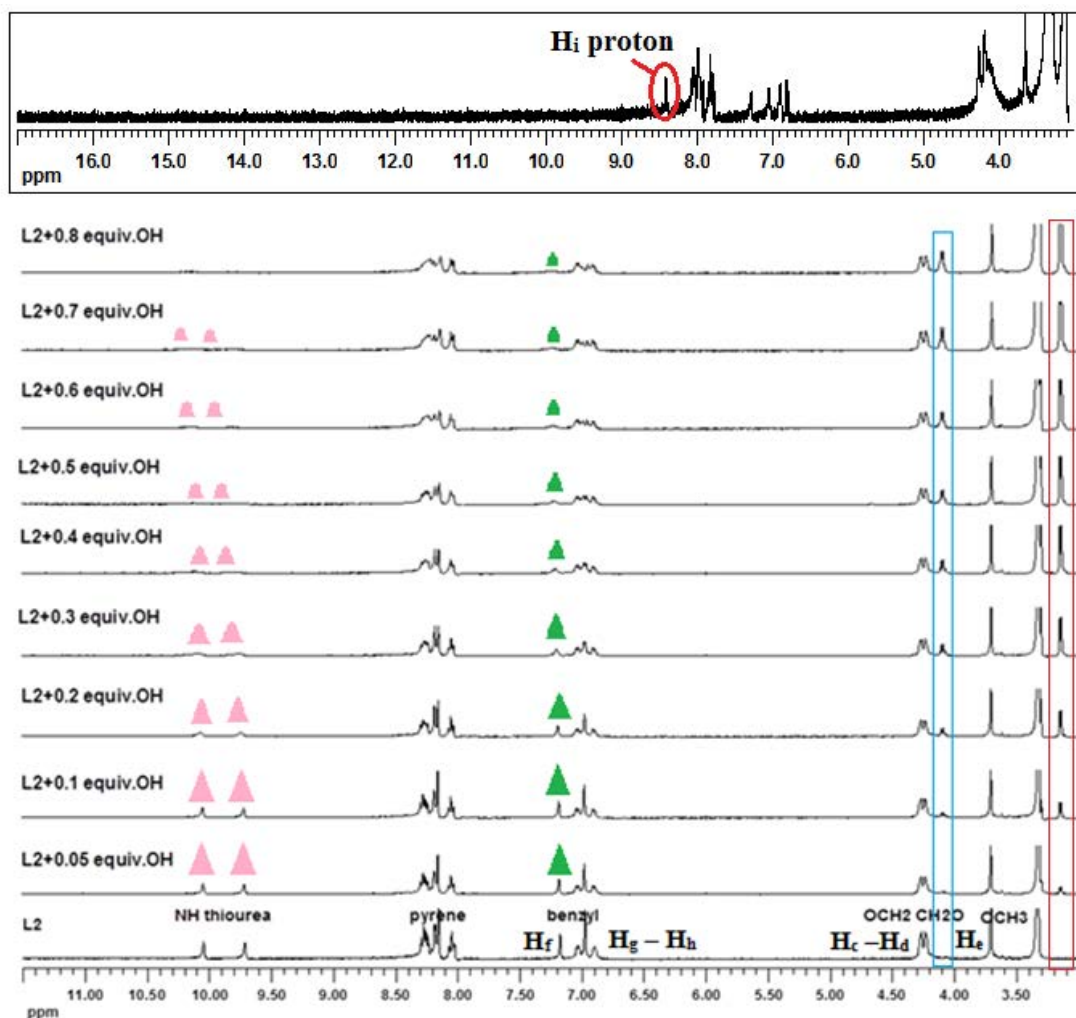
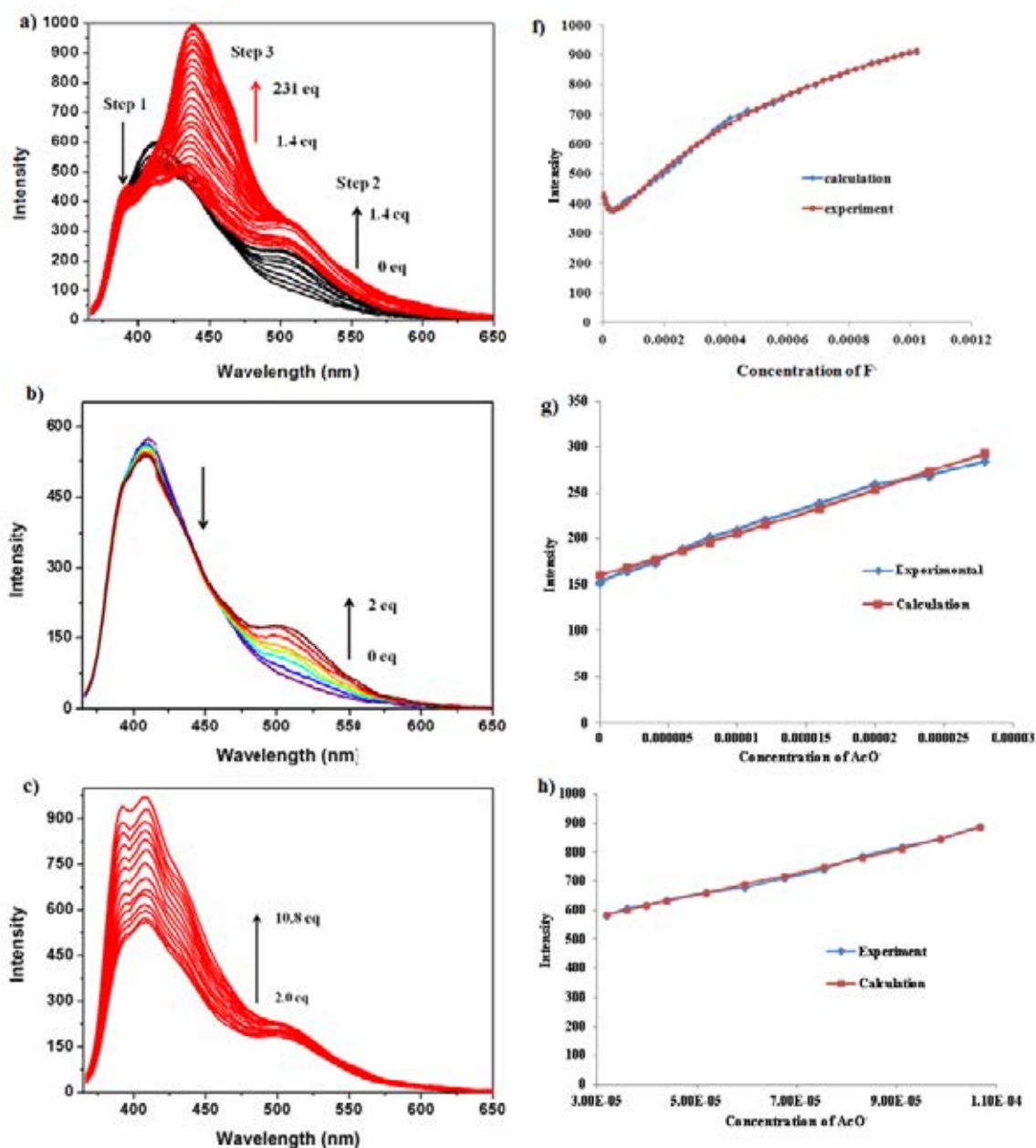


Figure 4.19 ^1H NMR titration spectra of **L2** in the presence of 0-0.8 equiv of tetra-*n*-butylammonium OH^- in d_6 -DMSO at 400 MHz.

While, ^1H NMR titration data of **L2** with AcO^- showed downfield shift and broad N-H and H_f protons (Figure A28). The result suggested that AcO^- formed H-bonding interactions with NH proton.

4.5.3 Determination of binding constants

From the fluorescence titration data, the binding constants (K_{ass}) for the formation of L2 with F^- , OH^- , and AcO^- were calculated via SPECFIT 32 program.



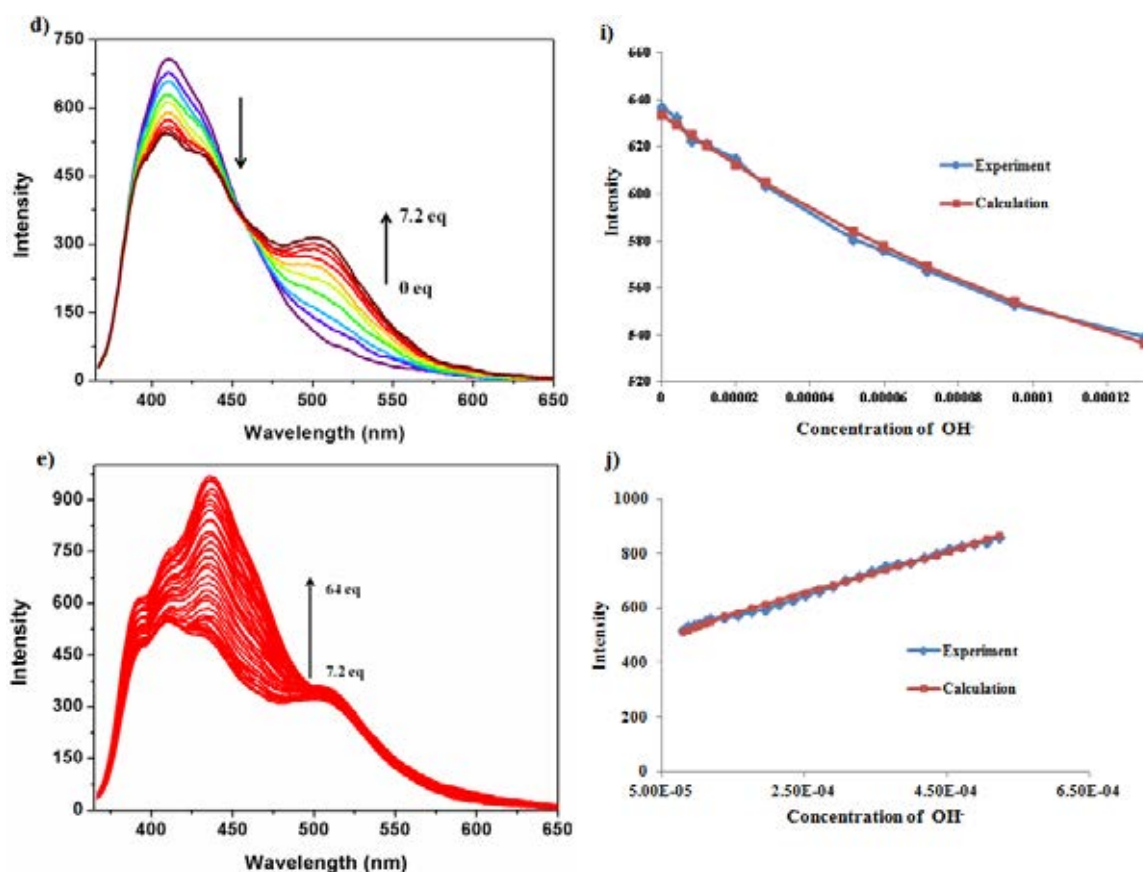


Figure 4.20 The fluorescence titration spectra of **L2** (10^{-5} M) upon the gradual addition of a) F^- (0-231 equiv.), b) AcO^- (0-2 equiv), c) AcO^- (2-10.8 equiv), d) OH^- (0-7.2 equiv.), and e) OH^- (7.2-64 equiv.) in DMSO and the compared experiment data calculated data from fluorescence titration of **L2** and f) F^- (0-1.4 equiv.), g) AcO^- (0-2 equiv), h) AcO^- (2-10.8 equiv), i) OH^- (0-7.2 equiv.), and j) OH^- (7.2-64 equiv.) for calculation of the binding constants (K_{ass}).

In SPECFIT 32 program give two data, 1) the binding constants (M^{-1}) and 2) the fitting graph (the plot of intensity versus concentration of anion). Figure 4.20a showed the emission intensity of **L2** upon adding F^- (0-231 equiv.). Then, these data were carried out to fit at 438 nm in SPECFIT 32 program to give a fitting graph as shown in Figure 4.20f and gave two binding constants ($\text{Log } \beta$) as shown in Table 4.4. The two binding constants ($\text{Log } \beta$) showed fitting in various ratios: **L2**: F^- , 2:1 (9.19 ± 0.53) and 2:2 (13.79 ± 0.64). From this result, it can be proposed that **L2** could formed complex with low concentration of F^- in a 2:1 fashion. At high concentration of F^- , the 2:2 fashion was dominated in the solution. The fitting graph in Figure 4.20g

and 4.20h gave binding constants of $\log \beta_1 = 4.3 \pm 0.2$ and $\log \beta_2 = 8.1 \pm 0.6$, respectively, for **L2** with AcO^- while **L2** with OH^- displayed $\log \beta_1 = 3.5 \pm 0.2$ and $\log \beta_2 = 6.8 \pm 0.4$ and the fitting graph in Figure 4.20i and 4.20j, respectively.

Table 4.4 Binding constant (M^{-1}) of receptor **L2** and F^- , OH^- , and AcO^- in DMSO via SPECFIT 32 program^a

L2·Anions	Log $\beta_1 \pm \text{SD}$ (host : guest)	Log $\beta_2 \pm \text{SD}$ (host : guest)	R²
F⁻	8.9 ± 0.1 (2:1)	11.9 ± 0.1 (2:2)	0.9736
AcO⁻	4.3 ± 0.2 (1:1)	8.1 ± 0.6 (1: 2)	0.9994 ^b , 0.9798 ^c
OH⁻	3.5 ± 0.2 (1:1)	6.8 ± 0.4 (1: 2)	0.9640 ^b , 0.9992 ^c

^a = Experiments were run in triplicate, ^b = Root mean square of the Log β_1 fitting graph (in Figure 4.20g for AcO^- and Figure 4.20i for OH^- , ^c = Root mean square of the Log β_2 fitting graph (Figure 4.20h for AcO^- and Figure 4.20j for OH^-)

The Job's plot of **L2** with anions (fluoride, hydroxide, and acetate) showed a maximum complexation at the mole fraction of 0.5 suggesting 1/1 or 2/2 binding mode as shown in Figure 4.21, Figure A29 and Figure A30.

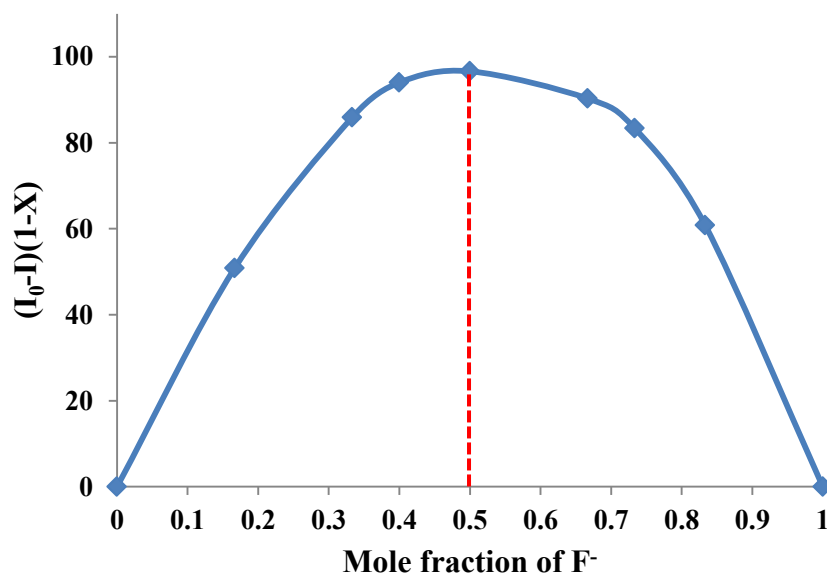


Figure 4.21 Job's plot of **L2** (5×10^{-6} M) with tetra-*n*-butylammonium fluoride in DMSO

4.6 Effects of concentrations on the emission spectra

The interactions of two pyrene molecules produced intramolecular and intermolecular excimer emission. The former produces a macrocyclic ring-closure product, while the latter results in a dimer and oligomer structures. The ratios of I_E/I_M of intramolecular interaction are independent from concentrations of ligand, while intermolecular interactions are not [39]. The possible structure of $L2 \cdot F^-$ complex was deduced from the relation of **L2** concentration (5×10^{-6} M to 5×10^{-8} M) with F^- 2.5 equiv. Figure 4.22, showed the fluorescence intensity ratios of excimer and monomer depended on the concentration of ligand that the ratios of I_E/I_M increased when concentrations of **L2** increased. From these results, indicated the structure of $L2 \cdot F^-$ complex could be an intermolecular pyrene-pyrene stacking as shown in Figure 4.23. However, plot of I_E/I_M in Figure 4.24 and 4.25 showed independence of I_E/I_M with

respect to concentration of AcO^- and OH^- . The binding mode of $\text{L2}\cdot\text{OAc}^-$ and $\text{L2}\cdot\text{OH}^-$ should be intramolecular pyrene-pyrene stacking as shown in Figure 4.26.

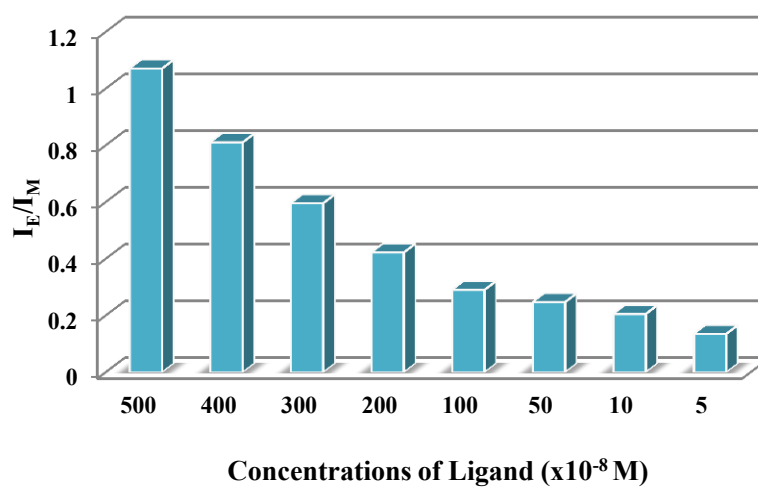


Figure 4.22 Plot of I_E/I_M of various concentrations of **L2** ($\times 10^{-8}$ M) with TBAF (2.5 equiv)

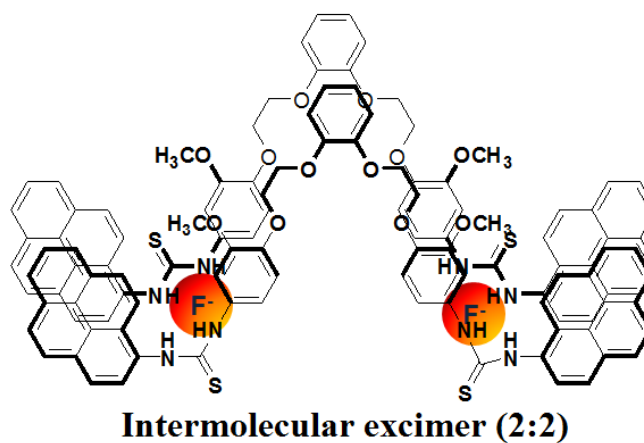


Figure 4.23 The possible structure of $\text{L2}\cdot\text{F}^-$ complex

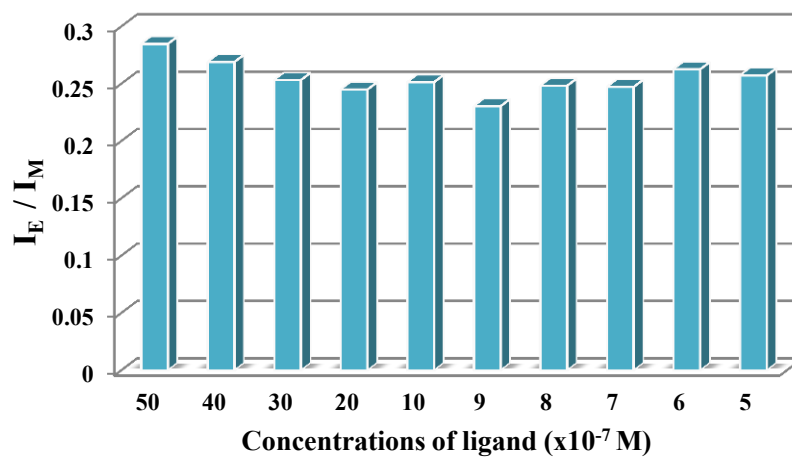


Figure 4.24 Plot of I_E/I_M of various concentrations of $L2$ ($\times 10^{-7}$ M) with TBAOAc (1.0 equiv)

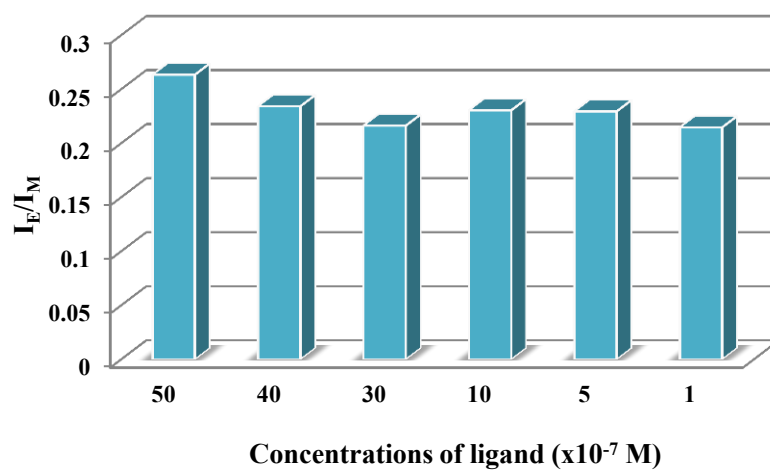
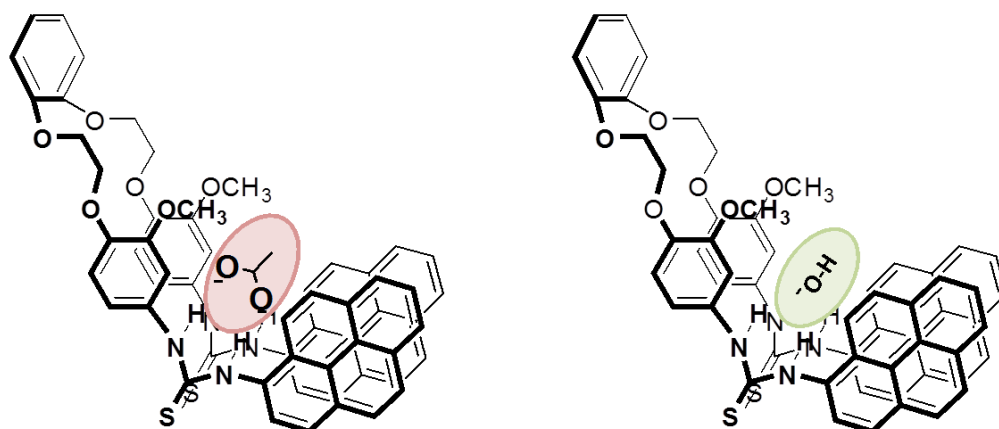


Figure 4.25 Plot of I_E/I_M of various concentrations of $L2$ ($\times 10^{-7}$ M) with TBAOH (1.5 equiv)



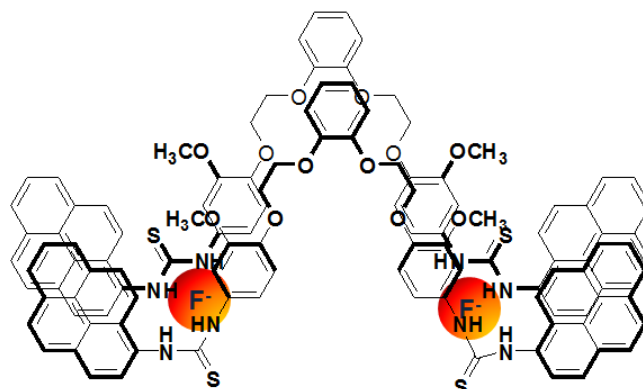
Intramolecular excimer (1:1)

Figure 4.26 The possible structure of $L2 \cdot OAc^-$ and $L2 \cdot OH^-$ complex

CHAPTER V

CONCLUSION

We have designed and synthesized compounds containing the benzenylamide unit linked to pyrene, **L1** and the dimeric pyrene thiourea linked to polyethylene glycol chain, **L2**. Attempts to synthesize **L3** were also carried out. However, the synthesis of **L3** was not successful. The fluorescence spectrum of free **L1** and **L2** in DMSO showed monomer bands at $\lambda_{em} = 381$ nm ($\lambda_{abs} = 346$ nm) and $\lambda_{em} = 410$ nm ($\lambda_{abs} = 350$), respectively. Quantum yields of **L1** and **L2** were 0.29 and 0.32, respectively. In fluorescence study, upon addition of anions to **L1** solution, a slightly change of the monomer band was observed. From experimental blank test, the result indicated that decreasing of monomer band of **L1** was occurred from the dilution effect rather than the addition of anions. In the case of **L2**, addition of tetra-*n*-butylammonium salts of F^- , AcO^- , and OH^- induced an excimer band at 515 nm. The order of intensity ratios between excimer and monomer bands (I_E/I_M) in **L2** varied as $F^- > OH^- \gg AcO^- > BzO^- > H_2PO_4^- > Cl^- > Br^- \approx I^-$. Due to smaller size and more basicity of F^- produced distinct excimer emission intensity compared to other anions. 1H NMR spectrum of **L2** when adding excess F^- showed a peak at 16.10 ppm due to the $[FHF]^-$ species. This indicated that F^- deprotonated the proton of N-H thiourea group of **L2**. In the case of OH^- the peak at 4.13 ppm due to water was observed and this also indicated that OH^- deprotonated N-H at thiourea group. The Job's plot experiment of **L2** and F^- showed a maximum mole fraction of fluoride at 0.5 which supported 2:2 complexation of $L2 \cdot F^-$ and the stability constants were calculated to be 8.9 ± 0.1 ($\log \beta_1$), and 11.9 ± 0.1 ($\log \beta_2$). The stoichiometries of **L2** and OH^- and AcO^- calculated using the same method were 1:1 and the stability constants were calculated to be 3.5 ± 0.2 ($\log \beta_1$) and 6.8 ± 0.4 ($\log \beta_2$) for $L2 \cdot OH^-$ and 4.3 ± 0.2 ($\log \beta_1$) and ($\log \beta_2$) 8.1 ± 0.6 for $L2 \cdot OAc^-$.



Intermolecular excimer (2:2)

The possible structure of $\mathbf{L2}\cdot\text{F}^-$ was the intermolecular pyrene-pyrene stacking complex because the fluorescence intensity ratios of excimer and monomer (I_E/I_M) depended on the concentration of the ligand. However, the binding mode of $\mathbf{L2}\cdot\text{OH}^-$ and $\mathbf{L2}\cdot\text{AcO}^-$ should be intramolecular pyrene-pyrene stacking because I_E/I_M ratios of OH^- and AcO^- were independent of $\mathbf{L2}$ concentration.

REFERENCE

- [1] Steed, J. W., Turner, D. R., and Wallace, K. J. Core concepts in supramolecular chemistry and nanochemistry. John Wiley&Sons, 2007.
- [2] Guha, S., Drew, G. B. M., and Banerjee, A. Construction of supramolecular helices and breaking the helicity by forming supramolecular β -sheet structures using suitable self-assembling pseudopeptide building blocks. Crystal Growth & Design 10 (2010): 4716–4721.
- [3] Steed, J. L., and Atwood, J. L. Supramolecular chemistry. New York: John Wiley&Sons, 2000.
- [4] Kondo, S.-I., Nagamine, M., Karasawa, S., Ishihara, M., Unno, M., and Yano, Y. Anion recognition by 2,2'-binaphthalene derivatives bearing urea and thiourea groups at 8- and 8'-positions by UV-vis and fluorescence spectroscopies. Tetrahedron 67 (2011): 943-950.
- [5] Kang, S. O., Begum, R. A., and Bowman-James, K. Amide-based ligands for anion coordination. Angew. Chem. Int. Ed. 45 (2006): 7882-7894.
- [6] Shao, J., Lin, H., and Lin, H-K. A simple and efficient colorimetric anion sensor based on a thiourea group in DMSO and DMSO-water and its real-life application. Talanta 75 (2008): 1015–1020.
- [7] Gac, L. S., Luhmer, M., Reinaud, O., and Jabin, I. Self-assembly via ionic interactions of calix[6]arene-based receptor displaying remarkable host-guest properties toward neutral guests. Tetrahedron 63 (2007): 10721–10730.
- [8] Kim, S. J., and Quang, D. T. Calixarene-derived fluorescent probes. Chem. Rev. 107 (2007): 3780-3799.
- [9] Gomez, D.E., Fabbrizzi, L., and Licchelli, M. Why, on interaction of urea-based receptors with fluoride, beautiful colors develop. J. Org. Chem. 70 (2005): 5717-5720.
- [10] Gunnlaugsson, T., Glynn, M., Tocci, M. G., Kruger, E. P., and Pfeffer, M. F. Anion recognition and sensing in organic and aqueous media using

- luminescent and colorimetric sensors. Coord. Chem. Rev. 250 (2006): 3094–3117.
- [11] Valeur, B. Molecular fluorescence principles and applications. New York: Wiley-Vch, 2001.
- [12] Xie, J., Menand, M., Maisonneuve, S., and Metivier, R. Synthesis of bispyrenyl sugar-aza-crown ethers as new fluorescent molecular sensors for Cu(II). J. Org. Chem. 72 (2007): 5980-5985.
- [13] de Silva, A. P., and others. Signaling recognition events with fluorescent sensors and switches. Chem. Rev. 97 (1997): 1515-1566.
- [14] Yang, J. S., Lin, C. S., and Hwang, C. Y. Cu²⁺-induced blue shift of the pyrene excimer emission: A new signal transduction mode of pyrene probes. Org. Lett. 3 (2001): 889-892.
- [15] Winnik, F. M. Photophysics of preassociated pyrenes in aqueous polymer solutions and in other organized media. Chem. Rev. 93 (1993): 587-614.
- [16] Cho, E. J., Ryu, B. J., Lee, Y. J., and Nam, K. C. Visible colorimetric fluoride ion sensors. Org. Lett. 7 (2005): 2607-2609.
- [17] Cho, E. J., and others. A new fluoride selective fluorescent as well as chromogenic chemosensor containing a naphthalene urea derivative. J. Am. Chem. Soc. 125 (2003): 12376-12377.
- [18] Kim, S. K., and Yoon, J. A new fluorescent PET chemosensor for fluoride ions. Chem. Commun. (2002): 770-771.
- [19] Kim, S. K., Bok, J. H., Bartsch, R. A., Lee, J. Y., and Kim, J. S. A fluoride-selective PCT chemosensor based on formation of a static pyrene excimer. Org. Lett. 7 (2005): 4839-4842.
- [20] Tongraung, P., Chantarasiri, N., and Tuntulani, T. Calix[4]arenes containing urea and crown/urea moieties: Effects of the crown ether unit and Na⁺ towards anion binding ability. Tetrahedron Lett. 44 (2003): 29-32.
- [21] Nerngchamnong, N., Chailap, B., Leeladee, P., Chailapakul, O., Suksai, C., and Tuntulani, T. Topological and metal ion effects on the anion binding abilities of new heteroditopic receptors derived from p-tert-butylcalix[4]arene. Tetrahedron Lett. 52 (2011): 2914-2917.

- [22] Choi, J. K., Kim, S. H., Yoon, J., Lee, K. H., Bartsch, R. A., and Kim, J. S. A PCT-based, pyrene-armed calix[4]crown fluoroionophore. J. Org. Chem. 71 (2006): 8011-8015.
- [23] Ghosh, K., and Adhikari, S. Colorimetric and fluorescence sensing of anions using thiourea based coumarin receptors. Tetrahedron Lett. 47 (2006): 8165–8169.
- [24] Luxami, V., and Kumar, S. Colorimetric and ratiometric fluorescence sensing of fluoride ions based on competitive intra- and intermolecular proton transfer. Tetrahedron Lett. 48 (2007): 3083-3087.
- [25] Chauhan, S. M. S., Bisht, T., and Grag, B. Anion sensing by phenazine-based urea/thiourea receptors. Tetrahedron Lett. 49 (2008): 6646-6649.
- [26] Qu, Y., Hua, J., and Tian, H. Colorimetric and ratiometric red fluorescent chemosensor for fluoride ion based on diketopyrrolopyrrole. Org. Lett. 12 (2010): 3320-3323.
- [27] Swamy, K. M. K., and others. Tandem Pseudopericyclic reactions: [1, 5]-X sigmatropic shift/ 6π -electrocyclic ring closure converting N-(2-X-Carbonyl) phenyl ketenimines into 2-X-Quinolin-4(3H)-ones. J. Org. Chem. 71 (2006): 8626-8628.
- [28] Lee, J. Y., Cho, E. J., Mukamel, S., and Nam, K. C. Efficient fluoride-selective fluorescent host: experiment and theory. J. Org. Chem. 69 (2004): 943-950.
- [29] Li, Y., Cao, L., and Tian, H. Fluoride ion-triggered dual fluorescence switch based on naphthalimides winged zinc porphyrin. J. Org. Chem. 71 (2006): 8279-8282.
- [30] Lin, C-I., Selvi, S., Fang, J. M., Chou, P. T., Lai, C. H., and Cheng, Y. M. Pyreno[2,1-*b*]pyrrole and bis(pyreno[2,1-*b*]pyrrole) as selective chemosensors of fluoride Ion: A mechanistic study. J. Org. Chem. 72 (2007): 3537-3542.
- [31] Zhang, J. F., Lim, C. S., Bhuniya, S., Cho, B. R., and Kim, J. S. A highly selective colorimetric and ratiometric two-photon fluorescent probe for fluoride ion detection. Org. Lett. 13 (2011): 1190–1193.

- [32] Yang, J. S., Lin, C. S., and Hwang, C. U. Cu^{2+} -induced blue shift of the pyrene excimer emission: A new signal transduction mode of pyrene probes. Org. Lett. 3 (2001): 889-892.
- [33] Kim, H. J., Kim, S. K., Lee, J. Y., and Kim, J. S. Fluoride-sensing calix-luminophores based on regioselective binding. J. Org. Chem. 71 (2006): 6611-6614.
- [34] Dahan, A., and others. Synthesis and evaluation of a pseudocyclic trithiourea-based anion host. J. Org. Chem. 72 (2007): 2289-2296.
- [35] Kim, H. K., Hong, J., Hong, A., Ham, S., Lee, J. H., and Kim, J. S. Cu^{2+} -induced intermolecular static excimer formation of pyrenealkylamine. Org. Lett. 10 (2008): 1963-1966.
- [36] Jung, H. S., and others. Cu^{2+} ion-induced self-assembly of pyrenylquinoline with a pyrenyl excimer formation. Org. Lett. 11 (2009): 3378-3381.
- [37] Thongkum, D., and Tuntulani, T. Fluoride-induced intermolecular excimer formation of bispyrenyl thioureas linked by polyethylene glycol chains. Tetrahedron 67 (2011): 8102-8109.
- [38] Abe, A. M. M., Helaja, J., and Koskinen, A. M. P. Novel crown ether and salen metal chelation driven molecular pincers. Org. Lett. 8 (2006): 4537-4540.
- [39] Wu, X. L., Luo, L., Lei, L., Liao, G. H., Wu, L. Z., and Tung, C. H. Highly efficient cucurbit[8]uril-templated intramolecular photocycloaddition of 2-naphthalene-labeled poly(ethylene glycol) in aqueous solution. J. Org. Chem. 73 (2008): 491-494.
- [40] Zhou, Y., Zhu, C., Gao, X., You, X., and Yao, C. Hg^{2+} -selective ratiometric and "Off-On" chemosensor based on the azadiene-pyrene derivative. Org. Lett. 12 (2010): 2566-2569.
- [41] Sirikulajorn, A., Duanglaor, P., Ruangpornvisuti, V., Tomapatanaget, B., and Tuntulani, T. tryptophan receptors containing acridine-based thiourea. supramol. Chem. 21 (2009): 486-494.
- [42] Chuentragool, P., Vongnam, K., Rashatasakhon, P., Sukwattanasinitt, M., and Wacharasindhu, S. Calcium carbide as a cost-effective starting material for

- symmetrical diarylethynes via Pd-catalyzed coupling reaction. Tetrahedron 67 (2011): 8177-8182.
- [43] Kendo, S-i., Sonoda, H., Katsu, T., and Unno, M. Improvement of solubility of 2,2'-binaphthalene derivatives bearing urea groups as anion receptors and their application to a chloride selective electrode. Sensors and Actuators B:Chem. 160 (2011): 684-690.
- [44] Bordwell, F. G. Equilibrium acidities in dimethyl sulfoxide solution. Acc. Chem. Res. 21 (1988): 456-463.
- [45] Boiocchi, M., Boca, L. D., Gomez, D. E., Fabbrizzi, L., Licchelli, M., and Monzani, E. Nature of urea-fluoride interaction: Incipient and definitive proton transfer. J. AM. CHEM. SOC. 126 (2004): 16507-16514.
- [46] Han, F., and others. Simple bithiocarbonohydrazones as sensitive, selective, colorimetric, and switch-On fluorescent chemosensors for fluoride anions. Chem. Eur. J. 13 (2007): 2880-2892.

APPENDIX

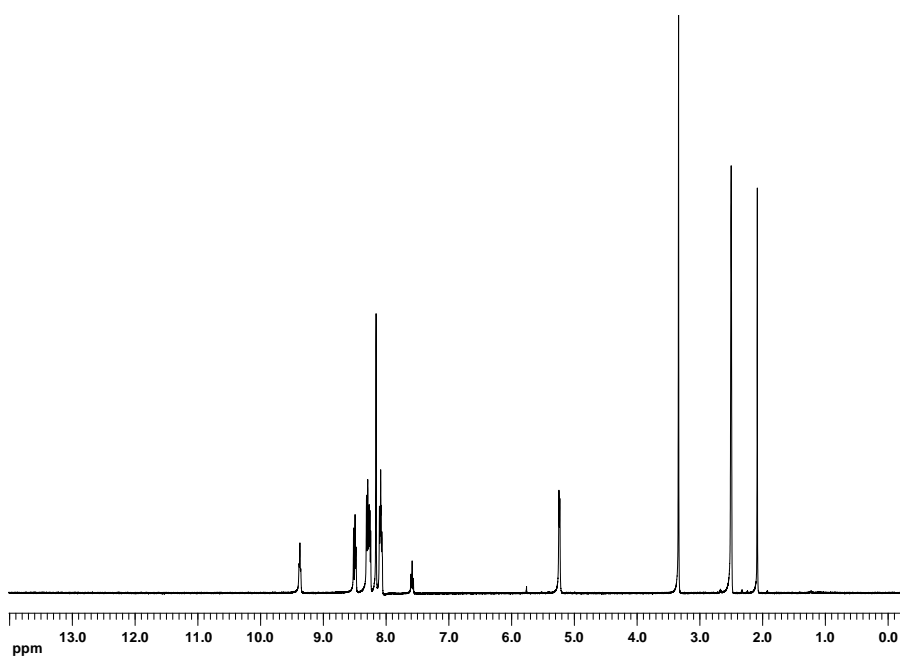


Figure A1 ^1H NMR spectrum of **L1** in d_6 -DMSO at 400 MHz

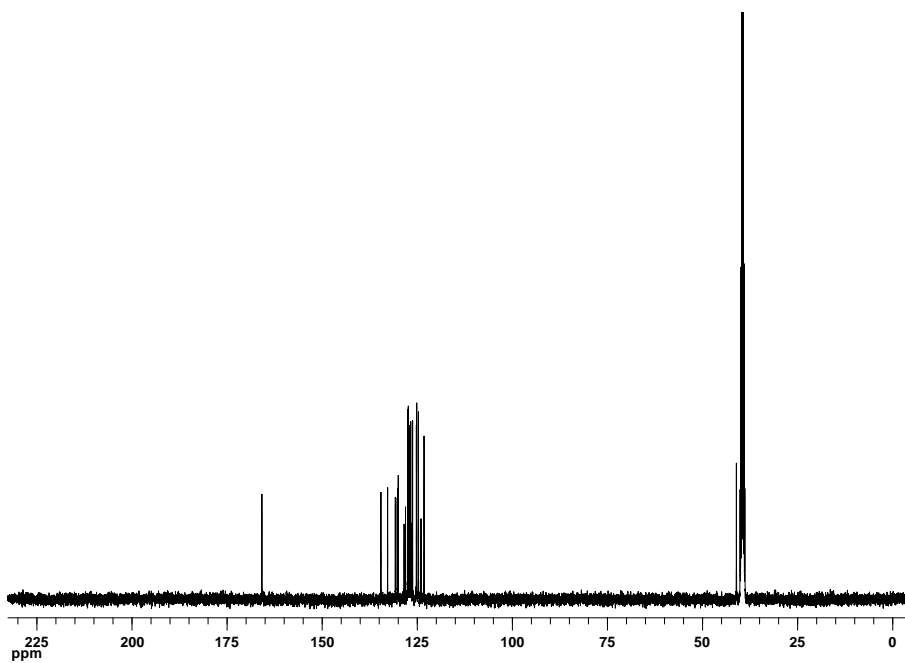


Figure A2 ^{13}C NMR spectrum of **L1** in d_6 -DMSO at 400 MHz

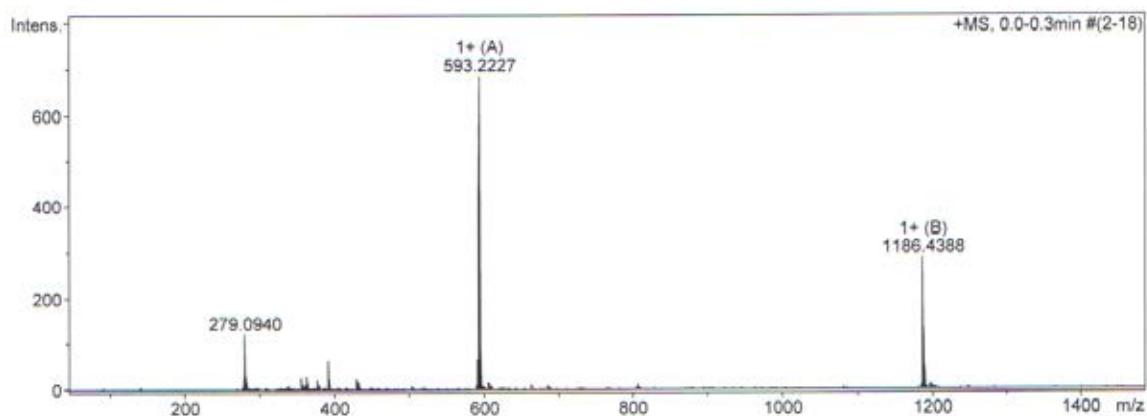


Figure A3 ESI-MS mass spectrum of **L1** as shown at 593.2227

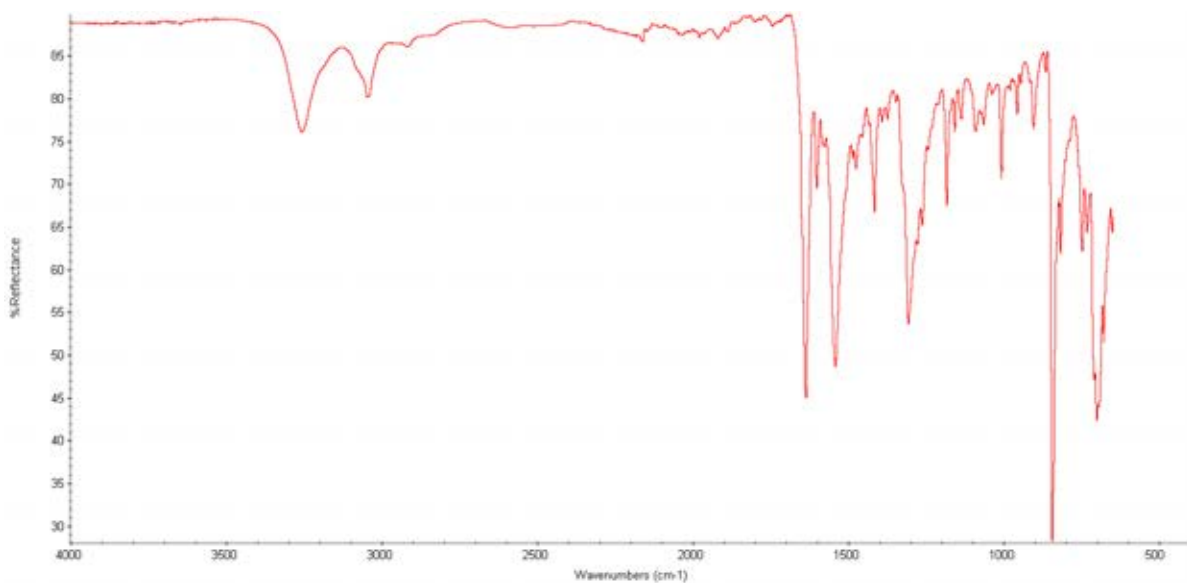


Figure A4 IR spectrum of **L1** in KBr

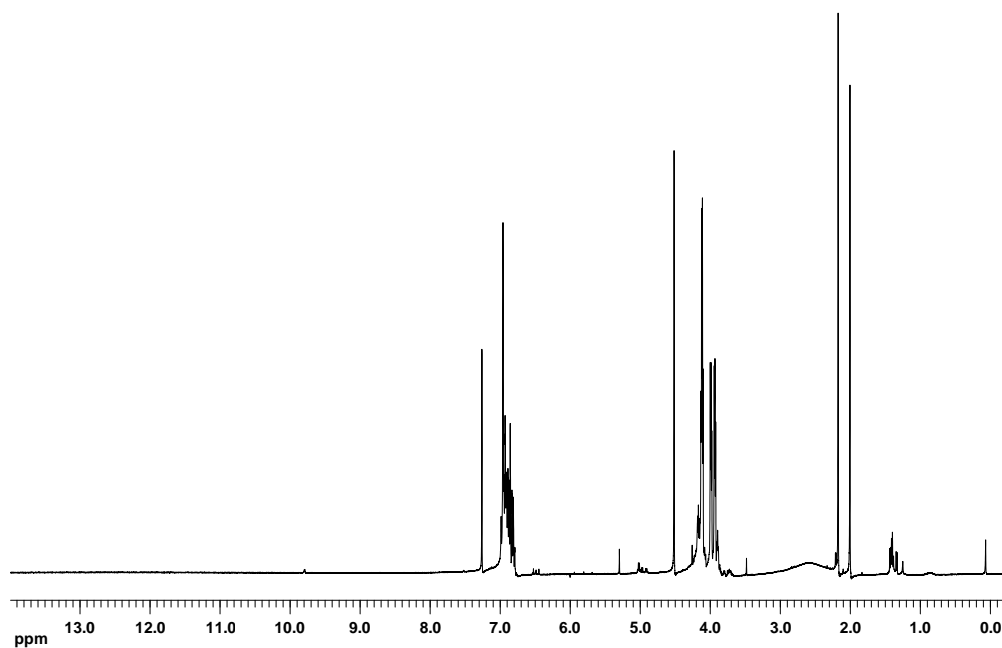


Figure A5 ¹H NMR spectrum of compound **1** in CDCl₃ at 400 MHz

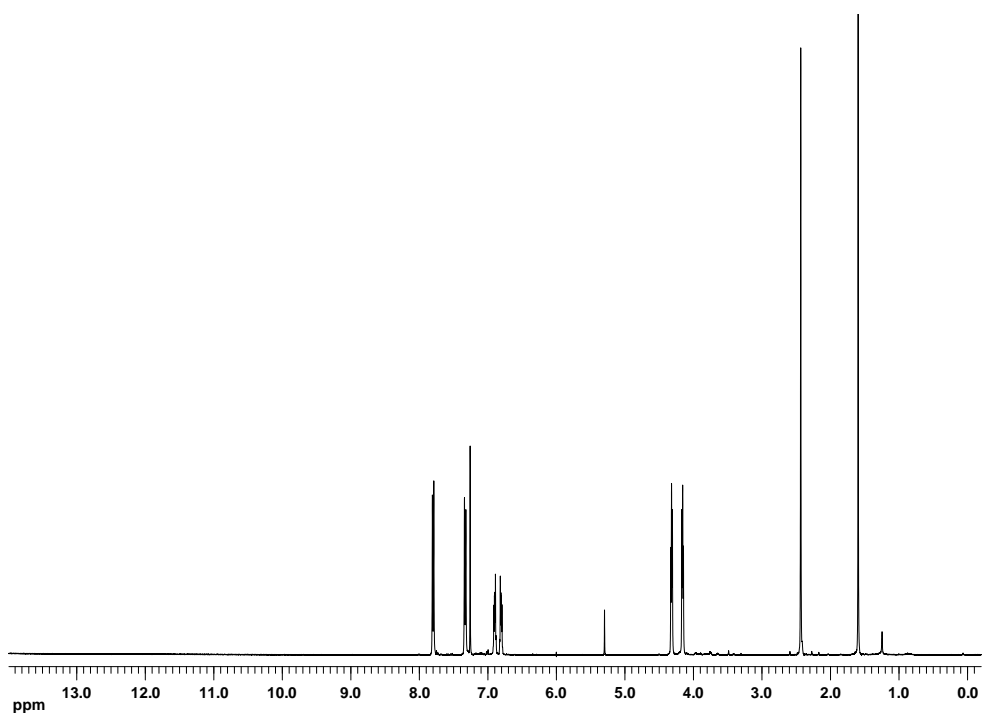


Figure A6 ¹H NMR spectrum of compound **2** in CDCl₃ at 400 MHz

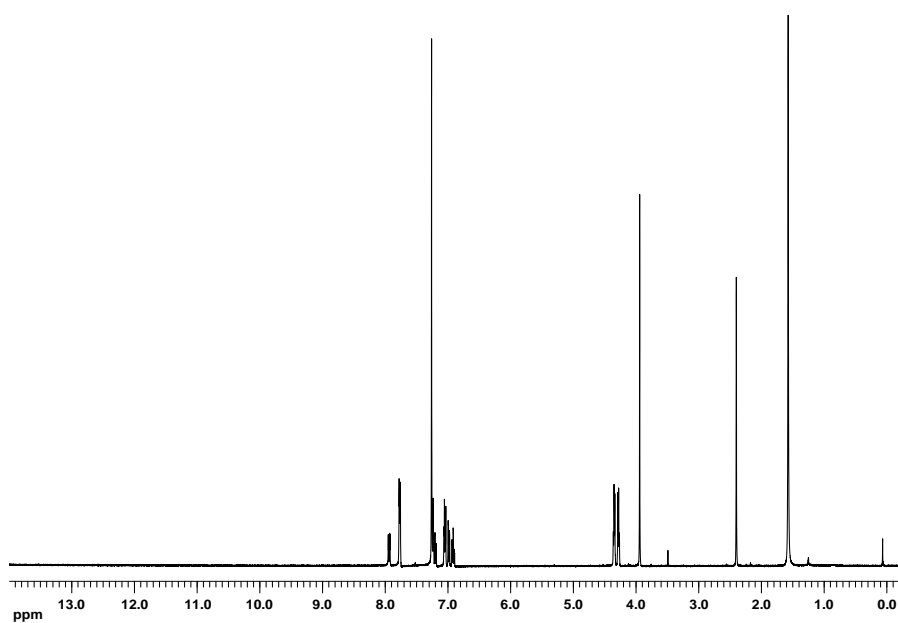


Figure A7 ^1H NMR spectrum of compound **4** in CDCl_3 at 400 MHz

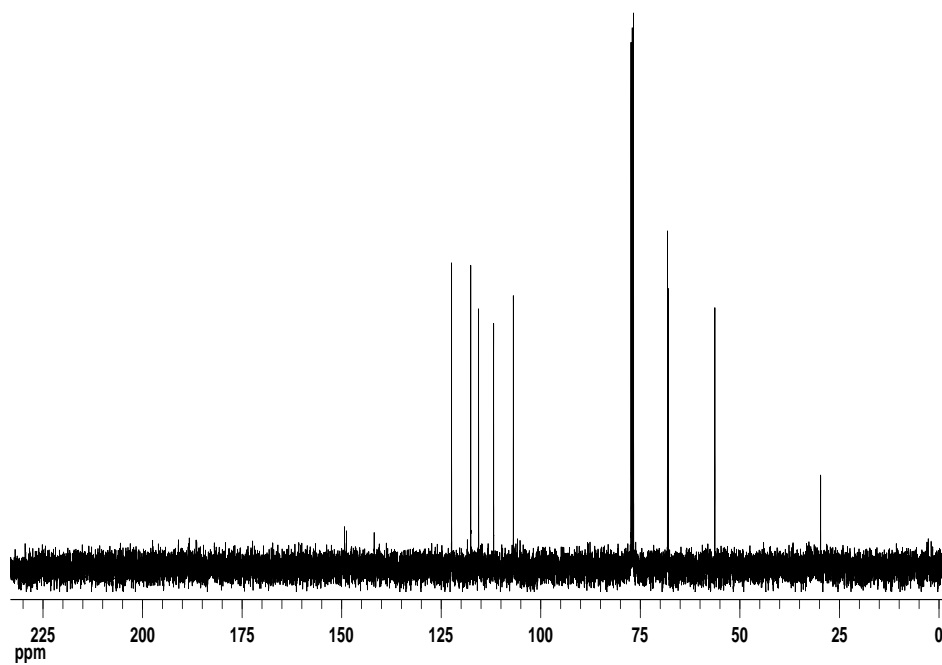


Figure A8 ^{13}C NMR spectrum of compound **4** in CDCl_3 at 400 MHz

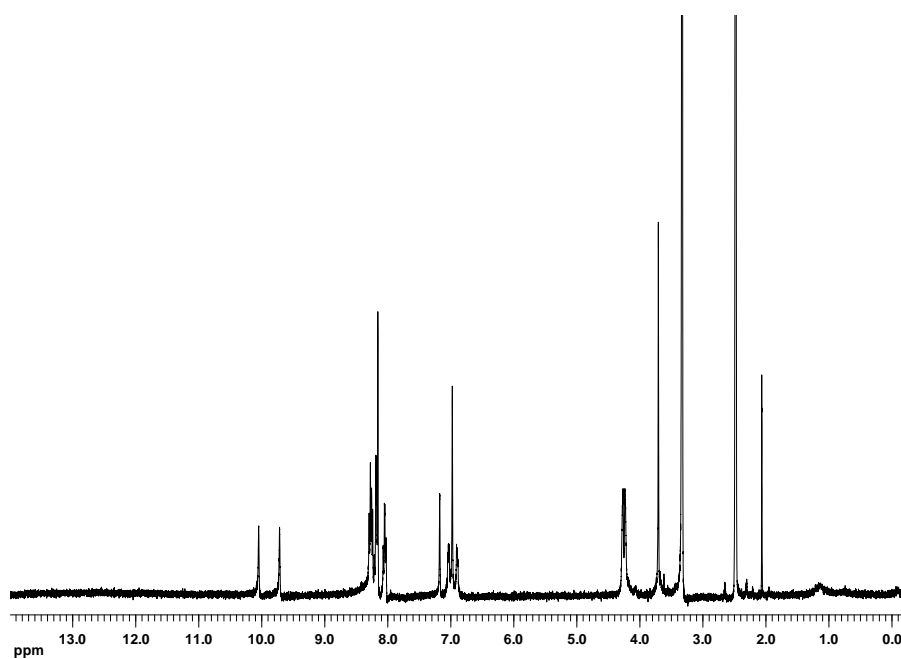


Figure A9 ^1H NMR spectrum of L2 in $\text{d}_6\text{-DMSO}$ at 400 MHz

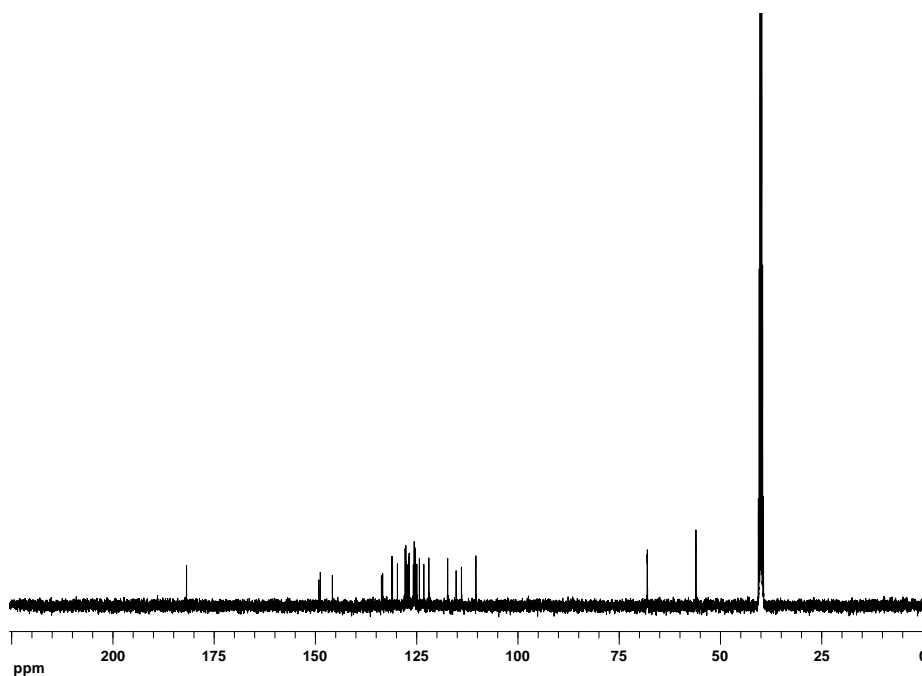


Figure A10 ^{13}C NMR spectrum of L2 in $\text{d}_6\text{-DMSO}$ at 400 MHz

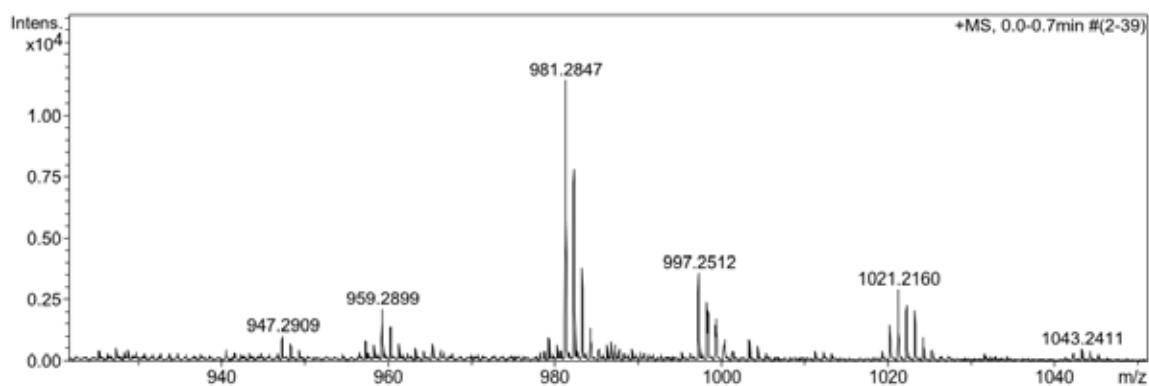


Figure A11 Mass spectrum (ESI-MS) of L2 as shown at 959.2899 m/z

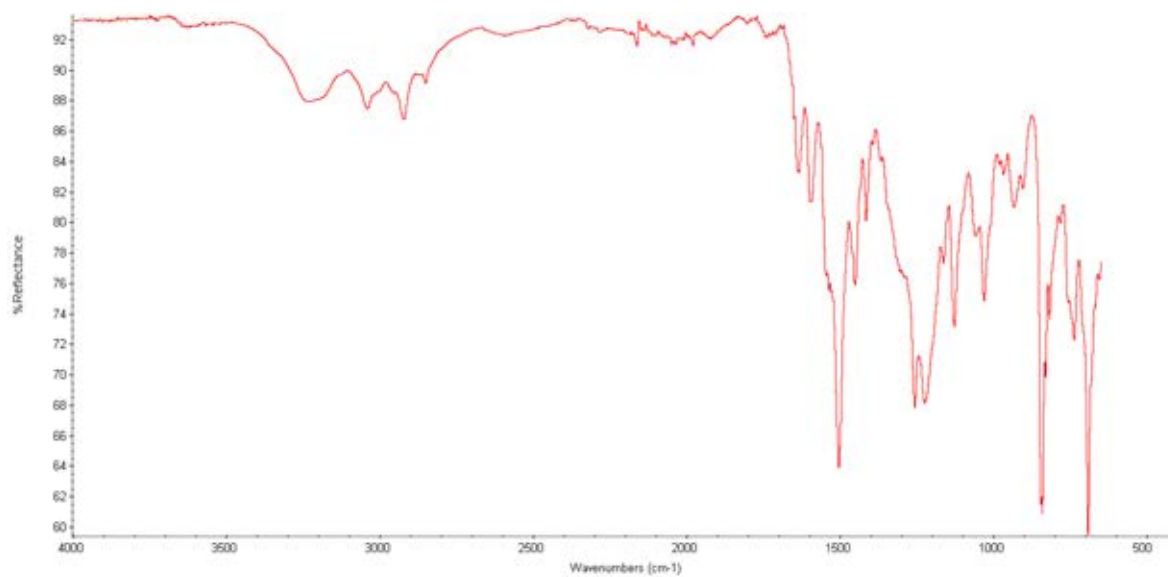


Figure A12 IR spectrum of L2 in KBr

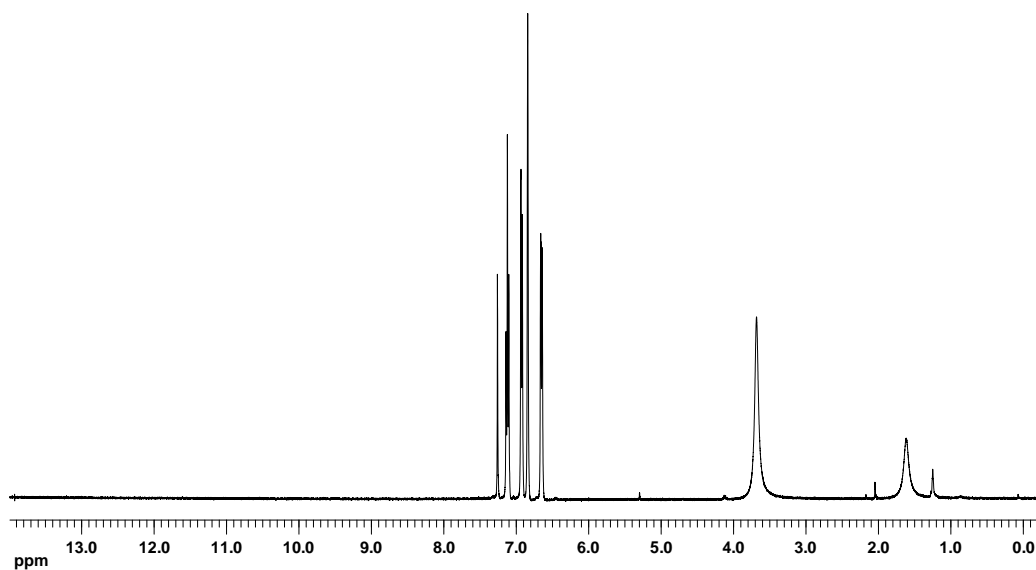


Figure A13 ^1H NMR spectrum of compound **6** in CDCl_3 at 400 MHz

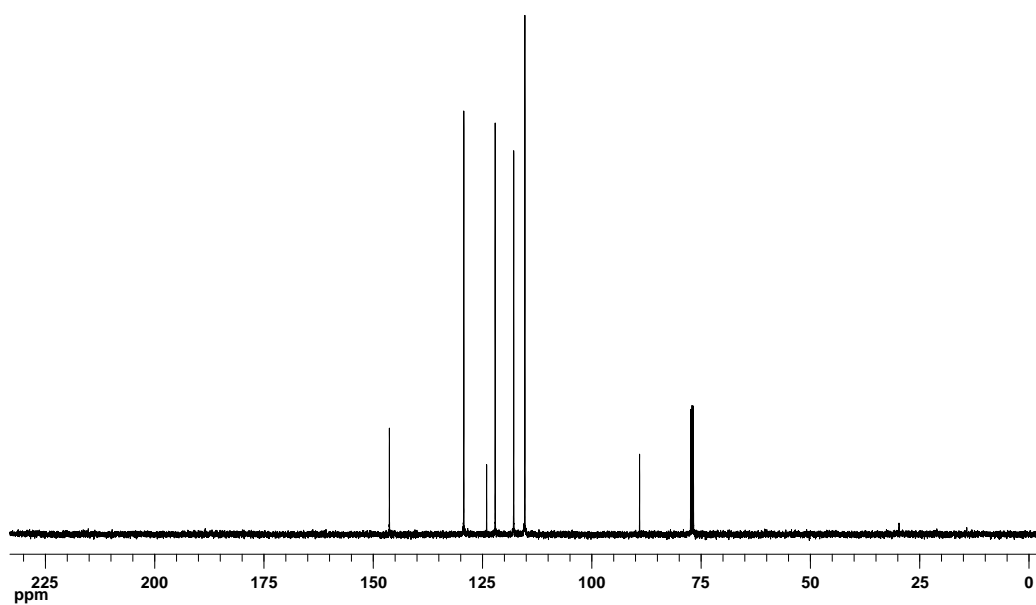


Figure A14 ^{13}C NMR spectrum of compound **6** in CDCl_3 at 400 MHz

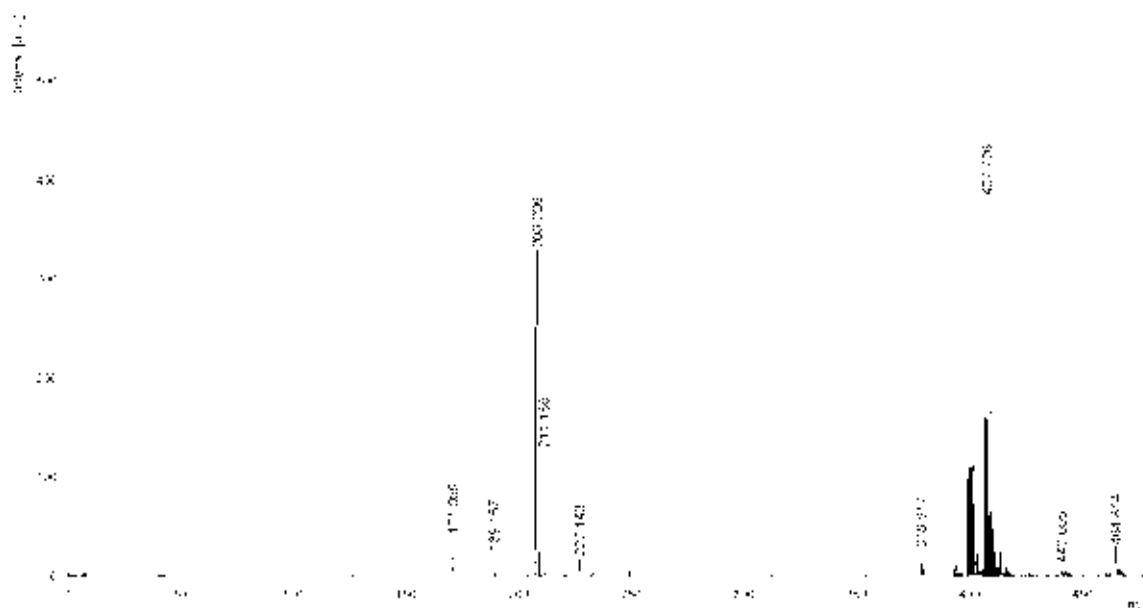


Figure A15 MALDI-TOF mass spectrum of compound **6** as shown at 208.206

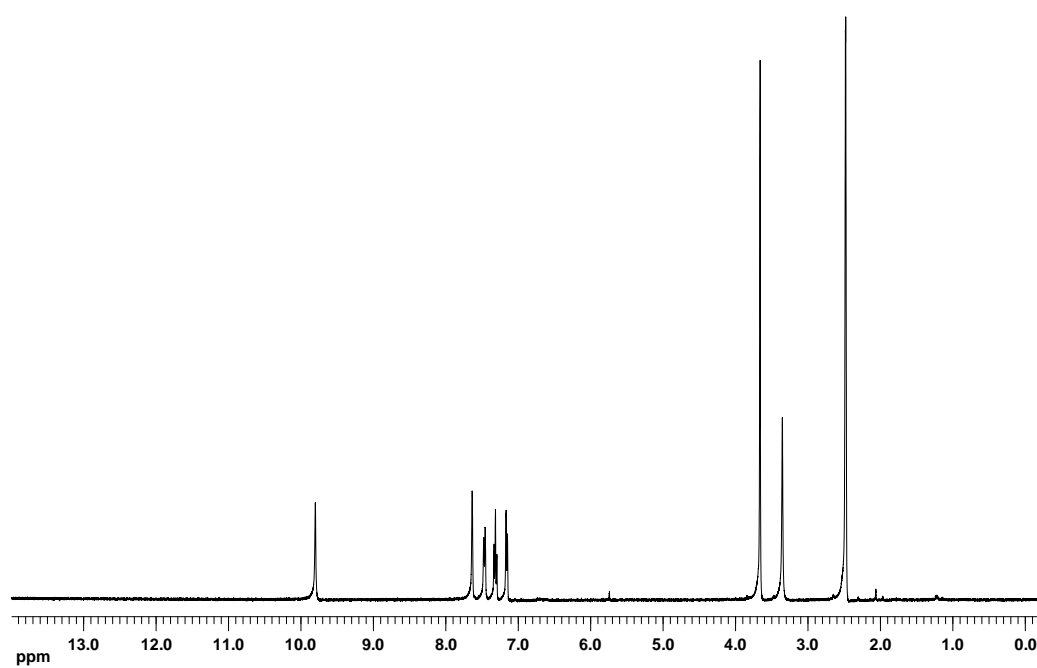


Figure A16 ¹H NMR spectrum of compound **7** in d₆-DMSO at 400 MHz

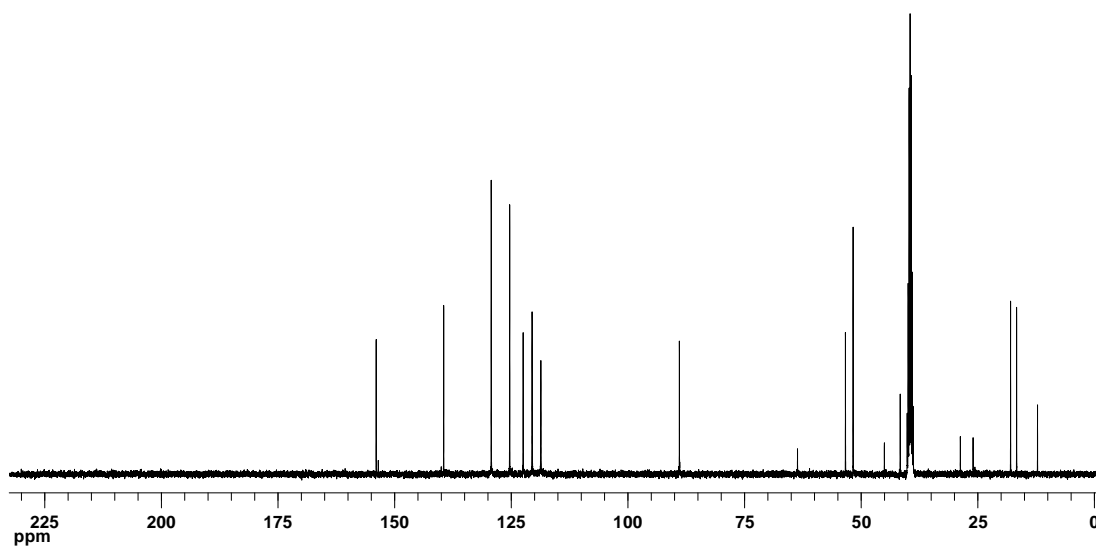


Figure A17 ^{13}C NMR spectrum of compound **7** in d_6 -DMSO at 400 MHz

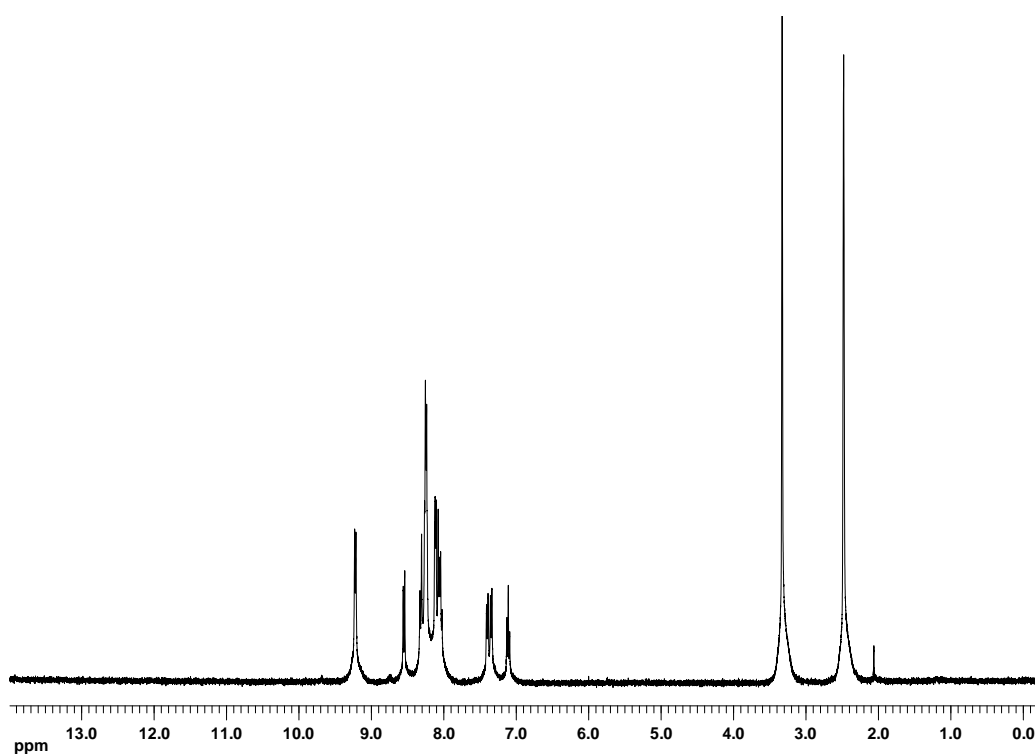


Figure A18 ^1H NMR spectrum of compound **8** in d_6 -DMSO at 400 MHz

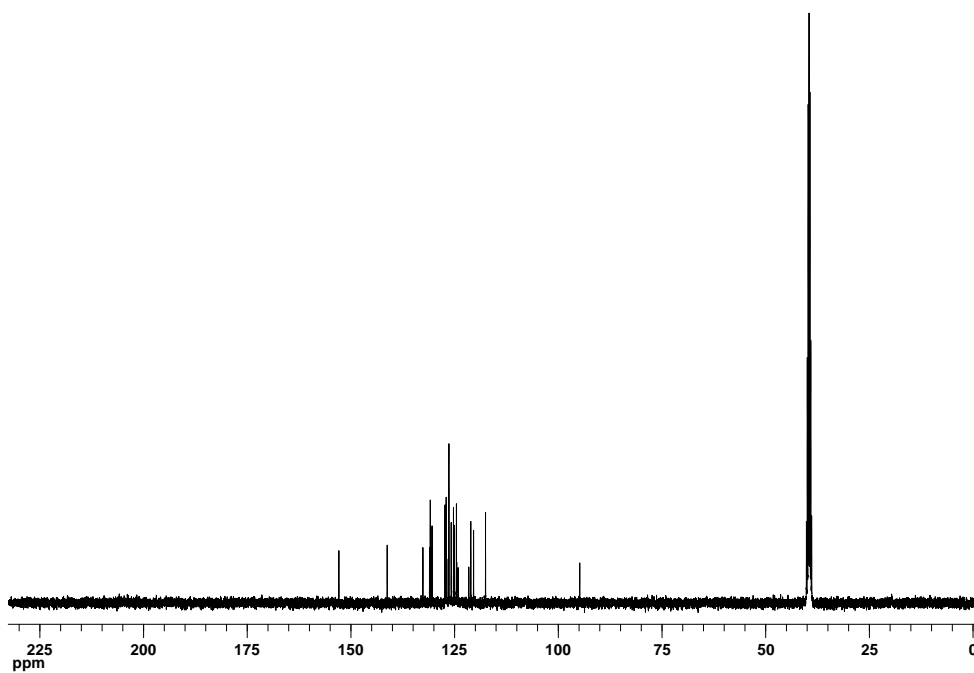


Figure A19 ^{13}C NMR spectrum of compound **8** in d_6 -DMSO at 400 MHz

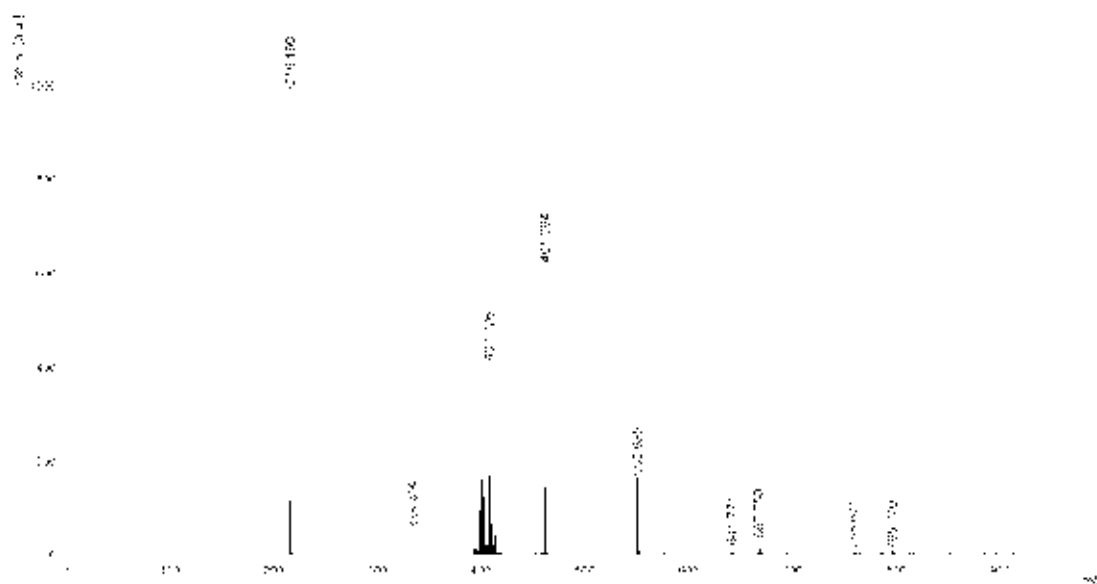


Figure A20 MALDI-TOF mass spectrum of compound **8** as shown at 461.394

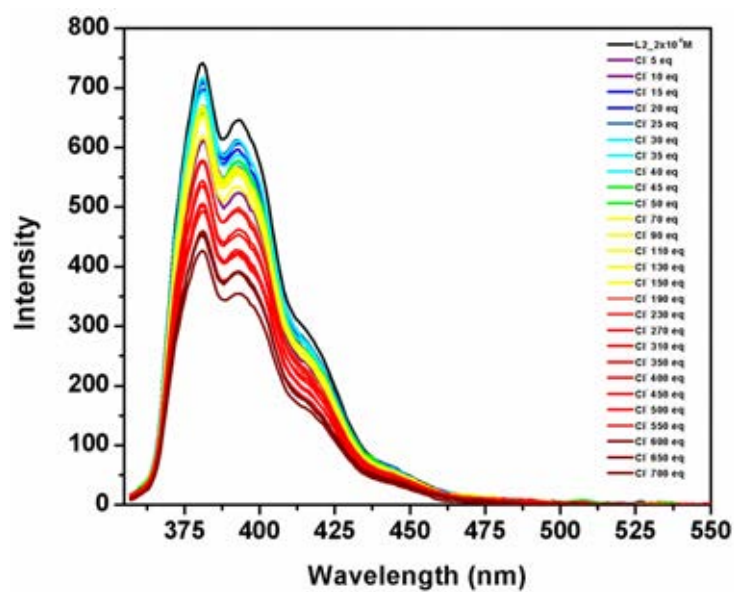


Figure A21 Fluorescence emission of L1 (2×10^{-6} M) with 0-700 equiv. of Cl⁻ salts in DMSO

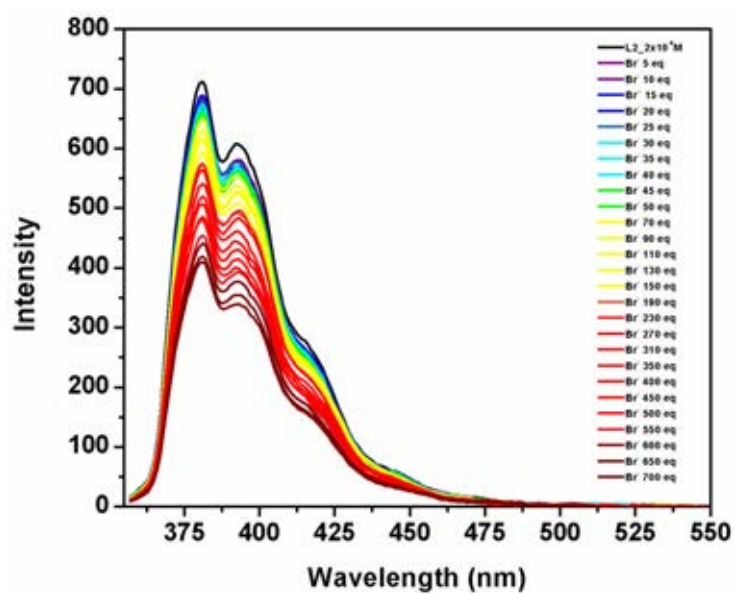


Figure A22 Fluorescence emission of L1 (2×10^{-6} M) with 0-700 equiv. of Br⁻ salts in DMSO

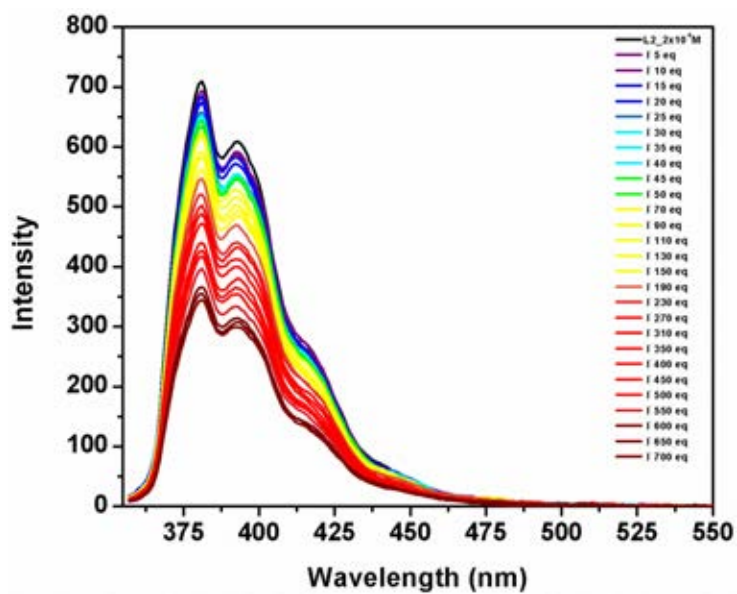


Figure A23 Fluorescence emission of L1 (2×10^{-6} M) with 0-700 equiv. of I⁻ salts in DMSO

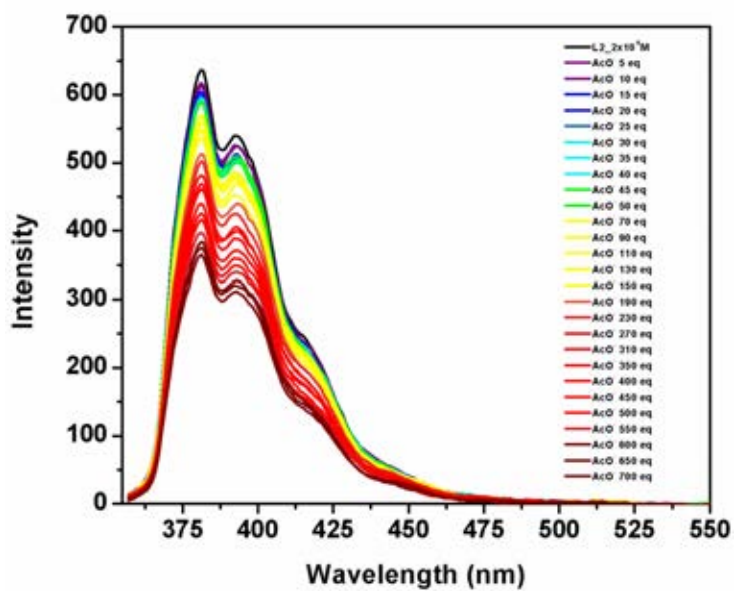


Figure A24 Fluorescence emission of L1 (2×10^{-6} M) with 0-700 equiv. of AcO⁻ salts in DMSO

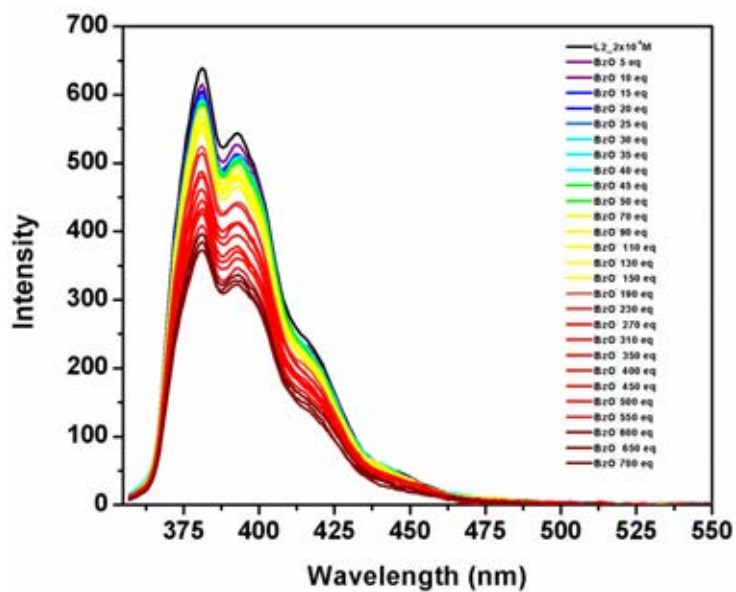


Figure A25 Fluorescence emission of L1 (2×10^{-6} M) with 0-700 equiv. of BzO⁻ salts in DMSO

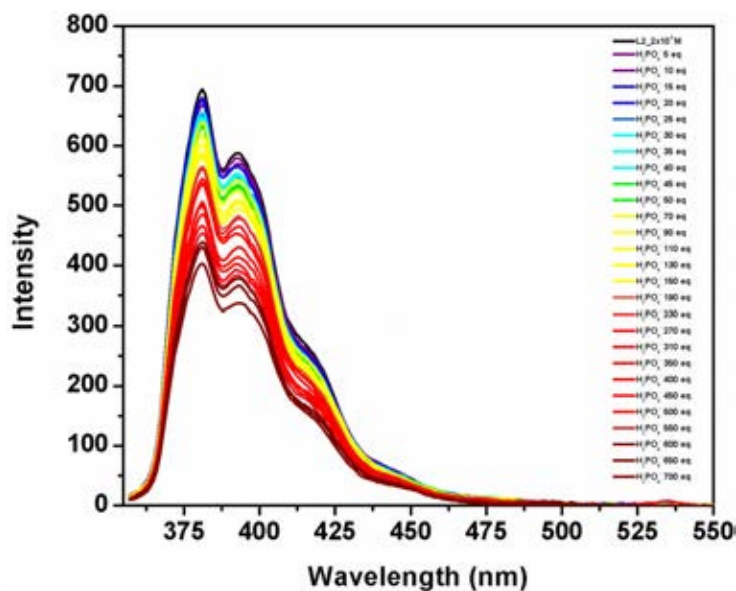


Figure A26 Fluorescence emission of L1 (2×10^{-6} M) with 0-700 equiv. of H₂PO₄⁻ salts in DMSO

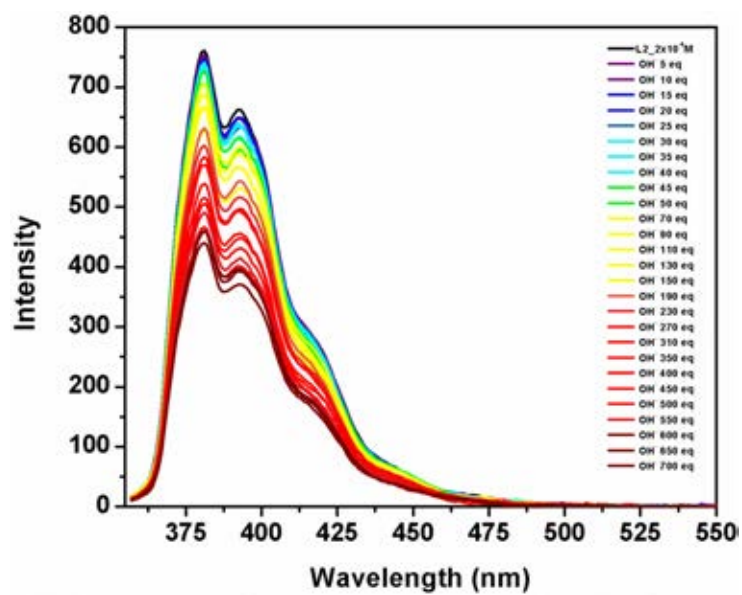


Figure A27 Fluorescence emission of **L1** (2×10^{-6} M) with 0-700 equiv. of OH^- salts in DMSO

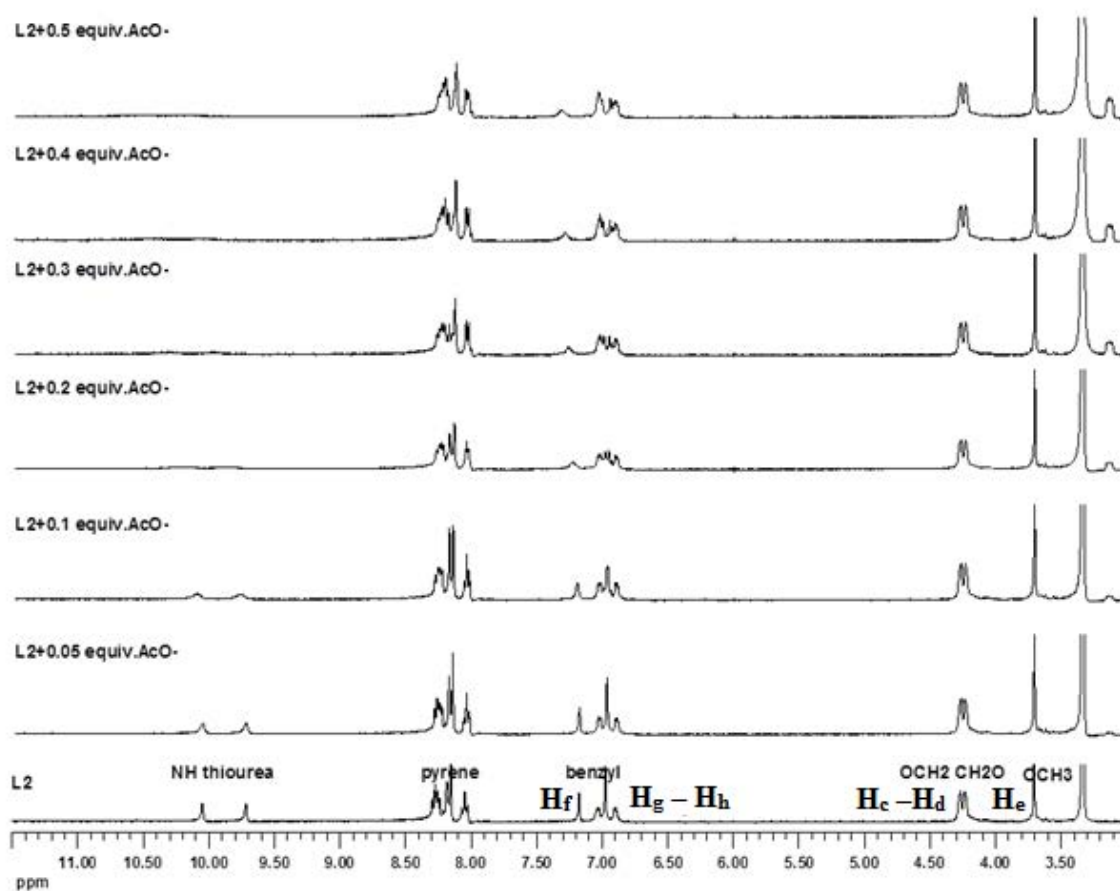


Figure A28 ^1H NMR titration spectra of L2 in the presence of 0-0.5 equiv of tetra-*n*-butylammonium AcO^- in d_6 -DMSO at 400 MHz.

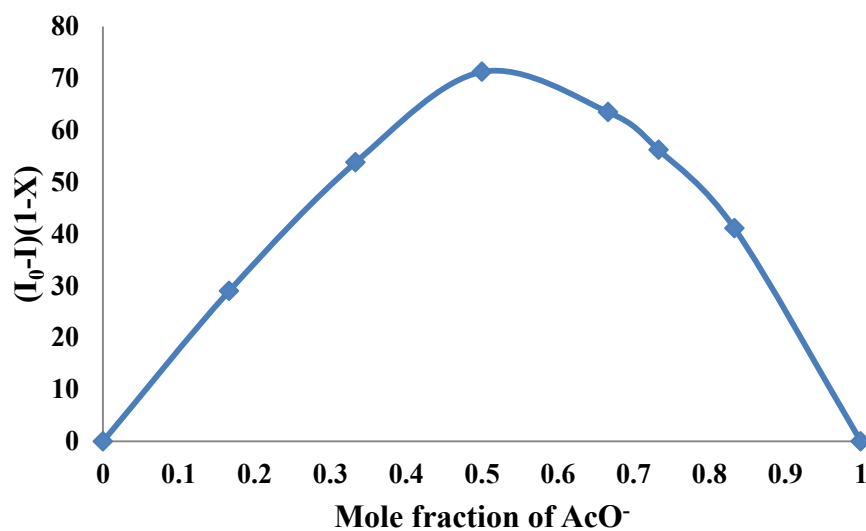


Figure A29 Job's plot of L2 (5×10^{-6} M) with tetra-*n*-butylammonium acetate in DMSO

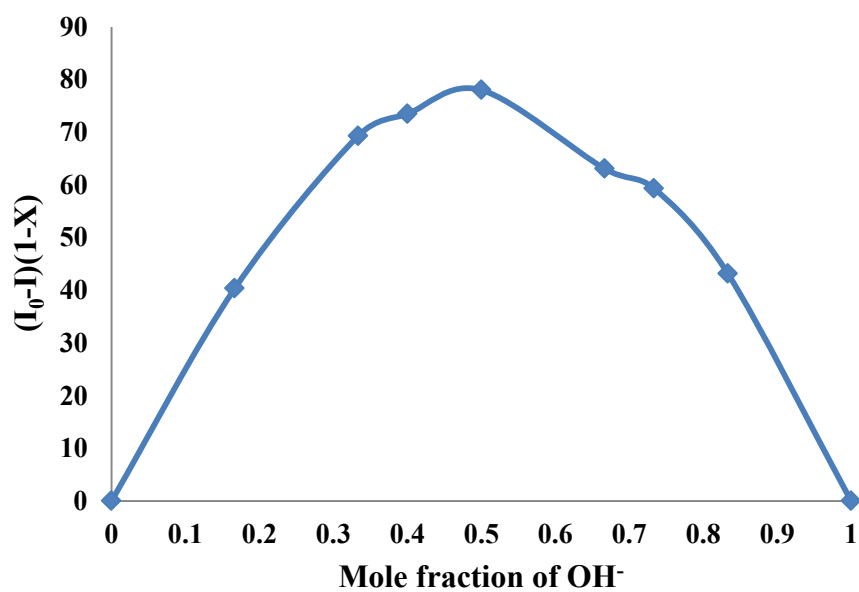


Figure A30 Job's plot of L2 (5×10^{-6} M) with tetra-*n*-butylammonium hydroxide in DMSO

VITAE

Name: Miss Yanee Pharat

Date of Birth: January 20, 1987

Education:

2009-2012 (being pursued) M.Sc. Candidate in inorganic chemistry
Chulalongkorn University, Bangkok, Thailand

Thesis Topic: **Structural Effects of Bispyrenyl Ureas
Linked by Polyethylene Glycol and Ethyne Spacers toward
Anion Binding Abilities.**

2005-2009 Maharakham University, Maharakham, Thailand.
Bachelor degree of Science majoring in Chemistry

Senior Project: **Cation Allosteric Effect in the Recognition of
Anions by Pseudo-Azacrown Ether Receptor.**

Grants:

2009-2011 Human Resource Development in Science Project (Science
Achievement Scholarship of Thailand, SAST) Scholarship

Presentation:

2012 Structural effects of bispyrenyl ureas linked by polyethylene
glycol chain towards their anion binding abilities, **Poster
presentation** in the 6th Pure and Applied Chemistry
International Conference (PACCON 2012), 11-13 January
2012, The Empress Convention Center, Chiang Mai, Thailand